Republic of Iraq
Ministry of Higher Education and Scientific Research
University of Babylon
College of Education for Pure Sciences
Department of Physics

Preparation and Characterization of Nanocomposite Films as a Model of Antibacterial Applications

A thesis

Submitted to the Council of the College of Education for Pure Sciences of University of Babylon in Partial Fulfillment of the Requirements for the Degree of Master in Education / Physics

by

Sarmad Munther Abdulkadhim Hussein

B. Sc. in Physics
(University of Babylon, 2013 A.D)

Supervised by

Prof.
Dr. Fouad Shakir Hashim

Prof.
Dr. Bahaa Hussein Salih

2022 A.D **1444 A.H.**

بِسْمِ اللَّهِ الرَّحْمَٰنِ الرَّحِيمِ

﴿وَيُطَافُ عَلَيْهِمْ بِآنِيَةٍ مِنْ فِضَّةٍ وَأَكْوَابٍ كَانَتْ قَوَارِيرَاْ (١٥) قَوَارِيرَ مِنْ فِضَّةٍ قَدَّرُوهَا تَقْدِيرًا (١٦)﴾

صدق الله العلي العظيم

سورة الانسان

الآية (١٥-١٦)

Dedication

This thesis is lovingly dedicated to the almighty God who gives me strength and good health while doing this. To the Noble Messenger, may God's prayers and peace be upon him, who illuminated the earth with the guidance of the message of Islam dedicate this effort.

My respective parents who have been my constant source of inspiration. They have given us the drive and discipline to tackle any task with enthusiasm and determination, without their love and support this thesis would not have been made possible. I also dedicate this thesis to my brothers and sister who supports me in everything, to my friends who helped me finished this project, to the martyrs of Iraq with all the love and appreciation.

Sarmad

Acknowledgements

First of all, my thanks to God Almighty for his grace and generosity, and I praise him very much.

I would like to express my deep thanks and appreciation to the kindergarten of love and the fountain of tenderness my dear mother, may God prolong her life, and to those who planted in me ambition and perseverance, my dear brothers and sister, for providing me with help, assistance, advice and their constant encouragement during the research period.

With the final touches on my thesis, I am pleased to extend my sincere thanks and appreciation to Prof. Dr. Fouad Shakir Hashim and Prof. Dr.Bahaa H. Rabee for suggesting the topic of research and for thier supervision and following-up.

I also extend my thanks to the Head of the Physics Department, Prof. Dr. Khaled Henein, and the graduate studies rapporteur in the physics department, Prof. Dr. Shurooq Sabah, for their efforts and assistance. In gratitude, I would like to thank my honorable professor and colleague, head of the department of biology sciences, Assistant Professor Dr. Adi Jassim Abdul Razzaq for his kind care and assistance throughout the study period.

I would like to express my gratitude to the assistant teacher Msc. Zainab Hameed Kareem for her assistance during the research period.

Finally, I would like to thank everyone who helped me in accomplishing this thesis.

Sarmad

Summary

PVA-PVP polymer blend and its nanocomposites with 5wt.% of ZnO and different (1, 2, 3 and 4) wt.% of Ag NPs were synthesized using solution casting method. The results were identified by Fourier transform infrared spectroscopy (FT-IR), X-ray diffraction (XRD), field emission scanning electron microscope (FE-SEM), optical microscope (OM), UV-Visible spectroscopy, A.C electrical properties, and its application as antibacterial activity. FT-IR spectra confirmed of the produce the functional groups present in polymer nanocomposite systems. XRD analysis confirmed the formation nanocomposite films more crystalline from the polymeric matrix. FE-SEM images showed agglomeration of small and close packed group of elliptical particles on the surface of the polymeric matrix as a result of adding different amount of NPs. The optical microscope images denote a good homogeneity and fine distribution of ZnO and Ag NPs, as well as charge transfer and complex formation inside the blend polymer films.

UV-Visible spectroscopy showed that the optimum value of transmittance for polymer blend film is about 98% in the regions Vis and NIR. Reduced the transmittance of the NC films towards ultraviolet rays qualifies it to use as a packaging for storage drugs regardless of cost. indirect allowed and forbidden transition energy gaps were determined from the absorption spectrum, which their values decreased with increasing the Ag NPs content. The A.C electrical properties showed that the dielectric constant and dielectric loss for all films decreases with the increase of the electric field frequency, and that its values increase with the increasing the Ag NPs content.

The antibacterial susceptibility test of synthesized NCs was made by agar disk diffusion method against two isolates of bacteria: gram- negative bacteria *Escherichia coli* and gram-positive bacteria *Staphylococcus aureus*. The results

showed that the NCs films have a high antibacterial activity compared with antibiotic IMIPENEM 10mcg, best growth inhibition zone was observed with ratio 4wt.% of Ag (34.567±3.066) against *E. coli*.

Contents

List of symbols		
Symbol	**Physical Meanings**	**Unites**
A	Absorbance	%
T	Transmittance	%
α	Absorption Coefficient	cm^{-1}
n	Refractive Index	-
k_o	Extinction Coefficient	-
I_o	The Incident Intensity of Light	Lumen
I_T	The Intensity of Ray Transmittance	Lumen
T_g	Glass Transition Temperature	^oC
T_m	Melting Temperature	^oC
r	Exponential Constant	-
H	Planck Constant	J.s
E_{ph}	Energy of Phonon	eV
E	Energy	eV
M_{oc}	Ocular magnification	40x
M_{obj}	Objective magnification	40x
c	Velocity of Light	m/s
R	Reflectance	%
t_o	The thickness of the film	µm
N	Complex Refractive Index	-
ε	Complex Dielectric Constant	-
ε'	Dielectric Constant	-
ε''	Dielectric Loss	F/cm
ε_r	The Real part of the dielectric constant	-
ε_i	The Imaginary part of the dielectric constant	-
σ_{opt}	Optical Conductivity	S^{-1}
D	The Electrical Displacement	C/m^2
δ	Dielectric loss angle	-

E_g^{opt}	Optical energy gap	eV
R_v	Volume Electrical Resistance	Ω
A_a	Area	m^2
ρ_v	Volume Resistivity	Ω .cm
K_B	Boltzmann Constant	JK^{-1}
P	Polarization	C/m^2
N_o	Number of Molecules per a Unit of Volume	-
M_e	Electrical Dipole Moment	C.m
E	Electrical Field Intensity	V/m
E_i	The Internal Field of a Molecule	V/m
ε_o	Vacuum permittivity	F/cm
V_m	Maximum Voltage	V
J	Imaginary Number	-
w	Angular Frequency	$rad.s^{-1}$
C	Capacitance	F
C_o	Capacitance Vacuum	F
C_P	Capacitor Containing an Insulator Material	F
I	Electrical Current	A
I_q	Capacitate Current	A
I_p	Conduction Current	A
R_P	Parallel Resistance	Ω

List of abbreviations	
Abbreviations	Physical Meanings
PVA	Poly (vinyl Alcohol)
PVP	Poly (vinyl pyrrolidone)
Ag	Silver
ZnO	Zinc Oxide
NPs	Nanoparticles
RT	Room temperature
IR	Infrared
MW	Molecular weights
FT-IR	Fourier transform infrared spectroscopy
XRD	The X-Ray diffraction (XRD)
FE-SEM	Field emission scanning electron microscope
OM	Optical microscopy
UV	Ultraviolet spectrum
V.B	Valence band
C.B	Conductive band
A.C	Alternating current
S. aureus	Staphylococcus aureus bacteria
E. coli	Escherichia coli bacteria
SPSS	Statistical package for the social sciences

List of figures

List of Tables

Chapter One

Fundamental Concepts and Literature Review

1.1 Introduction

Polymers have existed in our lives from the beginning of time, and they make up all of life's foundations (building blocks). Until the middle of the twentieth century, humans did not completely know the true nature of polymers. Polymers have infiltrated every aspect of our life. It's difficult to imagine today's society without man-made polymeric materials, with all of its luxury and convenience. Increased understanding of polymer structure property correlations, development of revolutionary polymerization methods, and availability of novel and low-cost monomers have all contributed to the concept of a completely tailor-made polymer becoming a reality in recent years [1]. Each molecule is made up of thousands of atoms joined by covalent chemical bonds, and the polymer is made up of enormous organic molecules (Large molecules) of repeating tiny structural units (monomers) united in a process called polymerization. Molecules in a polymer are attracted to one another by forces that vary depending on the polymer type [2].

The polymers are classified into three categories: natural, industrial and modified. Proteins, cellulose, starches, and rubber are examples of natural polymers; industrial polymers include poly (vinyl chloride), polyvinyl alcohol, nylons polyethylene, polypropylene, polyesters polycarbonate, …. etc. [3].

Today, their remarkable combination of properties, low weight and processability is responsible for the vast use of polymer materials. The polymer matrix and shaped polymer matrix composite were supplied with a large number of additives. The combination of two or more substances with various physical and chemical properties and distinct interface are known as a composite. Composite

products have a wide range of uses. In recent years, it has been discovered that adding nanoparticles to polymers causes significant changes in the polymer's structural, optical, and electrical characteristics [4]. Because of it is unique characteristics such as environmental friendliness, nontoxicity, water solubility, biodegradability, outstanding electrical and optical properties, chemical stability, excellent dielectric strength, and charge storage capacity.

polyvinyl alcohol (PVA) is classified as a basic polymer. PVA has a hydroxyl group that, through hydrogen bonding, can aid in the formation of an interpenetrating link in a polymer composite [5,6].

polyvinyl pyrrolidone (PVP) is a water soluble, biodegradable polymer with good features. Low toxicity, a high dielectric constant, and compatibility are just some of the benefits. Hydrogen bonds form when the hydroxyl group of PVA and the carbonyl group of PVP come together, resulting in contact. When polymers are combined with nanofillers, the fillers in the polymers are distributed uniformly [7, 8].

Several researchers have recently investigated PVA –PVP polymer mixes with different nanofillers. Wound dressings, articular cartilage replacements, and membranes for high-energy electrochemical devices all employ PVA –PVP mixes [5-7].

The word "nanotechnology" refers to the application of small quantities of material to processes such material separation, consolidation, and deformation by a single atom or molecule [9]. Polymer nanocomposite is a multicomponent system that contains minor elements (fillers) with a size of less than 100 nm in at least one dimension [10].

As a new generation of antimicrobial agent, nano metal oxides have been shown to have antibacterial properties, and researchers have advised employing

silver and zinc ions as excellent disinfectants against hospital pathogenic microorganisms [11]. Although scientists previously assumed that leftover metal ions may harm human health, tests revealed that the hazardous nature of ZnO NPs to different bacterial systems and human T cells is selective [12]. These findings showed that ZnO nanoparticles might be effective as antibacterial nanomedicine agents in specific therapeutic dosage regimes [11]. The current work deals with the synthesis of nanocomposites (PVA-PVP/ ZnO and Ag) and the study of their structural and optical properties for antibacterial applications.

1.2 Polymer Blend

Physical mixing of two or more distinct polymers without any chemical contact is referred to as a polymer blend. Both crystalline and amorphous polymers are used in the polymer mixes. Combining two or more polymer types is a useful technique for fabricating and producing materials with improved characteristics. Blending is regarded as one of the most important topics in polymer research and development for numerous reasons, one of which is that polymer blends provide a quick and inexpensive technique to produce novel polymeric materials. These materials have a variety of characteristics that are dependent on the qualities of their constituents. Also, polymer blends have a wide range of industrial uses due to improved attributes and cost savings. Compatibility, miscibility, and morphology are the three most important criteria that heavily influence the performance of polymer blends [13]. Polymer blends are created using five different processes: Melt blending, solution blending, latex blending, partial block or graft copolymerization, and the development of an interpenetrating polymer network are all examples of polymerization processes. Figure (1.1) shows illustrative image for preparation of polymer blend [14].

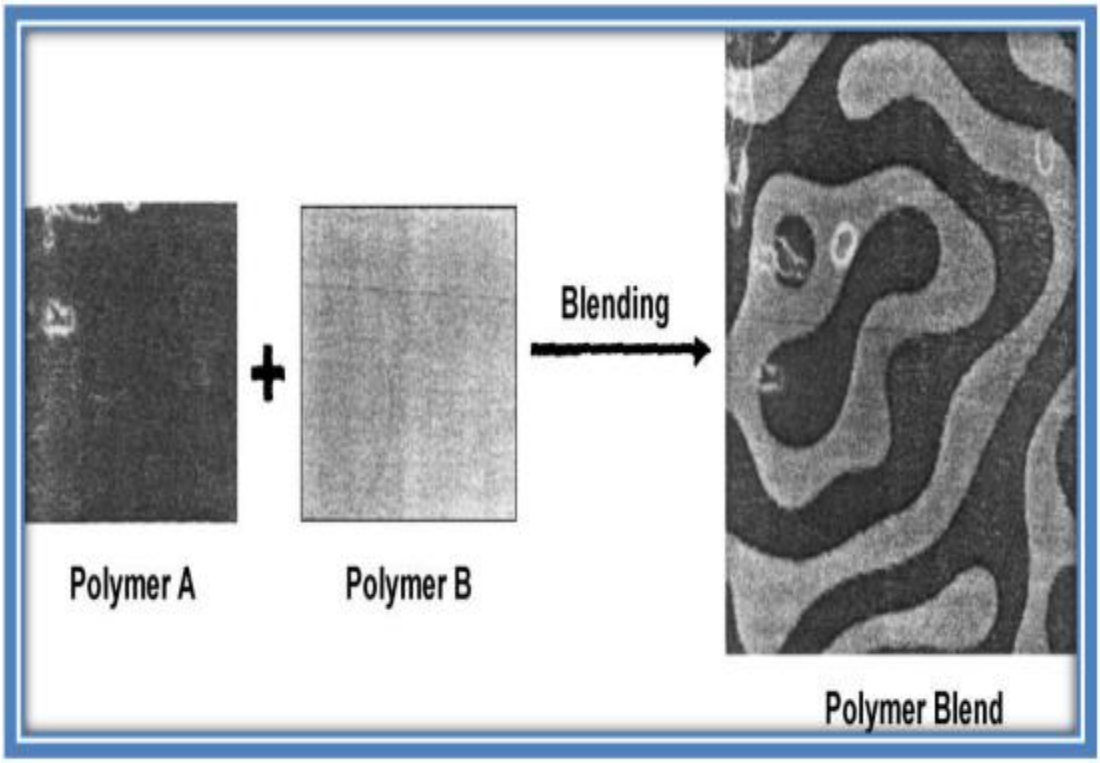

Fig. (1.1): Illustrative image for preparation of polymer blend [14]**.**

1.3 Nanomaterials

Nanomaterials research is a branch of materials science that focuses on nanotechnology. One billionth of a meter is a nanometer (nm). Nanomaterials are materials with a single unit ranging from (1-100) nanometers in size. Due to their size, form, and chemical composition, these materials frequently exhibit unique features [15]. One–dimensional nanomaterials e.g., surface films, two –dimensional nanomaterials e.g., strands or fibers, and three –dimensional nanomaterials are all possible e.g. particles. They can be solitary, fused, aggregated, or agglomerated and appear in spherical, tubular, and irregular forms. Nanomaterials include nanotubes, quantum dots, and fullerenes [16].

1.4 Polymer Nanocomposites

Polymer nanocomposite (PNCs) are defined as a type of material with unique properties. A polymer nanocomposite (PNCs) is a polymer or copolymer containing nanoparticles or nanofillers distributed throughout the polymer matrix. Inorganic particles are disseminated in an organic polymer matrix in at least one dimension to improve the quality attributes of the material [17]. PNCs are a modern kind of polymer that can be used instead of traditional filled polymers. Nanocomposites' filler dispersion increases their properties significantly when compared to pure polymers, are among these properties Increased tensile strength, conductivity, and thermal stability, in addition to reduced flammability. Nanoparticles added to polymer composites also resulted in a new line of composite materials with improved and unique properties. Platelets, fibers, and spheroids are examples of these [18,19].

1.5 Literature Review

Söderberg *et al.* in (1990) [20]**,** studied the antibacterial activity; Muller Hinton agar dilution assays were used to evaluate the minimum inhibitory concentrations (MIC) of zinc oxide for a variety of clinical isolates. Gram positive bacteria were found to be the most susceptible, according to the research. Even at the highest quantities tested (1024 pg/mL), gram negative aerobic bacteria and streptococci were seldom inhibited.

Feng *et al.* in (1998) [21]**,** studied the ion beam assisted deposition (IBAD) has been successfully used to produce a dense ultra-adherent and pinhole-free hydroxyapatite (HAp) layer on alumina substrates. After deposition the HAp-coated alumina was immersed in 20 ppm and 100 ppm $AgNO_3$ solution to carry out the ion exchange

between Ag^{+} and Ca^{2+} in HAp. An obvious antimicrobial effect against *Escherichia coli*, *Pseudomonas aeruginosa*, *Staphylococcus aureus* and *Staphylococcus epidermidis* was observed in the samples treated with 20 ppm $AgNO_3$ solution. In contrast to this, the untreated samples did not show any bactericidal effect. Scanning electron microscopy (SEM) studies showed that Ag-rich phases were homogeneously distributed on the surface. X-ray diffraction (XRD) demonstrated that the surface structure in the samples without Ag was HAp, whereas with Ag it is HAp and AgCaP. The minimum inhibitory concentration of $AgNO_3$ was measured to be 1.302 μg/ml. The release of Ag^{+} ions from the Ag-HAp films in simulated body fluid (SBF) solution was determined by atomic absorption spectroscopy.

Feng *et al.* in (2003) [22]**,** studied the resistivity and breakdown voltage of Ag – PVA nanocomposites , and it was discovered that the composite containing (20–30) nm Ag particles outperformed the matrix.

Kim *et al.* in (2007) [23]**,** studied the Ag ions or salts have long been studied for their antibacterial properties. The shape and size distribution of stable Ag nanoparticles were studied using a particle characterizer and transmission electron microscopy. Yeast, *E. coli*, and Staphylococcus aureus were used to test the antibacterial efficacy of Ag nanoparticles. Using Muller Hinton agar plates, Ag nanoparticles of varied concentrations were introduced to liquid systems in these assays. As a result, yeast and *E. coli* were reduced at low concentrations of Ag nanoparticles, however the growth inhibitory effects on S. aureus were minor. The effect of Ag NPs on microbial growth inhibition owing to free radical generation was investigated using electron spin resonance spectroscopy. Ag NPs may be effective as growth agents, according to these observations.

Al-Ramadhan *et al*. in (2016) [24]**,** studied the optical properties of (PVA-PVP/Ag) nanocomposites prepared by casting method using UV Vis spectroscopy at a wavelength (200-900) nm. The values of the energy gap of indirect transition (allowed and forbidden) decreased as nanoparticle concentration increased, refractive index increased as Ag amount increased, OM results showed homogeneous distribution, very smooth surface, and small roughness.

Ramesan *et al*. in (2018) [25]**,** prepared the nanocomposites of poly (vinyl alcohol) - poly (vinyl pyrrolidone) / silver-doped zinc oxide (Ag-doped ZnO), structural properties were checked by FT-IR spectroscopy. SEM, XRD, and optical properties (UV) and conductivity tests were used to evaluate the ternary mixes. The intermolecular interaction between the polar component of the mix and the metal oxide nanoparticles was shown by the FT-IR and UV spectra. The structurally ordered arrangements of nanoparticles inside the polymer matrix were determined using SEM and XRD patterns. The electrical characteristics of the composites, such as AC conductivity and dielectric properties, were shown to rise with an increase in nanoparticle content up to a particular concentration (5 wt. percent), after which the value decreased.

Teodorescu *et al.* in (2019) [26]**,** studied the (PVA) and sparked substantial scientific interest and is acknowledged as one of the most widely manufactured synthetic polymers in the world, having been produced for almost a century. This is owing to its extraordinary qualities, which have necessitated its widespread usage in a range of applications, particularly in the medical and pharmaceutical areas. However, research have indicated that PVA-based biomaterials have several constraints that can limit their usage or performance. To address these limitations, a variety of approaches have been described, one of which is blending with PVP. As

a result, our goal was to provide a thorough assessment of the present status of biomaterial synthesis, characteristics, and applications based on the synergistic impact of PVA and PVP combinations. Future biomaterials research was discussed, with PVA and PVP showcasing the exciting possibilities they may give.

Ismail *et al*. in (2019) [27]**,** studied Polyvinyl alcohol and polyvinyl pyrrolidone (PVA and PVP) films doped with lithium ions. Absorbance A and absorption index (α) were found to be higher in the findings. Optical band gap (E_g^{opt}) of the composites was significantly reduced by adding $Li_2\ SO_4$ from 2.98 to 2.196 eV. The effect of photon energy hv on the real dielectric constant ε_1, imaginary dielectric constant ε_2, and optical conductivity (σ_{opt}) was also investigated. The existence of charge transfer complexes in the host polymer as a result of the addition of modest quantities of Li ions is referred to as the indirect optical gap of the doped mix.

Panchal *et al.* in (2020) [28], studied the zinc oxide NPs and Ag/ZnO NCs with different Ag metal concentrations (0.5 wt. percent, 1wt. percent and 2wt. percent). The structural, optical, and electrical features of green generated NPs and NCs were monitored using several analytical techniques including as XRD, SEM, UV-Vis, and FT-IR. Antibacterial and dye degradation activities of green generated pure ZnO-NPs, as well as 0.5 wt. percent, 1wt. percent, and 2wt.% Ag- ZnO NCs, were examined. When compared ZnO NPs with other manufactured Ag-ZnO NCs, the results revealed that synthesized 1wt. percent Ag-ZnO NCs had significant photocatalytic and antibacterial activities.

Jassim and Hashim in (2021) [29]**,** studied the constant ZnO and varied ratios of Co_3O_4 NPs films made using the solution cast process, the polymer blend (PVA-PEG) and its nanocomposites. SEM, FT-IR, and XRD were employed to identify the products. In order to evaluate optical characteristics, UV-visible spectroscopy was

performed. According to the experimental findings, the FT-IR spectra of the generate the functional groups in polymer nanocomposite systems. XRD measurements indicated the emergence of more crystalline nanocomposite films from the polymeric matrix. SEM demonstrated a significant dispersion of ZnO and Co_3O_4 NPs on the surface of the polymeric matrix. According to the A.C electrical properties, the dielectric constant and dielectric loss for all films decrease with increasing electric field frequency, and their values grow with increasing wt. percent of Co_3O_4NPs.

1.6 The Aim of the Study

It is very important to apply various additives such as nanoparticles to polymers, due to the wide uses of polymers in various branches of industries in order to meet the increasing needs and requirements of these applications. Therefore, in this study we worked on synthesizing (PVA-PVP/ ZnO and Ag) nanocomposite films and studying the effect of NC on structural, optical, electrical properties and application it in the field of antibacterial.

Chapter Two

Theoretical Part

2.1 Introduction

This chapter gives a basic overview of the study's theoretical component, as well as physical concepts, scientific classifications, correlations, and laws that were utilized to explain the findings.

2.1.1 Polymer Classification Based on Structure

There are different kinds of polymers categorized according to their structure and as follows [30]:

A. Linear Polymers

Single molecular is the basic structural unit for polymers in a series of certain lengths that are connected in a linear form. Linear polymers may include totals twisted that are part of monomer but without any branch. As shown in figure (2.1 A).

B. Branched Polymers

This type of polymers consists of several branches that could be a Ladder and Comb or Crusader, which is usually present with different lengths. As seen in the figure (2.1 B).

C. Cross linked Polymers

This kind of polymers consists of chains from three dimensional linked together in more than one site and monomers bonding in effective totals that are chemical bonds. As shown in figure (2.1 C).

D – Network Polymers

Three-dimensional (3D) networks e.g., epoxies and phenol-formaldehyde. As shown in figure (2.1 D).

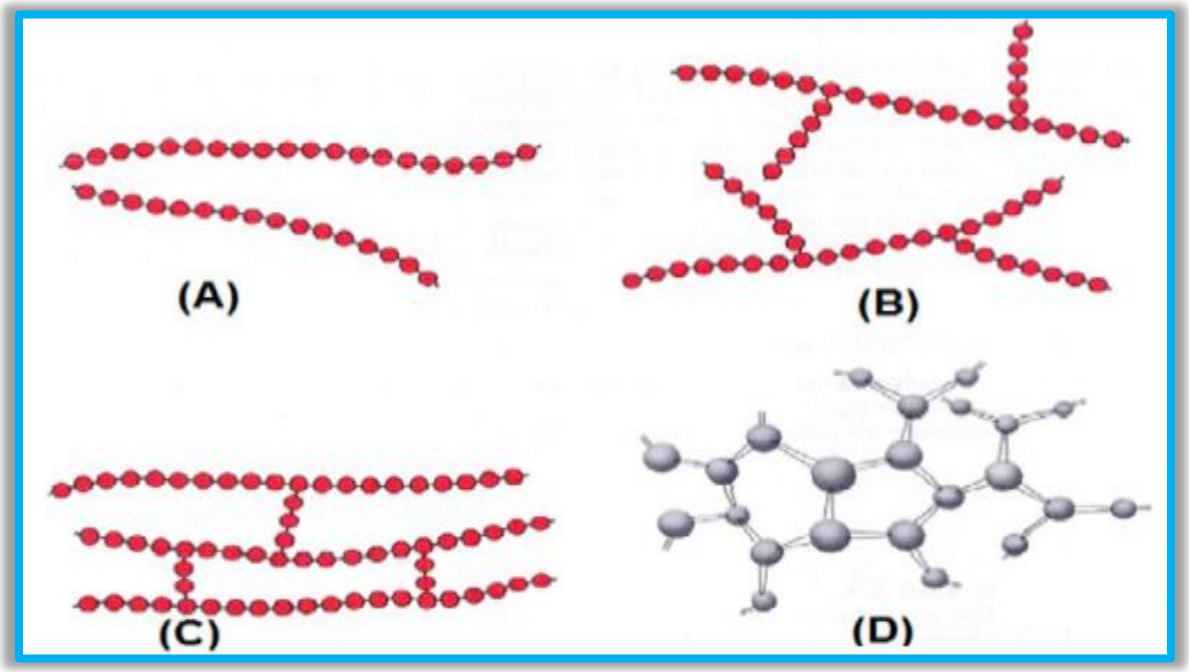

Fig. (2.1): Polymeric chains come in several forms: A. Linear ,B. Branched ,C. Cross-linked and D. Network [31].

2.1.2 Classification of Polymers Dependent on Homogeneity

Polymers are divided into three categories based on the homogeneity of repeating units:

A. Homopolymers:

Materials made from one monomer are termed homopolymers [32].

B. Copolymers:

If their materials are made from more than one type of monomer, they are termed copolymers [32].

C. Composite Polymers:

It is the process of adding material to homogenous polymers in order to modify some of their properties and the application of new recipes to them [33].

2.2 The Materials Used in the Study

2.2.1 Polyvinyl Alcohol (PVA)

PVA is one among the most well-known and oldest polymers., with partially hydrolysis and has the formula $(C_2H_4O)_n$, as shown in figure (2.2), currently used extensively in semiconductors applications [34].

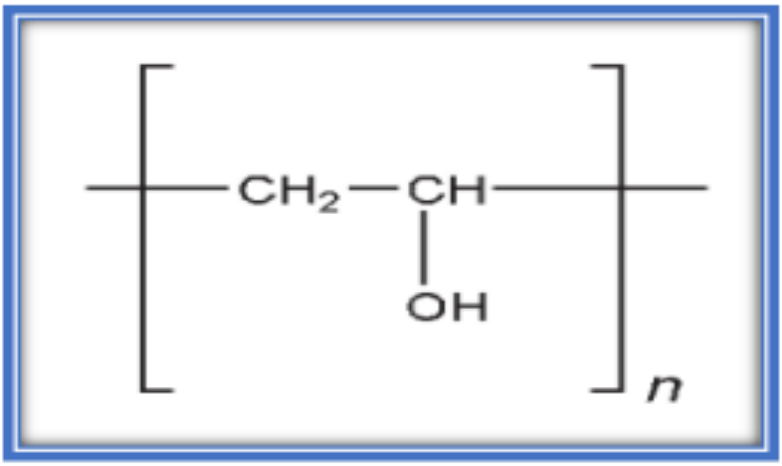

Fig. (2.2): The chemical structure of PVA [34].

PVA is an odorless, transparent, tasteless, and white or cream-colored water-soluble synthetic polymer that comes in the form of a granular powder [35]. PVA has the benefit of being able to mix with water, as well as being resistant to solvents, oils, and having outstanding adhesion to cellulosic materials. PVA's melting point is 230 ^oC for fully hydrolyzed grades, and (180 -190) ^oC for partially hydrolyzed grades. As a result, it is widely used in the paper and textile industries to make oxygen-resistant membranes for photographic film coating [36].

PVA possesses special properties, outstanding chemical stability, environmentally friendly, optical and electrical characteristics. The semi-crystalline existence – amorphous as well as crystalline regions, which cause interfacial effects that increase the physical properties – is important in polyvinyl

alcohol [37]. The key PVA physical and chemical properties are described in Table (2.1) [38].

2.2.2 Polyvinyl pyrrolidone (PVP)

Polyvinyl pyrrolidone (PVP), commonly called polyvidone or povidone, is a water-soluble polymer and other polar solvents [39]. PVP is a biocompatible, hemocompatible synthetic polymer that has been used as a biomaterial for many years. PVP is notable for its ability to interact with a wide range of hydrophilic and hydrophobic materials, and its pyrrolidone structure gives it capabilities comparable to those of a protein. This substance has a low immunogenicity, antigenicity, and toxicity. PVP has the formula $(C_6H_9NO)_n$, as shown in figure (2.3) [40].

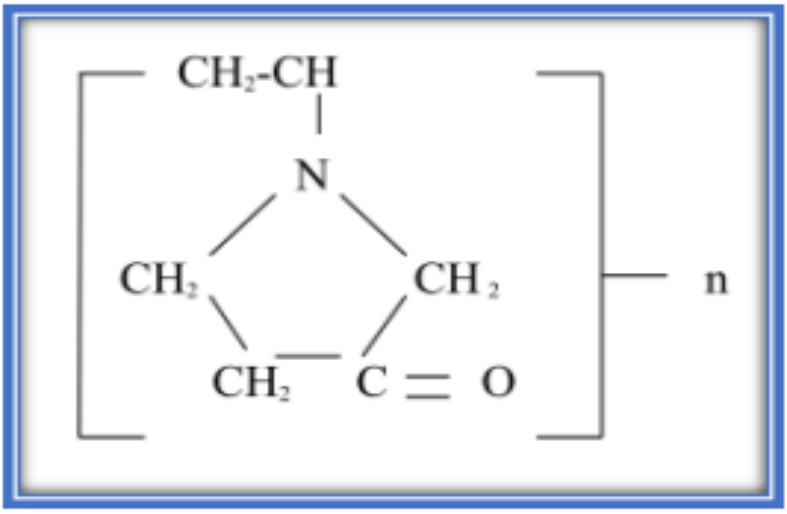

Fig. (2.3): The chemical structure of PVP [40].

PVP is amorphous and possesses an elevated glass transition temperature (T_g) due to the presence of the rigid pyrrolidone group, which is known to form various complexes with inorganic salts [41], as shown in Table (2.1).

Table (2.1) : Some physical and chemical properties of Polyvinyl alcohol (PVA) and polyvinyl Pyrrolidone (PVP) [38,41].

Properties	PVA	PVP
Appearance	White – to cream granule powder	White to creamy- white
Molecular formula	$(C_2H_4O)_n$	$(C_6H_9NO)_n$
Density g /cm^3	1.19 - 1.31	1.25
Solution pH	5-7	3-7
Refractive index	1.55	1.53
Glass transition temperature (T_g) ˚C	75 - 85	109
Melting temperature (T_m) ˚C	180 - 190	150-180

2.2.3 Silver (Ag)

Noble metal nanoparticles have lately become the subject of investigation because to their unique characteristics, which differ from those of bulk materials. The size, shape, and changes in the surroundings of nanoparticles all influence these qualities [42]. Silver nanoparticles have unique properties (optical, electrical, and magnetic qualities that are affected by size and form) that can be utilized as an antibacterial agent, biosensor materials, composite fibers, superconducting materials that can be used at a cryogenic temperature, cosmetics, and electronic components, which have piqued the interest of researchers. Ag NPs have been produced and stabilized using a variety of physical and chemical processes [43]. Physical and chemical characteristics of silver nanoparticles are described in Table (2.2) [44].

Table (2.2): The physical and chemical properties of silver nanoparticles [44].

Properties	Silver (Ag)
Atomic number	47
Mass number	107.86
Electronic configuration	$4d^{10}\ 5s^{1}$
Structure	FCC
Lattice constant (nm)	0.409
Density ($g.cm^{-3}$)	10.5
Melting temperature ^{o}C	961.8
Boiling temperature ^{o}C	2212
Electrical conductivity $(\Omega.cm)^{-1}$	6.30×10^{5}

2.2.4 Zinc Oxide

ZnO is a semiconductor material that belongs to the category of transparent oxides with great visual transparency, efficient UV absorbance with a broad band gap 3.37 eV, substantial binding energy of exciton (60 meV), and chemical stability (even under ambient conditions like sunlight, water and air) [45]. ZnO may be employed in bio-applications since it is non-toxic and ecologically friendly. It's a low-cost ingredient in conductive glass, white paint, and commercial sunscreens [46]. ZnO has a high cohesive energy of 1.89 eV, making it one of the most stable and radiation resistant materials in the direct band gap semiconductor family, ensuring extended life and a high degradation threshold for ZnO-based optoelectronic devices [47]. ZnO material is used as a liquid or cream to beautify the

skin or hair, and is used as a pomade in medical healing [48].There are a few simple physical parameters mentioned in Table (2.3) [49].

Table (2.3): Different properties of ZnO [49].

Parameters	Values
The lattice constants (at 300 K)	a = 0.32495 nm
	c = 0.52069nm
Dielectric constant of static	8.656
Refractive index (n)	2.008 ,2.029
Thermal conductivity	0.6 – 1.16 W/Km
Specific heat	0.125 cal/g K
Thermal constant at 573K	1200m V/K
Electron mobility	~210 cm^2 /V. s
melting point	2247 K
Molecular weight	81.406 g mol^{-1}
density	5.606 g/cm^3

2.3 Measurements of Structural Properties

2.3.1 Optical microscope (OM)

A compound optical microscope is an optical tool that magnifies an object (or specimen) and projects it onto the retina of the eye or onto an imaging device using visible light. The term "compound" refers to how two lenses, the objective lens and the eyepiece (or ocular), work together to generate the image's final magnification.

$$M_{final} = M_{obj} \times M_{oc}$$

Where: M_{obj} is objective magnification, M_{oc} is ocular magnification.

Both diffracted (rays that interact with the specimen) and non-diffracted (rays that pass through the specimen without deviating) rays are gathered by the objective lens in most kinds of transmitted light microscopy and contribute to picture generation [50].

2.3.2 Fourier Transforms Infrared (FT-IR)

Chemical analytical spectroscopy is Fourier Transforms Infrared (FT-IR). It tests the sensitivity of infrared with the amount of light waves. The wavenumbers consist of infrared light classified into three zones, far-infrared, mid-infrared and near-infrared, ranging from (4 ~ 400) cm^{-1}, (400 ~ 4000) cm^{-1} and (4000 ~ 14000) cm^{-1}, respectively. The allowable use of this technology depends on detecting the vibration of the chemical functional group in a sample. Where, as the contact takes place between the infrared light and the substance, the chemical bonds will stretch. Here, independent of the rest of the molecule composition, the infrared radiation is captured by the chemical functional group at a particular wavenumber range, More complex molecules contain more than one bond [51].

The idea behind this method is that chemical bonds vibrate at various frequencies. FT-IR spectroscopy is a powerful tool for identifying different types of chemical bonds in a molecule by creating a molecular "fingerprint" in the form of an infrared absorption spectrum. Molecular bonds vibrate at different frequencies depending on the components and the type of interaction. FT-IR may be used to identify unknown compounds, detect organic and inorganic additives at low levels, and analyze chemical structure change and solvent residue since it can reveal information about a material's chemical bonding or molecular structure without damaging [52].

2.3.3 The X-Ray diffraction

It is possible to apply XRD to investigate the crystallization process, unit cell lattice parameter detail, crystal structure, crystal orientation, and crystallite size, which is a fast and effective approach. The constructive interference of a monochromatic beam of X-rays is used to produce the XRD peaks after scattered of

each set of lattice planes in the sample at specific angles, where the distribution of the atoms determines the peak intensities within lattice. Therefore, The periodic atomic fingerprint of materials is represented by XRD pattern [53].

The sample holder, X-ray tube, and X-ray detector are the three basic components of an X-ray diffractometer. The cathode ray tube is responsible for creating X-rays by burning the filament to create electrons, which are subsequently driven toward a target by a voltage and attack the target substance. When electrons with sufficient energy displace inner shell electrons of the target material, X-ray spectra are produced [54].

When X-ray light of wavelength (λ) is projected at an angle (θ) onto a crystal lattice, the incoming X-rays interact constructively with the sample if the circumstances meet Bragg's law, as shown in figure (2.4) [55]:

$$2d_{hkl}\sin\theta = n\,\lambda \qquad (2.1)$$

Where: $d_{hkl} = \frac{d}{n}$, θ: is Bragg diffraction angle (degree) and λ is wavelength for incident X-ray beam (Å).

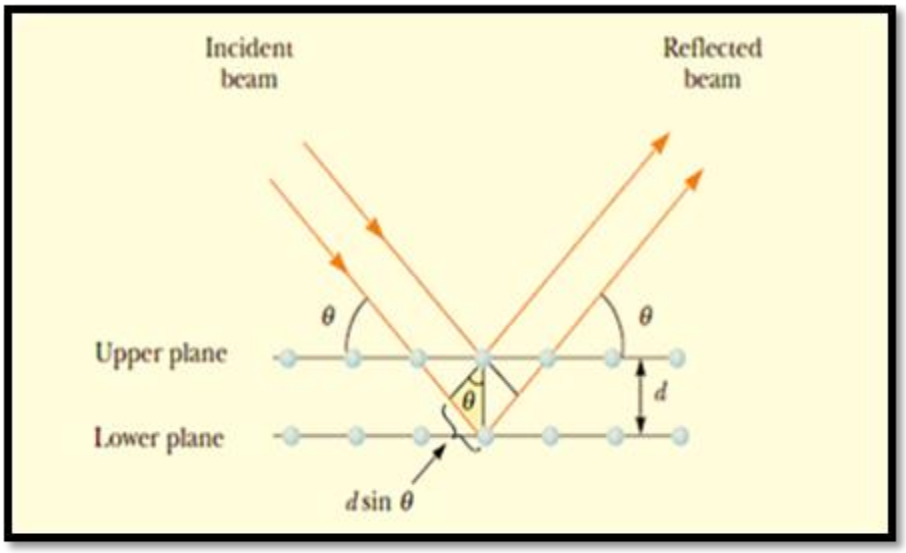

Fig. (2.4): Bragg's Diffraction [55].

The structural factors of any material are determined by X-ray diffraction, which is crucial in explaining many of the material's physical properties. In the case of the cubic structure, which represents the dominant pattern of the structure (Ag), (a, b, c) represent the lattice constants, and thus it is calculated using the equation [56]:

$$a = d_{hkl}\sqrt{h^2 + k^2 + l^2} \qquad (2.2)$$

where (h, k, l) represents Miller's coefficients.

In the case of the hexagonal structure, which is the dominant pattern in the composition of (ZnO), the lattice constant can be extracted from the following equation [57]:

$$\frac{1}{d_{hkl}^2} = \frac{4}{3}\left(\frac{h^2+hk+k^2}{a^2}\right) + \frac{l^2}{c^2} \qquad (2.3)$$

2.3.4 Field Emission Scanning Electron Microscope (FE-SEM)

Field emission scanning electron microscope (FE-SEM) is a type of electron microscope that uses light to produce images. Light is replaced by electrons in a

FESEM microscope (negatively charged particles). A field emission source is used to free the electrons. In a zigzag pattern, electrons scan the item [58].

2.4 The Optical Properties

The optical characteristics of polymer composites are being investigated in order to better understand the kind of internal structure of polymer and the nature of bonds; as well as to expand the spectrum of polymer applications.

Knowing a polymer composite's absorption and transmittance spectrums can help detect a variety of optical qualities over a wide range of wavelengths. We can determine the type of bonds, orbits, and energy beams by examining them in the ultraviolet spectrum. The visible spectrum research gives enough knowledge about a matter's behavior for solar applications. The infrared spectrum is crucial for understanding the overall structure of polymer composites and the constituents that make up their chemical composition [59].

2.4.1 Absorbance (A)

In order to get good absorption, the optical depth should be high for energies above the band gap, and reflectivity should be small. Absorbance is defined as the ratio of absorbed light intensity (I_A) to incident light intensity (I_o) depending on the kind of material [60]:

$$A = I_A / I_0 \qquad (2.4)$$

2.4.2 Transmittance (T):

The formula for calculating transmittance (T) is to divide the intensity of rays transmitting from the film (I_T) by the intensity of incoming rays on it (I_o) [61]:

$$T = I_T / I_0 \qquad (2.5)$$

2.4.3 Absorption coefficient (α):

The absorption coefficient is the decrease in energy in the flow of incident ray in the direction of wave propagation in relation to the distance unit. (α) depends on the photon energy (hυ), material characteristics, and forbidden band gap. Photon energy is taken from the following equation [62]:

$$E = h\nu \quad (2.6)$$

The frequency is (ν), while the Planck constant is (h).

The photon will be transmitted if the incident photon energy is smaller than the forbidden band gap, and transmittance is given by the equation:

$$T = (1-R)^2 . e^{-\alpha t} \quad (2.7)$$

Where: T transmittance, R: is the reflectance, $\boldsymbol{a}$ means the absorption coefficient. If it is assumed that the thickness of the films (dt), the intensity of incident photons is expected to be (dI) in direct proportion to both intensity (I) and thickness dt, i.e. [63]:

$$dI = -\alpha I\, dt \quad (2.8)$$

If the incidence ray's intensity (I_o) is incident on a material with thickness (t_t) and transmittance ray's intensity (I_T), we get:

$$\int_{I_\circ}^{I_T} \frac{dI}{I} = \int_0^{t_t} -\alpha dt \quad (2.9)$$

$$\ln I_T - \ln I_0 = -\alpha t_t \quad (2.10)$$

$$\frac{I_T}{I_\circ} = e^{-\alpha t_t} \quad (2.11)$$

$$T = e^{-\alpha t_t} \quad (2.12)$$

$$\frac{1}{T} = e^{\alpha t_t} \quad (2.13)$$

$$2.303 \log(\frac{1}{T}) = \alpha t_t \quad (2.14)$$

$$A = \log\left(\frac{1}{T}\right) \quad (2.15)$$

$$2.303 \times A = \alpha t_t \quad (2.16)$$

$$\alpha = \frac{2.303 \times A}{t_t} \quad (2.17)$$

2.4.4 The fundamental absorption edge

The basic absorption edge is a sudden increase in absorbance that occurs when the amount of absorbed energy radiation is about equal to the band energy gap; As a result, the basic absorption edge shows the energy differential between the up point of the valance band and the bottom point of the conduction band. Figure (2.5) shows three types of absorption zones [64].

A. High absorption region

Magnitude (α) in the part A is greater than or equal to $10^4 cm^{-1}$. The magnitude of the prohibited optical band gap (E_g^{opt}) can be introduced from this area.

B. Exponential region

The value of (α) in component B is in the range $1\ cm^{-1} < \alpha < 10^4\ cm^{-1}$. It refers to the transition from extended levels at the top of the valence band to localized levels in the conductive band and vice versa, from local levels in (V.B.) to extended levels at the bottom of the conductive band and vice versa (C.B).

C. Low absorption region

Value of (α) in component C is relatively tiny. it's around $\alpha < 1 cm^{-1}$. The transition happens in this area as a result of structural faults causing state density inside space motion [65].

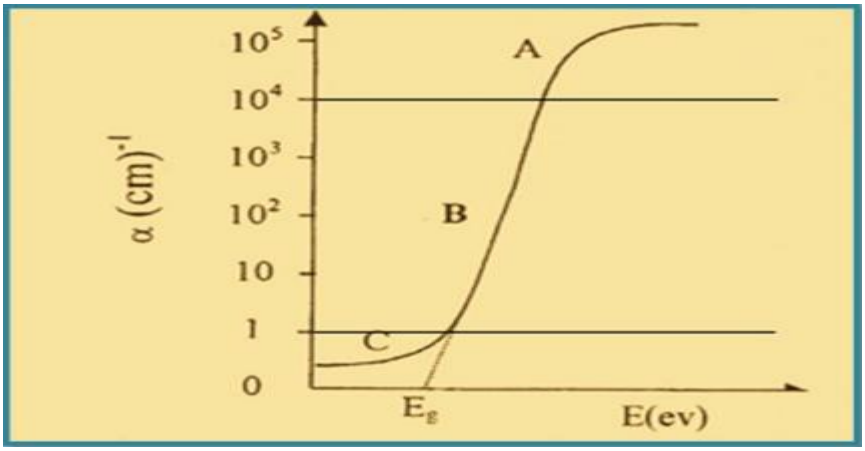

Fig. (2.5): Absorption edge variation with absorption regions [65].

2.4.5 The electronic transitions

Electronic transitions are divided into two categories:

2.4.5.1 Direct transition

When bottom of conductive band is exactly above the top of valence band in semiconductors, this transition happens, implying their wave vector K is the same, i.e., ΔK=0. The absorption appeared in this stage when hυ ≥ Eg. This form of transition is necessitated by the Law of Conservation of Energy and Momentum, which has two kinds [65]:

a. Direct allowed transition

As seen in figure (2.6.a), the transition occurs among top and bottom points of (V.B.) and (C.B.).

b. Directly forbidden transitions

As indicated in figure (2.6.b), this transition occurs towards the top (V.B.) and bottom (C.B.) points. The optical band gap energies were calculated using a Tauc diagram and the equation below [66]:

$$\alpha h\nu = B\,(h\nu - E_g^{opt})^{\,r} \qquad (2.18)$$

Depending on the kind of material, (B) is constant, and (ν) is the frequency of the incoming photon. The index r identifies the type of electronic transition between the energy bands; the values r of 1/2 and 3/2 are associated with the allowed and forbidden – direct transition.

2.4.5.2 The indirect transitions

Conduction band (C.B) does not have a bottom that is higher than the top of valence band (V.B) in an indirect band gap, in other words, the maximum of the V.B is found at different k-vectors than the minimum of the C.B. In this case, ($\Delta K \neq 0$), and this transition type must include the absorption or emission of a phonon, for the energy and momentum conservation laws Indirect transitions are divided into two categories [67]:

a. allowed indirect transitions

As illustrated in figure (2.6.c), these transitions occur between the highest point of the efficiency band and the lowest point of the conduction band in a distinct area of K–space.

b. Forbidden indirect transitions

As illustrated in figure (2.6.d), these transitions happen between the near points at the top of the valence band and the near points at the bottom of the conduction band, these transitions happened. To travel in the direction of phonon absorption, the absorption coefficient is given by [62]:

$$\alpha h\nu = B\,(h\nu - E_g^{opt} \pm E_{ph})^{r} \qquad (2.19)$$

where E_{ph} denotes phonon energy, (-) denotes phonon absorption, (+) denotes phonon emission, r denotes the exponential m transition, and $r = 2$ denotes permitted indirect transition while $r = 3$ indicates a forbidden indirect transfer.

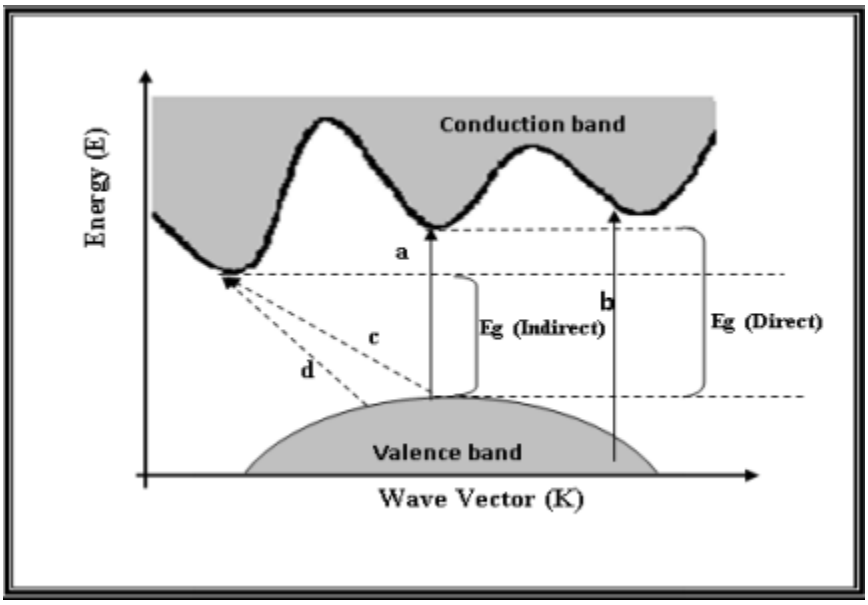

Fig.(2.6): Types of electronic transitions [62].

2.4.6 Refractive index

By dividing the speed of light in vacuum by the speed in light inside the material, the refractive index is computed. The following formulae are used to calculate the film's refractive index (n):[68]:

$$n = \frac{1+R}{1-R} + \left[\frac{4R}{1-R^2} - k_{\circ}^2\right]^{1/2} \qquad (2.20)$$

The reflectance R of the material with Transmittance (T) and Absorbance (A) is given by the relation [57]:

$$R = 1 - [Te^{A}]^{2} \qquad (2.21)$$

Depending on the refractive index, it can be determined the polarizability (P) by the relation [57]:

$$P = \frac{3}{4\pi}\left(\frac{n^2-1}{n^2+1}\right) \quad (2.22)$$

2.4.7 Extinction coefficient (k_o)

As seen in the equation below, the extinction coefficient is defined as the imaginary component of the complex refractive index N:

$$N = n - ik_o \quad (2.23)$$

Extinction coefficient could be found using the relation [69]:

$$k_o = \alpha\lambda/4\pi \quad (2.24)$$

where (λ) is the incident ray's wavelength.

2.4.8 Dielectric constant (ε)

At optical frequencies represented by light waves, the dielectric constant demonstrates matter's capacity to polarize; it may respond to numerous frequencies in a very difficult way, and electronic polarity dominates other forms of polarization. The real and imaginary dielectric constants may be computed using the equation below [70]:

$$\varepsilon = \varepsilon_r - i\varepsilon_i \quad (2.25)$$

where (εr, εi) are the dielectric constant's real and imaginary components. The n and k numbers are proportional to the real and imaginary components of the dielectric constant [70].

$$\varepsilon = N^2 \quad (2.26)$$

$$(n - I\,k)^2 = \varepsilon_r - i\varepsilon_i \quad (2.27)$$

From equation (2.25) the dielectric constant's real and imaginary can be written as following [71]:

$\varepsilon_r = (n^2 - k^2)$ (2.28)

$\varepsilon_i = (2nk)$ (2.29)

2.4.9 Optical conductivity

The optical conductivity (σ_{op}) depends directly on the refractive index (n) and absorption coefficient (α) by the following relation [72]:

$\sigma_{op} = \alpha\, n\, c/4\pi$ (2.30)

c is the velocity of light, α is the absorption coefficient.

2.5 Electrical Properties

The electrical properties of the material depend on the chemical composition, the arrangement of atoms in the solid and the presence of defects in the energy gap. In several ways, such as the annealing, this defect can be reduced. The electrical properties are also highly dependent on the preparation technique and the deposition conditions [73].

Matter can be classified according to its electrical conductivity into insulators, semiconductors and conductors. Conductivities for some polymers are (~ 10^{-17} Ω^{-1} cm^{-1}) for polyethylene, (10^{-16} Ω^{-1} cm^{-1}) for polystyrene and (10^{-12} Ω^{-1} cm^{-1}) for polyamides. The electrical properties are designed to understand the number, origins, and actions of a charge. This includes the exact composition of the substance, the chemical composition, and the shape of the substance [74].

2.6 A.C electrical Conductivity

A.C conductivity differs from D.C conductivity in that the electric field frequency during D.C conductivity is constant, but the electric field frequency during A.C conductivity is variable. When an insulator is placed in a low –frequency

electric field, the newly created or permanent dipoles can follow the change of the applied electric field without leaving any residue, so the value of the dielectric constant becomes equal (ohmic conductivity is equal to zero). At the other side, in more calculations, the frequency of the electric field is determined by the frequency of electric polarization; complex dielectric constants would be available [75].

The dielectric constant is the ratio of a capacitor's capacitance with an insulator material between its conducting plates to a capacitor's capacitance with a vacuum between the plates of the same size [30].

When an alternating potential $V = V_m e^{jwt}$, is applied across a capacitor c filled with an insulator, the current passing through the capacitor precedes the potential by a phase of $\pi/2$ as in figure (2.7 A) [30]:

$$I = jwCV \qquad (2.31)$$

where w is the applied field's angular frequency ($w = 2\pi f$), j is an imaginary integer ($j = \sqrt{-1}$), and Vm is the voltage maximum.

This demonstrates that the electrical current is equal to the current's amount Ip in the same phase with V and Iq with a phase difference $\pi/2$, that is [76]:

$$I = I_p + jI_q \qquad (2.32)$$

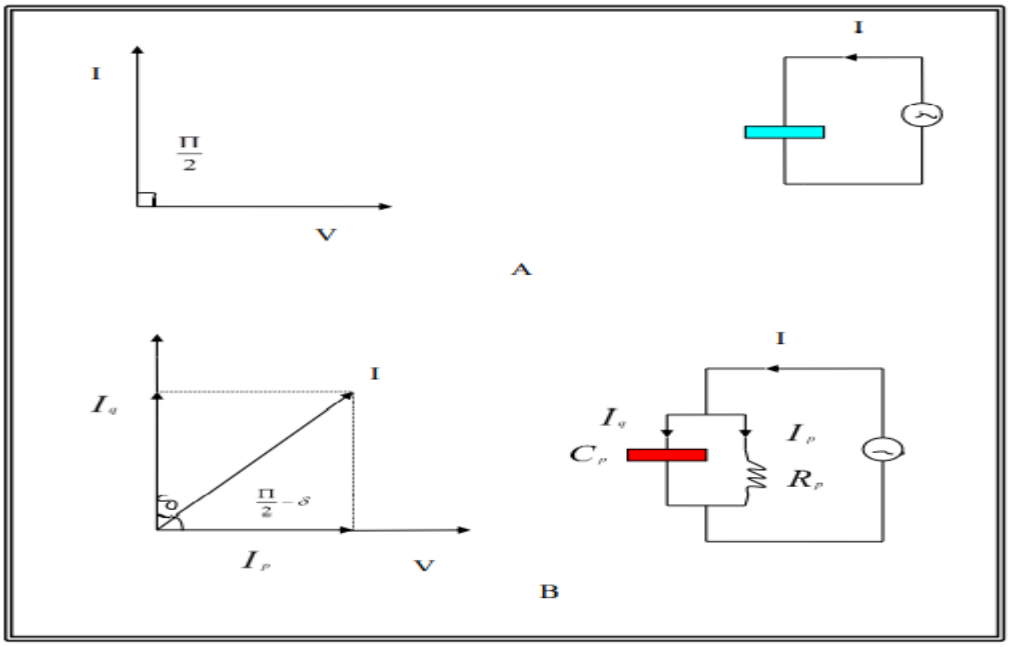

Fig. (2.7): A. The analogous circuit to a perfect capacitor, B. The analogous circuit to a non-ideal capacitor [76].

The equation defines the capacitance of a condenser made up of two parallel plates [77]:

$$C = \varepsilon_{\circ} \frac{A}{d} \qquad (2.33)$$

Substituting equation (2.33) in equation (2.31), you get:

$$I = jw\varepsilon\varepsilon_{\circ}VA / d \qquad (2.34)$$

The allowability (ε) has to be a complicated number. The electric current is a complicated variable because it has both real and imaginary components, as indicated in equation (2.32) [78]:

$$\varepsilon = \varepsilon' - j\varepsilon'' \qquad (2.35)$$

when ε″ is dielectric loss

So, acquire the following:

$$I = jw\varepsilon_{\circ}\frac{A}{d}(\varepsilon' - j\varepsilon'')\,V \qquad (2.36)$$

When we compare equations (2.36) and (2.32), we can see that:

$$Ip = w\,\varepsilon''\varepsilon_{\circ}\frac{A}{d}V \qquad (2.37)$$

$$Iq = w\,\varepsilon'\varepsilon_{\circ}\frac{A}{d}V \qquad (2.38)$$

Figure (2.7 B) shows that the loss factor (tanδ) is given by the following equation:

$$\tan\delta = \frac{Ip}{Iq} = \frac{\varepsilon''}{\varepsilon'} \qquad (2.39)$$

The electrical energy that is lost in the insulator is converted into thermal energy. In electrical applications, the significance of knowing the power factor is quite beneficial. In the high frequency insulator, excessive power factor will cause heat, resulting in a power outage [79].

The capacitor (c) can be represented by an ideal capacitor connected in parallel with a resistance Rp at low frequencies. So:

$$I = Ip + jIq = \frac{V}{R_P} + jwCPV \qquad (2.40)$$

Obtain the impedance as a result of this:

$$1/Z = 1/R_P + jwCP \qquad (2.41)$$

Equations (2.37), (2.38), and (2.40) may be written as follows:

$$R_p = d/(w\,\varepsilon''\varepsilon_{\circ}A) \qquad (2.42)$$

$$\varepsilon'' = \frac{1}{w\,R_P C_{\circ}} \qquad (2.43)$$

$$C_P = \frac{\varepsilon'\varepsilon_{\circ}A}{d} \qquad (2.44)$$

$$\varepsilon' = \frac{C_P}{C_\circ} \qquad (2.45)$$

Dissipated strength in the insulator is expressed by the presence of an alternative conductivity, using equation (2.39) [79]:

$$\sigma_{a.c} = w\, \varepsilon'' \varepsilon_\circ \qquad (2.46)$$

$\sigma_{a.c}$ is the temperature created in the insulating material as a result of the field alternation and the rotation of the dipole in its position (or the vibration of the charges)[77].

2.7 Antibacterial Mechanisms of Nanoparticles

NPs must come into touch with bacterial cells in order to perform their antimicrobial effect. Electrostatic attraction [80], van der -Waals forces [81], receptor ligand interactions [82], finally hydrophobic interactions [83]. NPs enter the bacterial membrane and aggregate throughout the metabolic route, altering the cell membrane's shape and function. The NPs then interact with DNA, lysosomes, ribosomes, and enzymes in the bacterial cell, causing oxidative stress, heterogeneous modifications, changes in cell membrane permeability, electrolyte balance issues, enzyme inhibition, protein deactivation, and gene expression changes as shown in figure (2.8) [84].

The most important mechanism of Nanoparticles toxicity to bacteria is damage to cell membrane, besides cell membrane damage, generation of reactive oxygen species, disturbance in metal/metal ion homeostasis, protein and enzyme dysfunction and geno-toxicity [84].

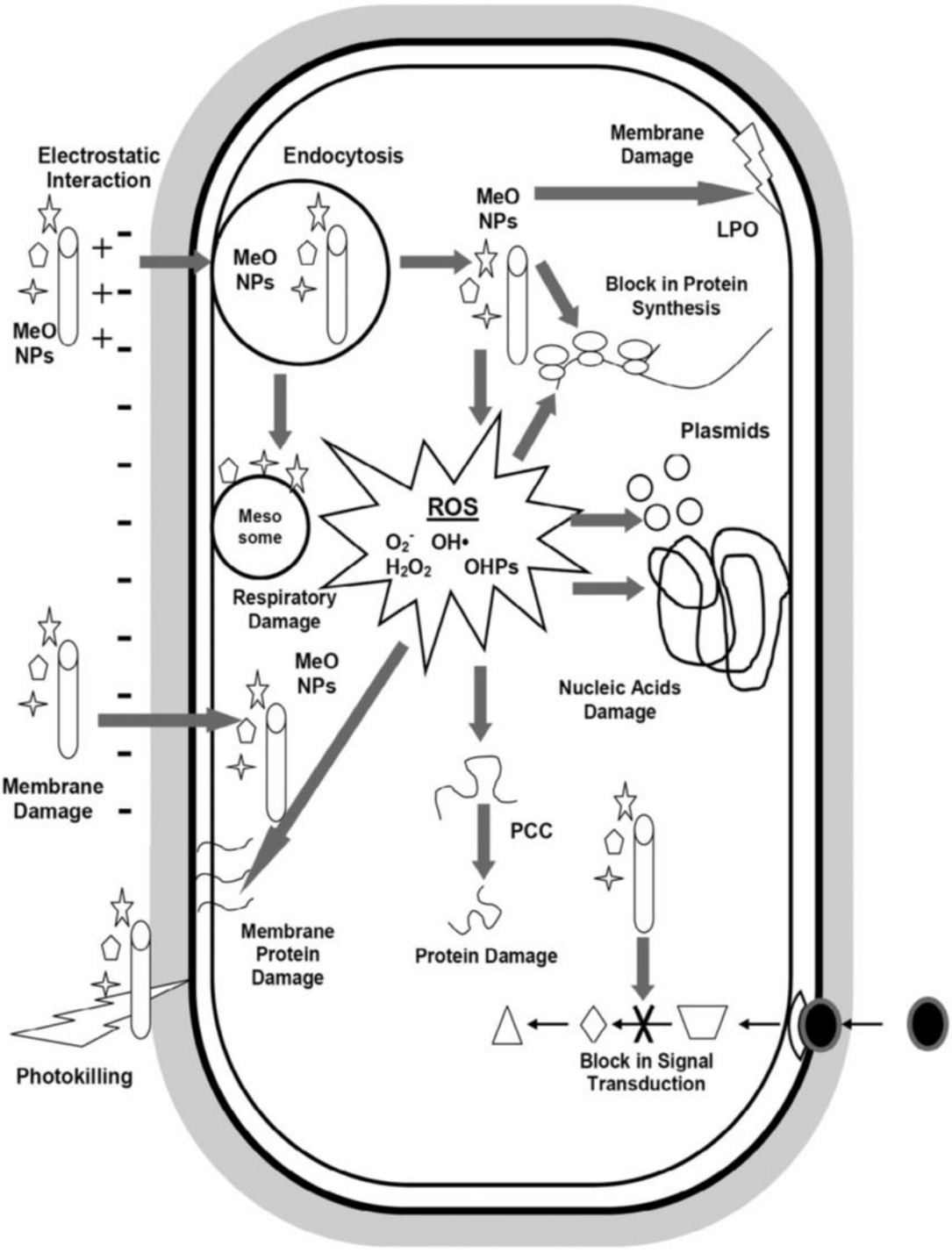

Fig. (2.8): Overview of Antimicrobial Mechanisms by Metal Oxide Nanoparticles. ROS: Reactive Oxygen Species, LPO: Lipid Peroxidation [84].

2.8 Bacterial Isolates Utilized in the Study

2.8.1 *Escherichia coli*

It is one of the most common gram-negative bacteria on the planet. *E. coli* is a facultative anaerobic bacterium, which means that it can live both with and without oxygen. Lactose fermentation is characterized by a non-spore forming, motile, rod-shaped bacterium. [85]. *E. coli* is one of the most prevalent bacteria found in the human intestine, and it grows best in 37°C [86]. At 37°C, a pH of 6.0-7.0 is excellent for growing bacteria in a culture, with a minimum pH of 4.4 and a maximum pH of 9.0 required for growth [87].

2.8.2 *Staphylococcus aureus*

Staphylococcus is discovered in pus following a surgical infection in a knee joint in Aberdeen in 1880. Sir Alexander Ogston, a surgeon from Scotland. The term was changed to *Staphylococcus aureus* by Friedrich Julius Rosenbach, who was attributed under the official naming process at the time. [88].

The gram-positive, round-shaped bacteria *S. aureus* (golden staph is another name for it) Gram – positive nonmotile, nonspore-forming cocci with a diameter of 0.5–1.0 μm that appear alone, in pairs, and in clusters. It is a facultative anaerobe that can grow without oxygen and is typically positive for catalase and nitrate reduction. It may be found in the nose, respiratory system, and on the skin and is a normal part of the body's flora [89].

S. aureus causes a number of skin problems, including abscesses, respiratory infections, and food poisoning. Virulence factors such as powerful protein toxins and the synthesis of a cell-surface protein that binds and inactivates antibodies are frequently produced by pathogenic strains to aid infections [90].

Pneumonia, meningitis, osteomyelitis, endocarditis, toxic shock syndrome, bacteremia, and sepsis are all symptoms of *S. aureus*, as are pimples, impetigo, boils, cellulitis, folliculitis, carbuncles, scalded skin syndrome, and abscesses, as well as pneumonia, meningitis, osteomyelitis, endocarditis, toxic shock syndrome. It's still one of the top five causes of hospital – acquired infections, and it is a leading cause of wound infections following surgery [91].

Chapter Three

Experimental Part

3.1 Introduction

This chapter covers the preparation and processing steps of the sample, as well as a description of the equipment and methods used in the preparation and measuring process, such as, Fourier Infrared Transform Spectrometer (FT-IR), X-Ray Diffraction (XRD), Field Emission Scanning Electron Microscope (FE-SEM), Optical Microscope (OM), and Optical Spectrometer. Also measuring the application for antibacterial activity.

3.2 The Utilized Materials

The substances used in this research are:

3.2.1 Matrix material

1. Polyvinyl alcohol (PVA)

PVA (partially hydrolyzed, molar weight = 160,000 g. mol^{-1}) is the world's biggest synthetic, water-soluble polymer by volume. The melting point 180-190 ^{o}C. linear formula is $(CH_2CH(OH))_n$. Provenance of PVA from (Central Drug House, Ltd., Company) Indian.

2. Polyvinyl Pyrrolidone (PVP)

PVP is a white powder with high purity (99.9 %), molar weight = 60,000 g. mol^{-1}. The melting point is (150-180) ^{o}C, linear formula is $(C_6H_9NO)_{n.}$ It could be obtained from (Direvo industrial biotechnology, Germany).

3.2.2 Additive materials and solvent ethanol

1. Zinc oxide (ZnO)

ZnO is an inorganic compound with particle size (20-30) nm. It's a solid white powder that is soluble in water. Its melting point is 2247 K, a molecular weight is 81.406 g mol^{-1}, and a density is 5.606 g/cm^3. Brand name is (HW NANO, in Jiangsu China).

2. Silver (Ag)

It was obtained as powder from (Sky Spring Nanomaterials, lnc., 2935Westhollow Dr. Houston, TX77082, ph:281-870-1700) company with particle size (20-30) nm and high purity (99.95%).

3. Ethanol

Ethanol is a kind of organic substance ethanol is also known as ethyl alcohol. It can also be called grain alcohol, drinking alcohol, spirits, or just alcohol. It is a basic alcohol with the chemical formula (C_2H_6O) . (CH_3-CH_2-OH) is another way to write the formula., which is sometimes abbreviated as EtOH. Ethanol, with a faint characteristic odor, is a colorless, poisonous, flammable liquid. It's a psychoactive element in alcoholic beverages, as well as a recreational drug. Ethanol is created naturally by yeast fermentation of carbohydrates or by petrochemical processes like ethylene hydration. As an antiseptic and disinfectant, it does have medicinal uses. It is utilized to make organic chemicals, as well as a chemical solvent and an alternative fuel source. Ethanol has a Formula: C_2H_5OH, Boiling point: 78.37 °C, Density: 0.789 g/cm^3, 46.07 g mol^{-1} Molecule mass, C_2H_5-OH is the molecular formula, solubility and fully miscible in water.

3.2.3 Bacteria used in this research

Two isolates of bacteria were used: bacteria *Escherichia coli* Gram-negative and bacteria *Staphylococcus aureus* Gram-positive. that was previously diagnosed, were obtained from collage of science / University of Babylon.

3.3 Preparation of (PVA-PVP/ZnO and Ag) Nanocomposites

Films of a polymer mixture (PVA - PVP) were prepared by solution casting technique. Both PVA and PVP polymers have good water solubility. This is due to the formation of strong H bonds between the functional group of polymers and water molecules (hydrophilic property). 0.8g of PVA was dissolving in 60 ml of deionized water. The solution was prepared by mixing with a magnetic stirrer for 1hr at room temperature, then continue for another hour under ~80^{o}C to get a good mix, afterwards, it was added 0.2g of PVP and Stir enough to get a homogeneous solution, then the solution casted into Petri dish and solvent is allowed to vaporize slowly at room temperature conditions for 144 hour. The synthesized dried film is taken off from the Petri dishes and kept in vacuum desiccators. NCs films were prepared from PVA- PVP/ 5wt.% ZnO and different wt.% (1, 2, 3 and 4) of Ag as listed in Table (3.1). It was obtained according to the following:

Used the solid-state method, as shown in Fig. (3.1), for mixing the ZnO and Ag NPs alone, which include dissolving it by ethanol solvent with continuous grinding in a crucible ceramic for 90 min, then dried at 60˚C for 4 hours before adding it to the polymer solution. Mixture of the polymers were continuing as in previous steps interspersed with the use of ultrasonic for 15 mints to prevent any agglomeration even get a homogeneous solution. The casting film kept at RT conditions for 144 hours to dry. The uniform thickness was (120±5) μm measured by Digital Vernier Caliper.

Fig. (3.1): Solid state method.

Table (3.1): Summarized the under-study nanocomposite films contents

The sample name	PVA (g)	PVP (g)	ZnO (g)	Ag (g)
PVA-PVP	0.8	0.2	0	0
PVA-PVP / 5wt.% ZnO	0.76	0.19	0.05	0
1wt.% Ag	0.7524	0.1881	0.05	0.01
2wt.% Ag	0.7448	0.1862	0.05	0.02
3wt.% Ag	0.7372	0.1843	0.05	0.03
4wt.% Ag	0.7296	0.1824	0.05	0.04

3.4 Process Chart of (PVA-PVP) Polymer Blend and its NC Films Synthesis

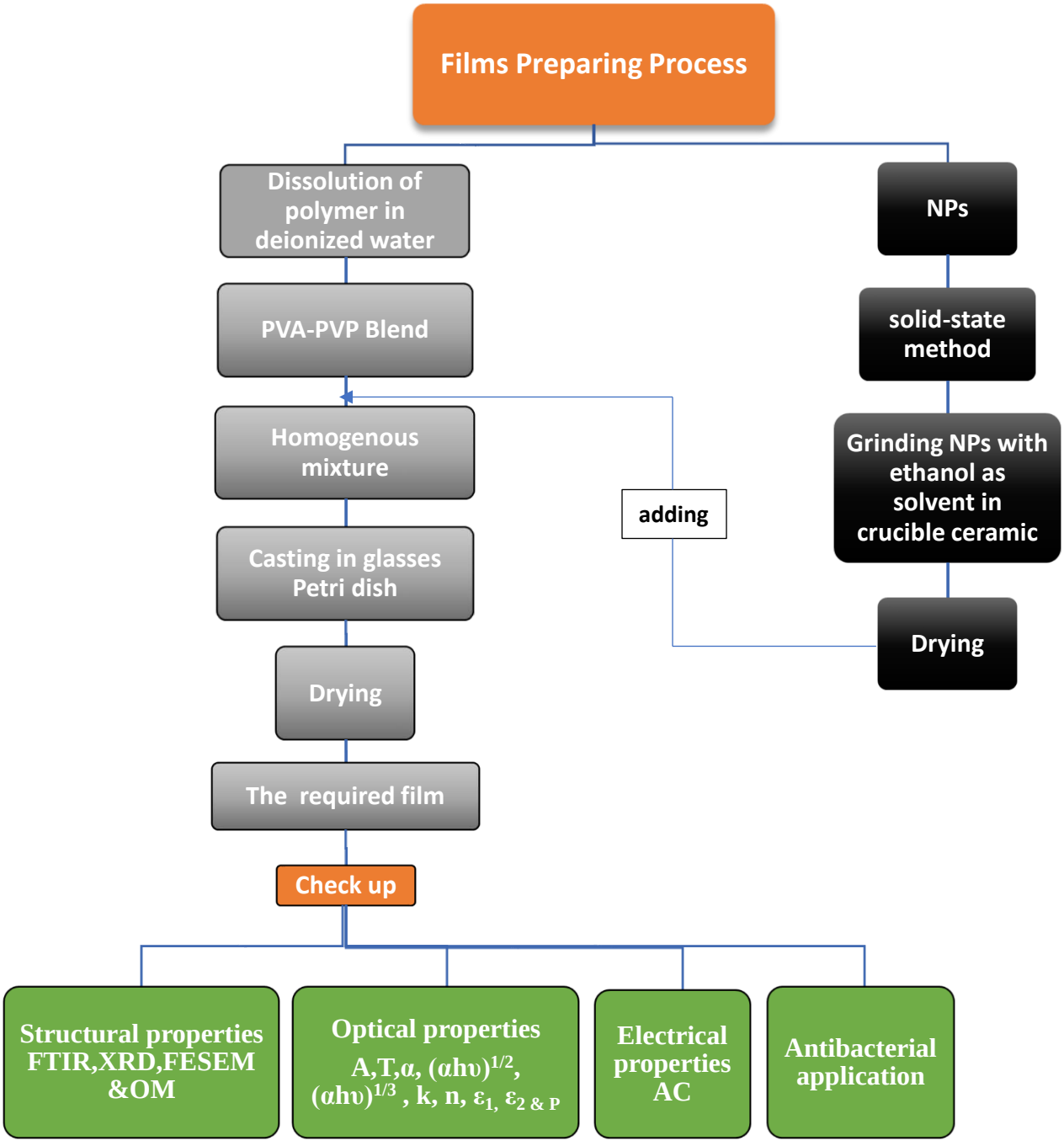

Fig. (3.2): Schematic diagram of experimental work.

3.5 Measurements of Structural Properties

3.5.1 Spectral characterization for FT- IR

FT-IR spectra were captured using an FT-IR (Bruker company type vertex -70, German origin). The spectrum of wave numbers considered is (500–4000) cm^{-1}. FT-IR has been introduced in the physics department/ education college for pure science/ University of Babylon.

3.5.2 X-Ray diffraction (XRD)

By studying the diffraction of X-rays for any material, the crystal structure of this material is identified. When an X-ray beam strikes the membrane at an angle within the range (2θ = 20˚-80˚), Bragg reflections on parallel crystal surfaces cause peaks to arise, during which constructive interference occurs for X-ray waves.

The crystal structure of the prepared thin films has been determined by using (Rigaku-binary (RAW), Ultima Iv, Japan). The following are the specifications for an X-ray diffractometer (XRD):

(Target Cu Kα1 radiation of 1.54060 Å, Current = 30 mA, Voltage = 40 kV, Step = 0.08 deg, scanning speed= 0.25 deg/min., and measurement temperature 25 °C).X-ray diffraction was examined at university of Tehran.

3.5.3 Field emission scanning electron microscope (FE-SEM)

The structural properties and nanoparticles size, shape and morphology of NCs films were analyzed by field emission scanning electron microscope (FE-SEM) (TESCAN Mira3, Company TESCAN, Czech Republic). The examination was carried out in the laboratory of the university of Tehran.

3.5.4 Optical microscope (OM)

The change of surface morphology samples of (PVA-PVP/ZnO and Ag) nanocomposites is observed applying the optical microscope. This used OM was provided by Olympus (Top View, type Nikon-73346). It is used in the university of Babylon/ Physics department/ college of education for pure sciences.

3.6 Optical Properties Measurements.

The absorption spectrum of (PVA-PVP/ZnO and Ag) nanocomposites have been recorded in the wavelength range (190-1100) nm by using the double beam spectrophotometer (Shimadzu, UV-1800 Å). The absorption spectrum has been recorded at room temperature. A computer program (UV Probe software) was employed to obtain the absorbance, optical constants, transmittance, absorption coefficient, extinction coefficient, dielectric constant (real and imaginary parts), refractive index and energy gaps. It is implemented at the university of Babylon /college of education for pure sciences/ department of physics.

3.7 Measurement of A.C. Electrical Conductivity

The A.C. electrical conductivity was measured by LCR meter type (HIOKI 3532-50 LCR Hi TESTER (Japan)) in university of Babylon / college of education for pure sciences/ department of physics. Fig. (3.3) demonstrates a diagram for the system of A.C electrical measurement. Only (1cm) from each one of the samples were taken and put between two electrodes and by different frequencies from (100Hz-5MHz) at room temperature. The capacity (C_P) and dissipated factor (D) have been recorded for all samples. Dielectric constant, dielectric loss and conductivity were calculated from this data.

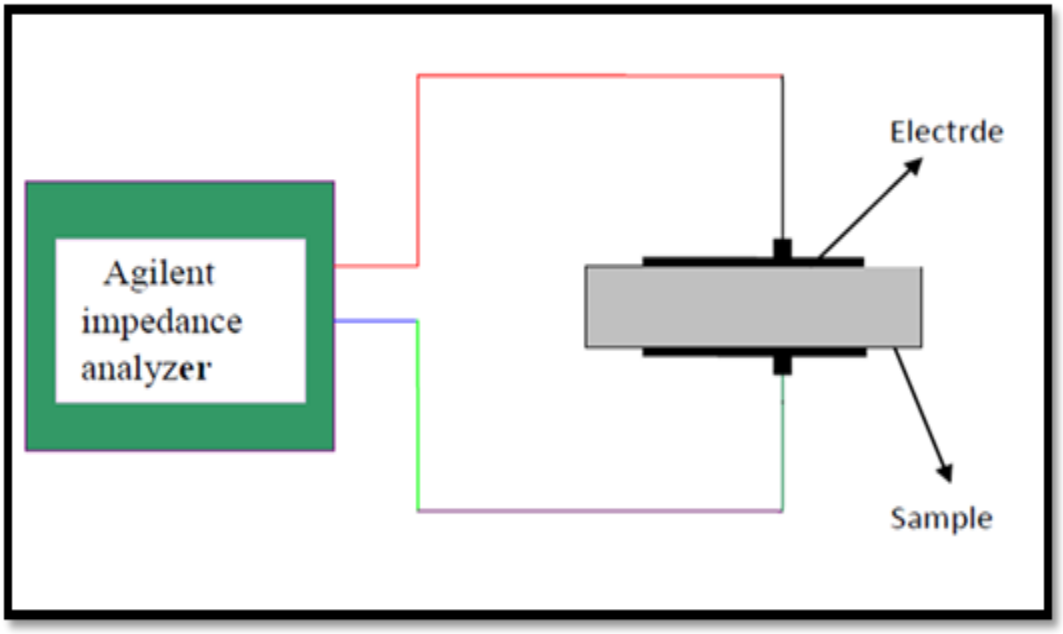

Fig. (3.3): Schematic diagram for A.C

3.8 Application of (PVA-PVP/ ZnO and Ag) Nanocomposites for Antibacterial Activity

3.8.1 The preparation of the bacterium inoculum

Four- five isolated colonies were selected from an 24hrs culture and diluted in Mueller Hinton broth to a turbidity like to 0.5 McFarland turbidity standard.

3.8.2 Antibacterial susceptibility test for nanocomposites

The antibacterial susceptibility test of synthesized nanocomposites was made by agar disk diffusion method.

3.8.3 Agar disk diffusion method:

Antibacterial activity of synthesized nanocomposites was performed by agar disk diffusion method. 20 ml of sterilized Mueller Hinton agar was placed in Petri dishes. After media solidification, 0.1 ml of each bacterial isolates were spread on

the surface of media, the Petri dishes were left for 5 minutes, then 6 mm diameter disk from each NCs were placed in each Petri dish.

The polymer blend pure was considered as negative control, the Petri dishes then incubated at 37^{o}C for 24hrs. The zones of inhibition were measured and expressed as millimeter in diameter, the experiment was performed in triplicate.

3.9 Statistical Analysis

Data were represented as a mean with standard deviation. For statistical analysis, Statistical Package for the Social Sciences (SPSS) version 23, Duncan's post hoc test was used and a P value ≤ 0.05 was considered to be significant difference. The correlation between Ag ratios and the inhibition zone in bacteria strains was also tested.

Chapter Four

Results and Discussion

4.1 Introduction

This chapter comprehensive evaluation the results obtained for the effect of ZnO and different ratios of Ag NPs on the structural, optical and electrical properties of (PVA-PVP) polymer blends and analysis of the results based on changes.

4.2 Structural Properties

4.2.1 Fourier transform infrared radiation (FT-IR) of the casting samples

FT-IR spectroscopy is one of the tools to provide useful information regarding the interactions between their functional groups. IR analysis is carried out on a FT-IR transmission profile spectrum to characterize the interface of pure (PVA-PVP) polymeric blend and its NC films with 5wt.% ZnO and different (1, 2, 3and 4) wt.% of Ag NPs under the investigated at RT in wavenumber (500-4000) cm^{-1} ranges.

Figure (4.1) illustrates the FTIR spectra of PVA-PVP blend and its NCs with ZnO and different wt.% of Ag NPs. FTIR spectrum of pure blend is corresponding to the broadness stretching vibrations of O–H (PVA and PVP), medial alkyne (disubstituted) C≡C group, C=O stretching of the ester group carbonyl groups (PVA), C=N stretching vibration occurs at 3274.36 cm^{-1}, 2360.45 cm^{-1}, 1653.12 cm^{-1} and 1243.13 cm^{-1}respectively [92]. The absorption peak at 1086.57 cm^{-1} corresponds to the C–O stretch for secondary alcohol were observed in PVP-PVA hydrogels. The IR spectra of (pure blend/ inorganic NPs) NCs contains all the characteristic peaks of PVA, PVP and the added NPs. Comparing the characteristic wavenumbers of blend with those representing the NCs, it can be noticed that there are slightly shifted toward higher wavenumbers, as a result of the addition of different wt.% of Ag NPs especially at 3274.36 cm^{-1}. Also, the transmittance

decreases with the increasing ratios of Ag NPs that assigned to increase the density of NPs. From this analysis, it is understood that there are no new peaks of absorption, therefore no interactions between polymer matrix and NPs. For more information and details see appendix A.

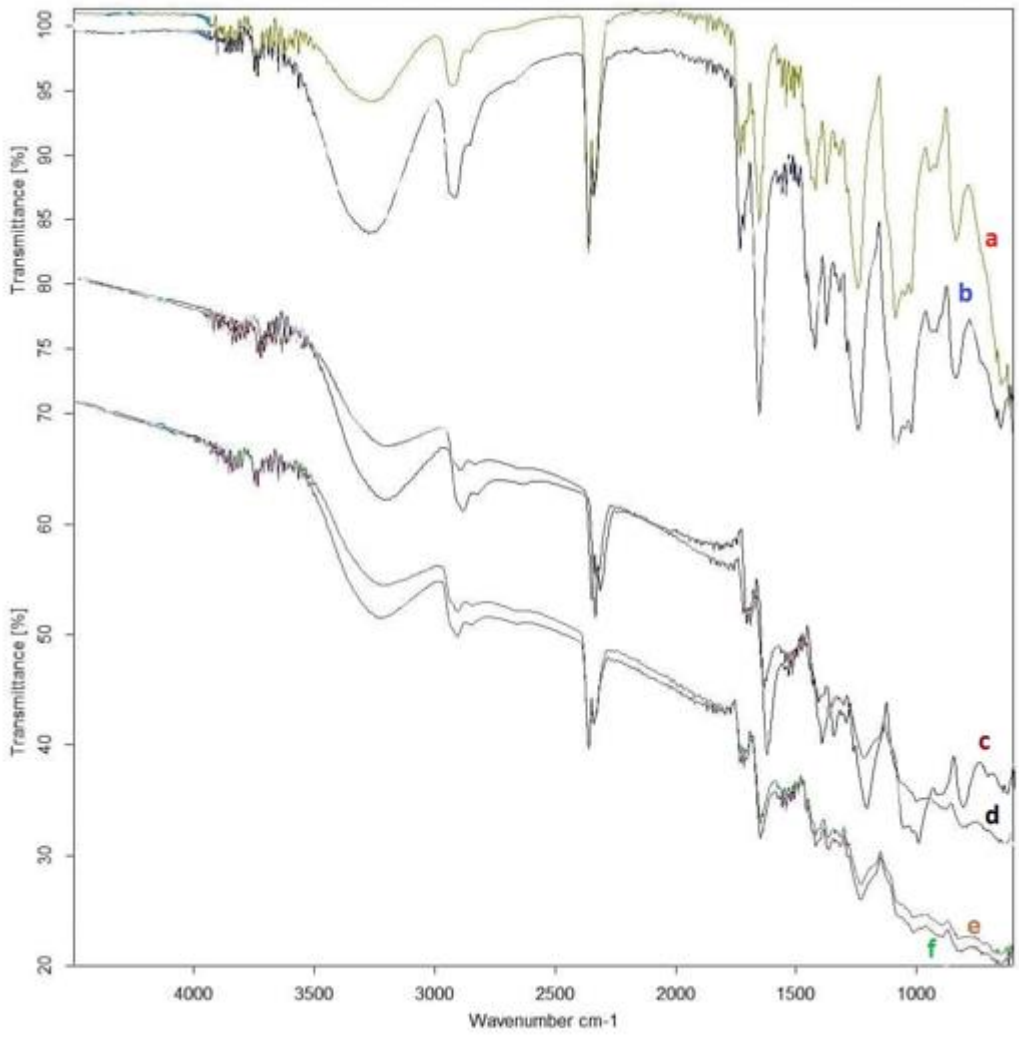

Fig. (4.1): FTIR spectra of a. (PVA-PVP) blend, b. (PVA-PVP/ 5wt.% ZnO), c. 1wt.% Ag, d. 2wt.% Ag, e. 3wt.% Ag and f. 4wt.% Ag NCs.

4.2.2 X-Ray diffraction (XRD)

X-ray diffraction is a common and non-destructive technique for the study of material crystallographic structures. PVA-PVP polymer blend and its NC films with 5wt.% ZnO and different (1, 2, 3 and 4) wt.% of Ag NPs were characterized by XRD technique as shown in figure (4.2). The XRD pattern of the pure polymer blend film had an obvious diffraction peak centered at around 2θ=19.4464°- 20.090° Bragg reflection. This strong peak corresponds to the (101) reflection, demonstrating the existence of crystalline PVA aggregates. The (101) diffraction can be explained by the interference effect between PVA macromolecules in the direction of intermolecular H bonds, or due the orthorhombic reflection of PVA polymer. At higher angles (especially at about 41°), some diffused peak displayed on a broader region can be observed showing the diffraction of pure water in the amorphous zone [26]. Thus, it can be concluded that PVA has a semicrystalline nature with domains of structural order and disorder. The 2θ values and planes for crystalline wurtzite hexagonal structure ZnO were respectively 31.9012° (100), 34.533° (002), 36.393° (101), 47.66° (102), 56.684° (110), 62.937° (103), and 68.313° (112), with lattice constant of a = 3.244 Å and c=5.157 Å, which are in close agreement with the values mentioned in the literature [28][29], and are coherent with the reported values (JCPDS Card No. 36–1451). Also, the 2θ values and planes for crystalline cubic phase Ag were respectively 38.371° (111), 44.458°(200), 64.735°(220), and 77.520°(311), with lattice constant of a = 4.065 Å, which are in close approval with the values mentioned in the research [28], and are coherent with the reported values (JCPDS Card No. 04–0783). The nanocomposites related peaks on the XRD spectrum of the NCs films became sharper revealing that it had higher crystallinity. The wurtzite hexagonal structure ZnO peak (101) is dominate in (PVA-PVP/ 5wt.% ZnO) NC film, while in other NC films the dominate peak is (111) belonging to the

cubic Ag structure. Very little shifted towards the larger angles is due to the micro strain generated in the chain polymer nanostructure by ZnO and Ag additives [93]. No extra impurity peaks are found as observed in XRD patterns, which means obtaining high purity films from the mixture of polymer and impurities. The XRD obtained data indicates that when metal and metal oxide was incorporated into polymer blend it became more crystalline than the pure films.

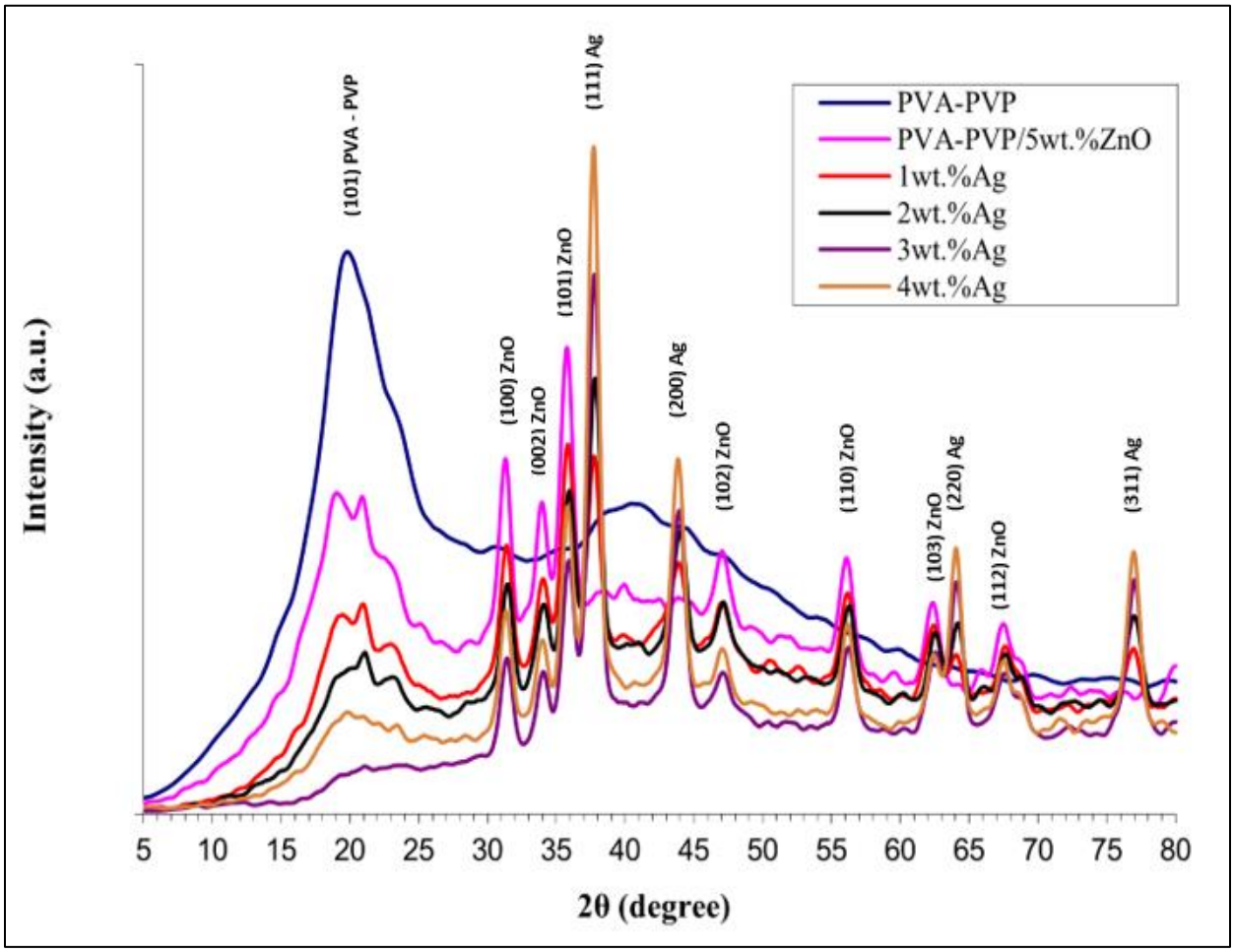

Fig. (4.2): XRD patterns of PVA-PVP and it's NCs with ZnO and different weight % of Ag NPs.

4.2.3 Field emission scanning electron microscope (FE-SEM)

Surface morphological features of PVA-PVP polymeric blend and its NCs with ZnO and different (1,2,3, and 4) wt.% of Ag NPs were identified using FE-SEM at a magnification of 200 kx. The addition of ZnO NPs showed agglomeration of small and close packed group of elliptical particles with slightly varying sizes, as the dense structure is formed due to evaporation of water as showed in figure (4.3, b). Silver addition at different ratios results in hampering the formation. PVA-PVP / ZnO with different (1,2, and 3) wt.% of Ag NCs showed reduction in the agglomeration as showed in figures (4.3, c, d and e), but in 4wt.% the NCs again showed agglomeration as showed in figure (4.3, f). Similar behaviour was reported in the research [28].

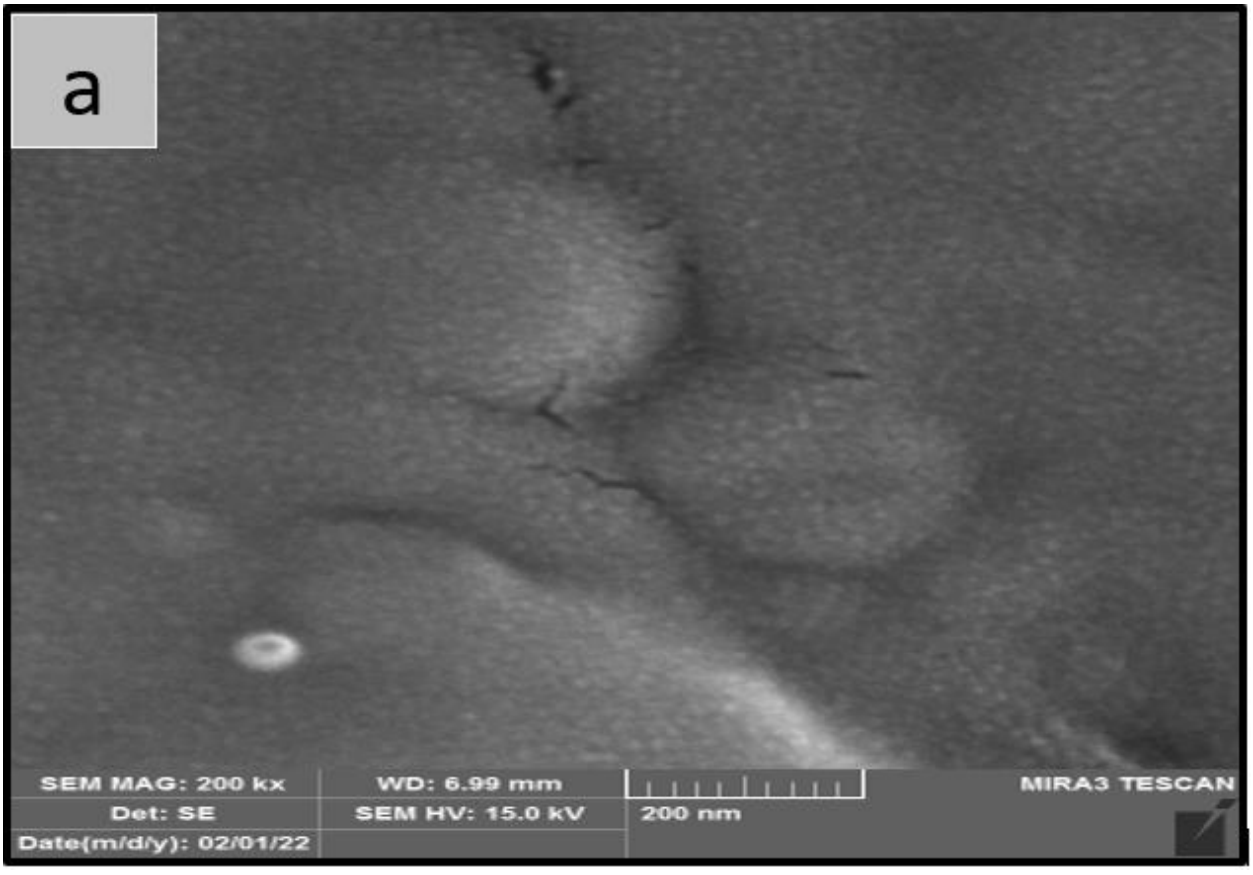

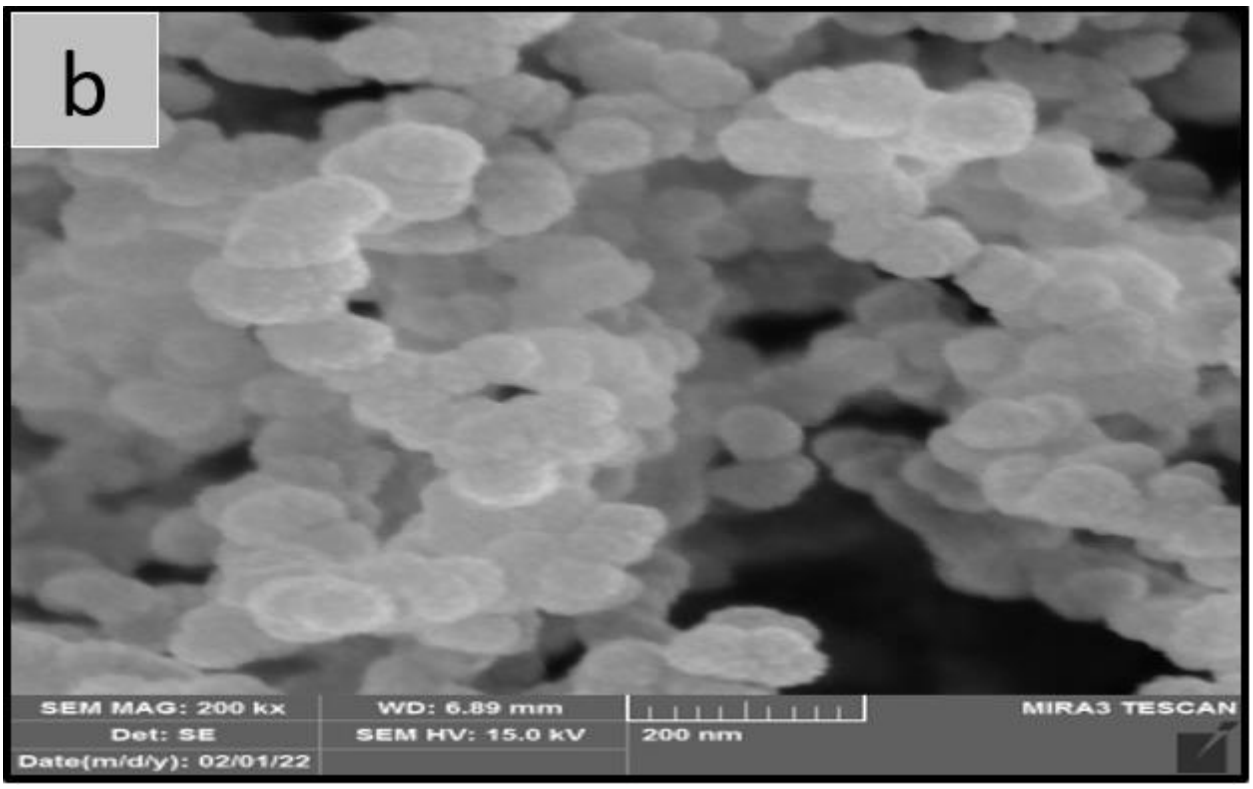
b
SEM MAG: 200 kx
WD: 6.89 mm
Det: SE
SEM HV: 15.0 kV
Date(m/d/y): 02/01/22
200 nm
MIRA3 TESCAN

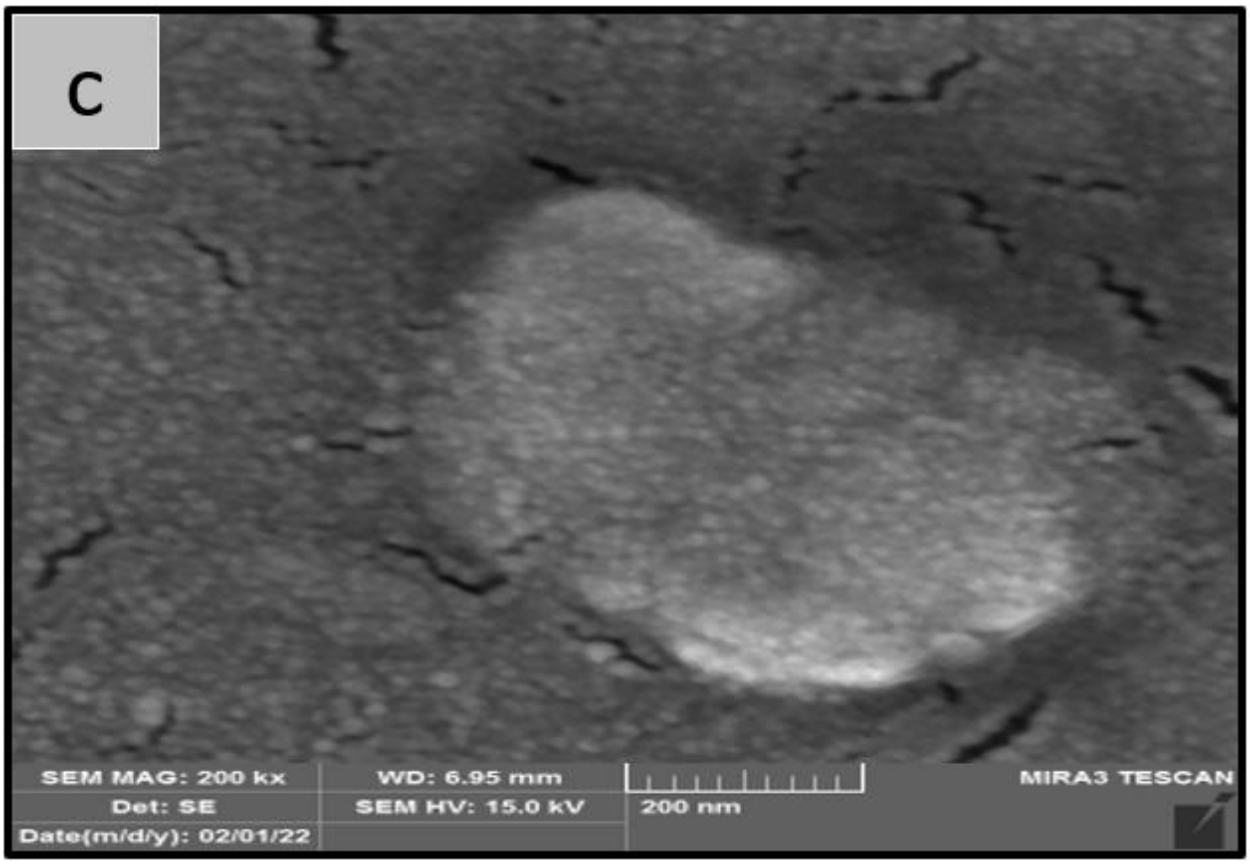
c
SEM MAG: 200 kx
WD: 6.95 mm
Det: SE
SEM HV: 15.0 kV
Date(m/d/y): 02/01/22
200 nm
MIRA3 TESCAN

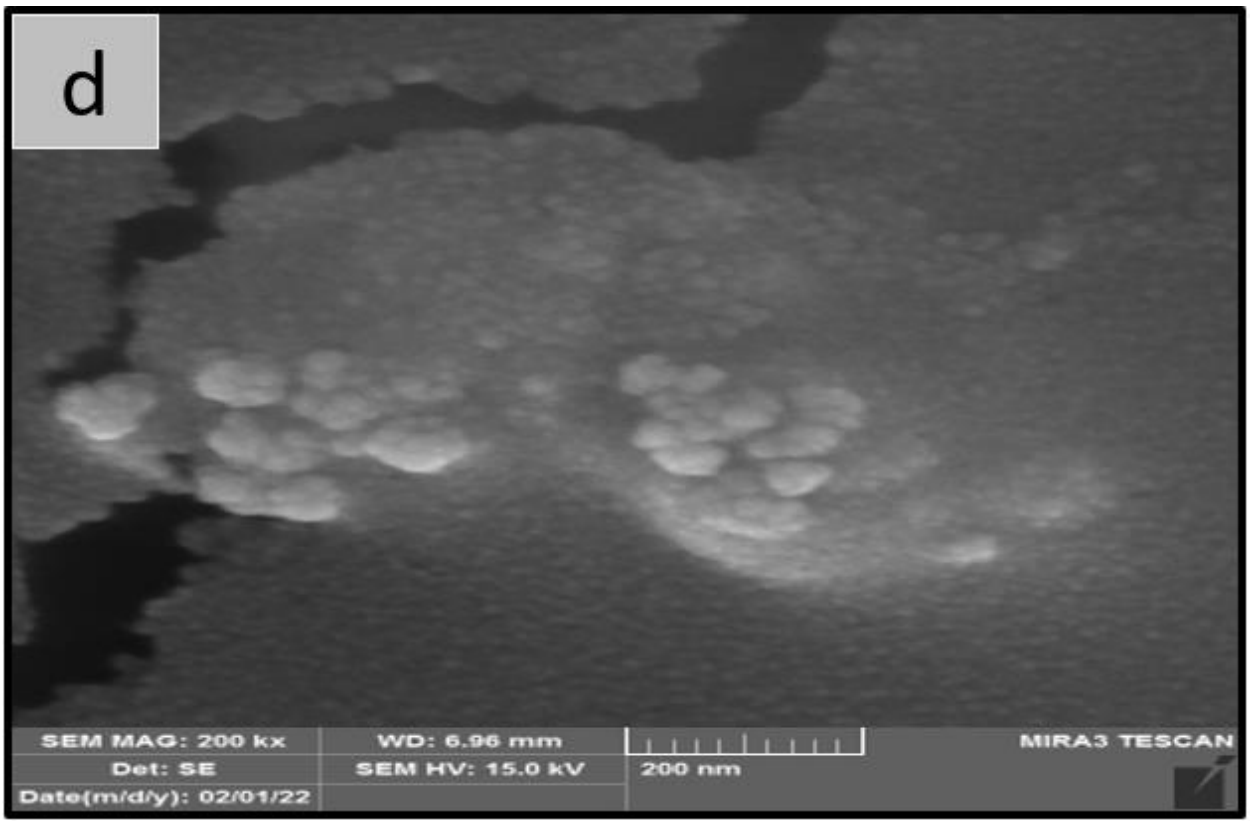
d
SEM MAG: 200 kx
WD: 6.96 mm
Det: SE
SEM HV: 15.0 kV
Date(m/d/y): 02/01/22
200 nm
MIRA3 TESCAN

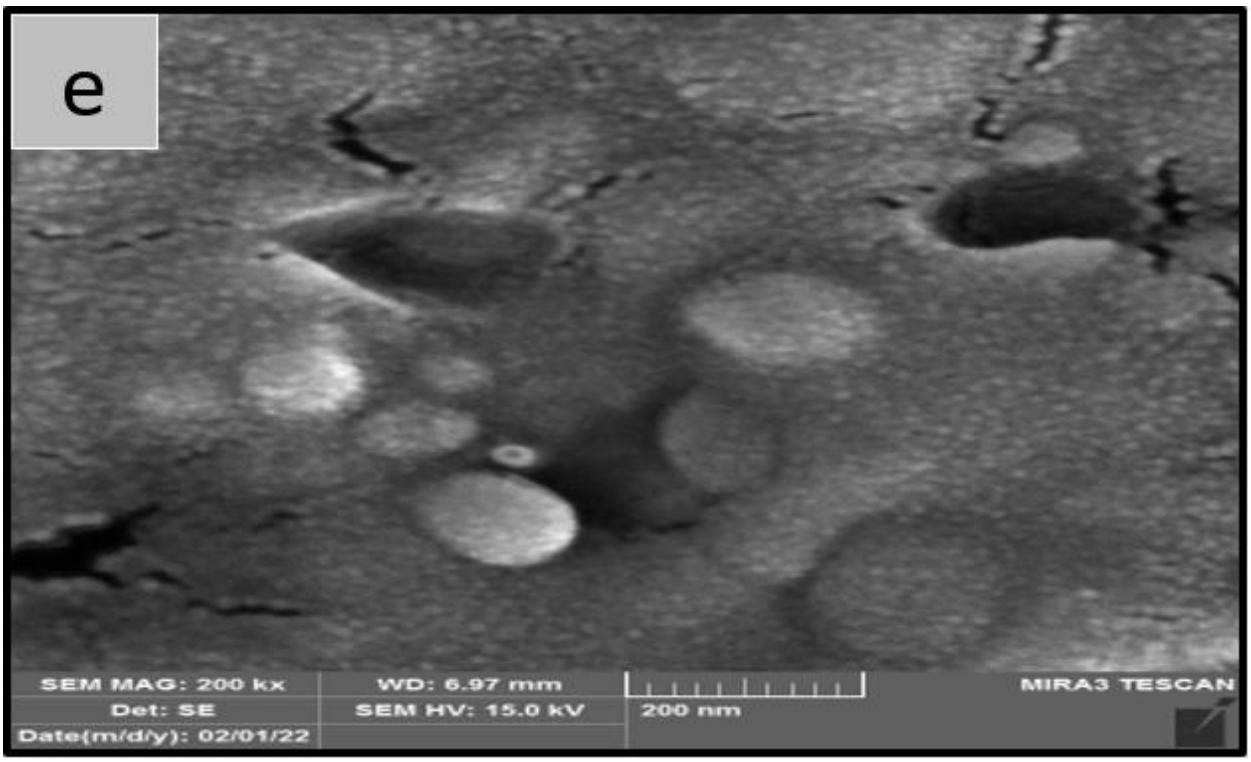
e
SEM MAG: 200 kx
WD: 6.97 mm
Det: SE
SEM HV: 15.0 kV
Date(m/d/y): 02/01/22
200 nm
MIRA3 TESCAN

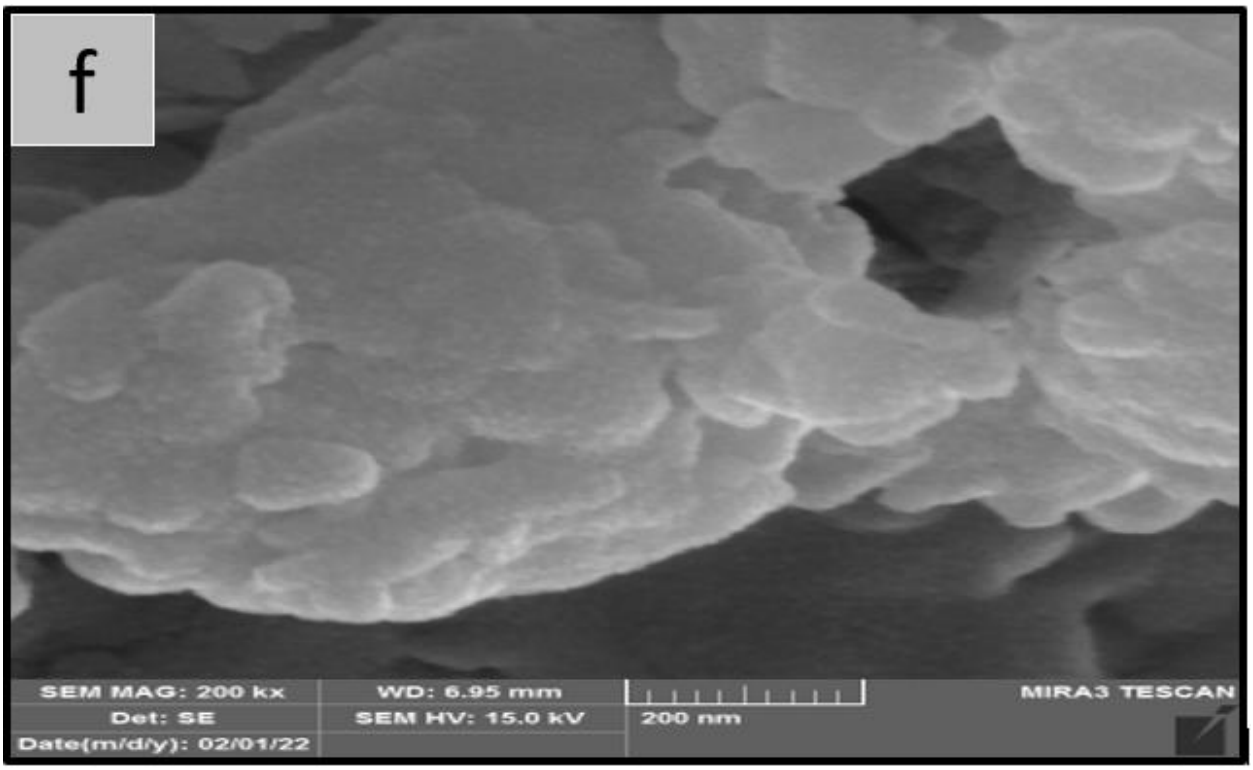

Fig (4.3): FESEM for, a. (PVA-PVP) blend, b. (PVA-PVP/ 5wt.% ZnO), c. 1wt.% Ag, d. 2wt.% Ag, e. 3wt.% Ag and f. 4wt.% Ag NCs.

4.2.4 Optical microscopy (OM) of the casting samples

The photomicrographs of the surface of (PVA-PVP) blend and its NCs with ZnO and different wt.% of Ag NPs at magnification power (40x) were shown in figure (4.4). The surface image of polymer blend film displayed in part (a) indicates a homogeneous phase without phase separation, in other ward it has a finer morphology with smooth surface, showing at this blend ratio the outstanding miscibility of PVA and PVP. From such figure (part b-f), it can be seen, that ZnO and Ag NPs are well dispersed on the surface of the polymer blend films and this apparent more evident with the increase in the wt.% of Ag. The NCs shows nearly elliptical structure of particles of uniform shape. This is because the NPs have a large surface area while the polymeric solution containing different polar groups has a high affinity for ZnO and Ag which leads to the orientation of the

nanoparticles within the polymer chain and thus the NC structure becomes more compact and thus the consistency of the material increases. This provided a suitable preparation method for preparing NC films.

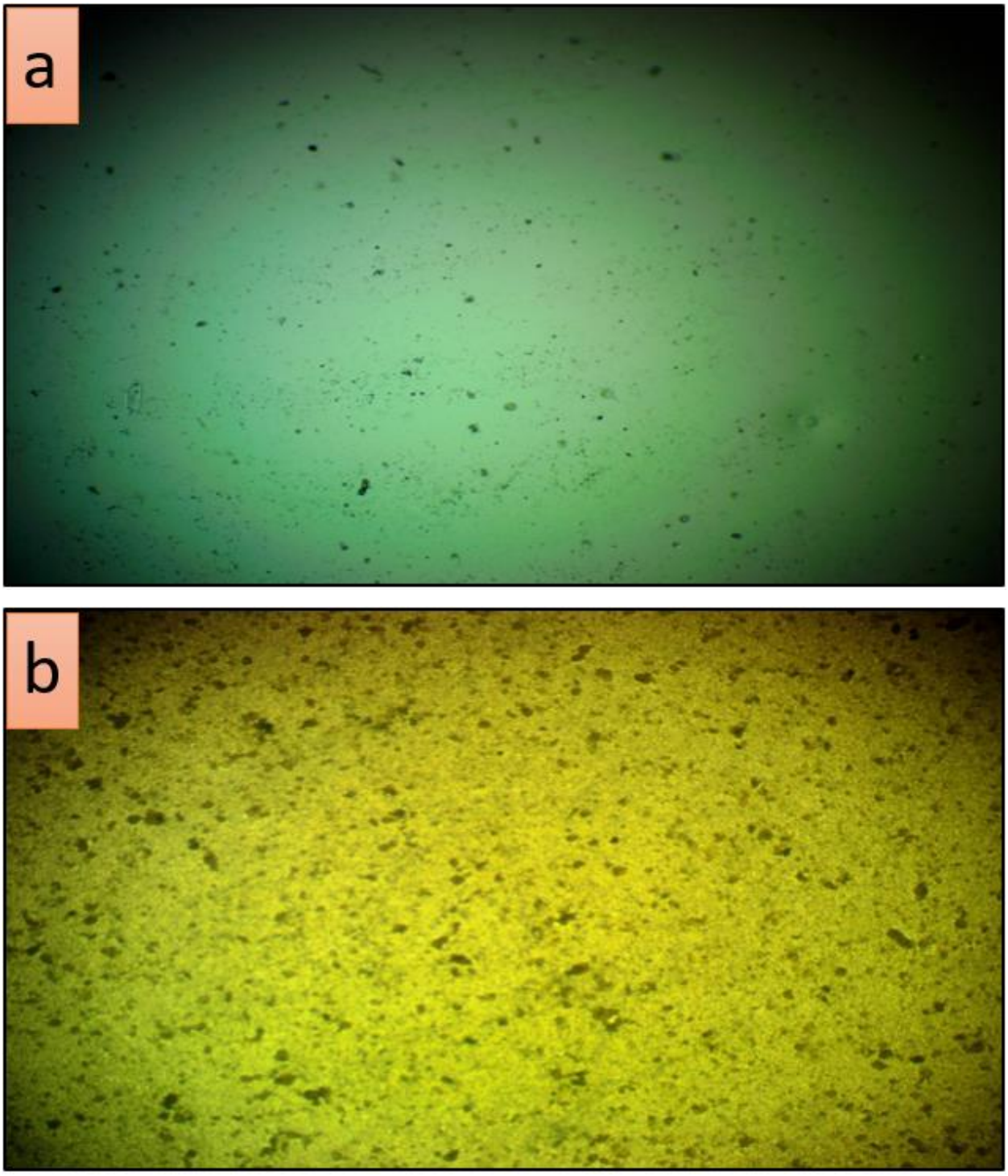

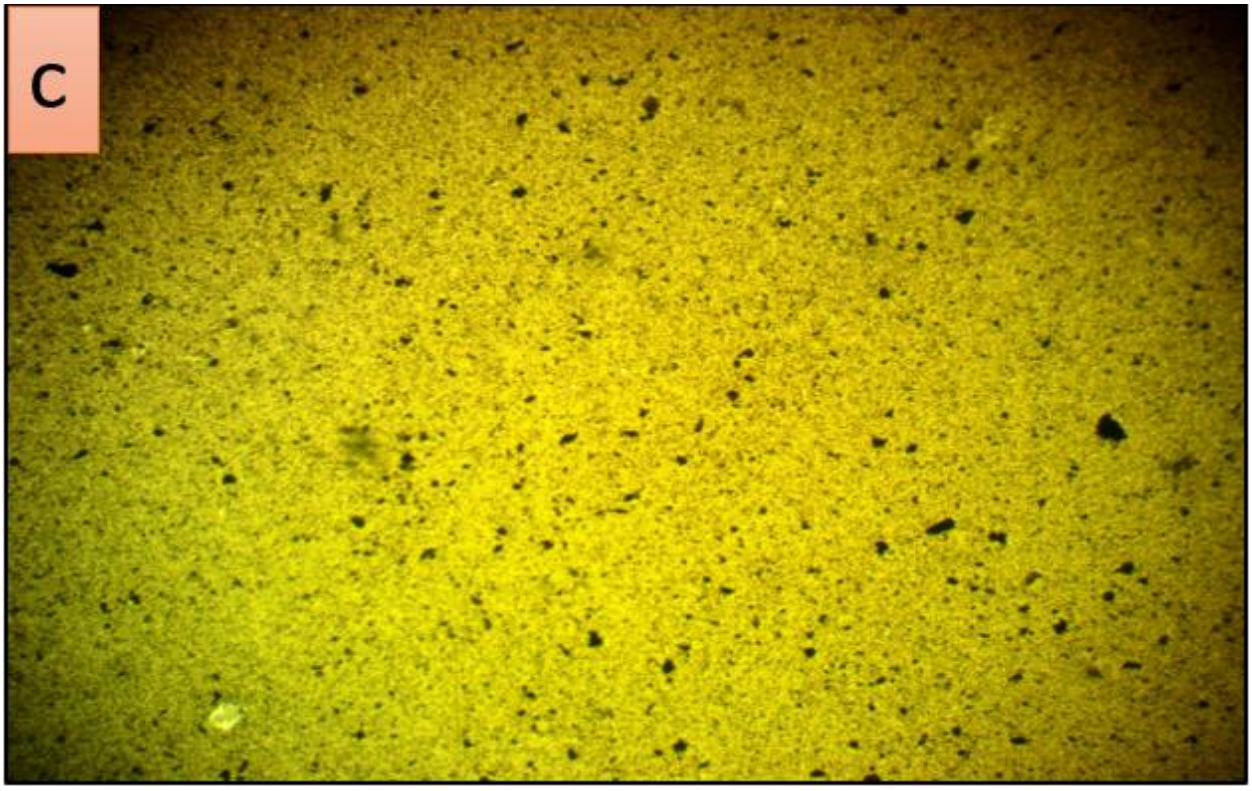
c

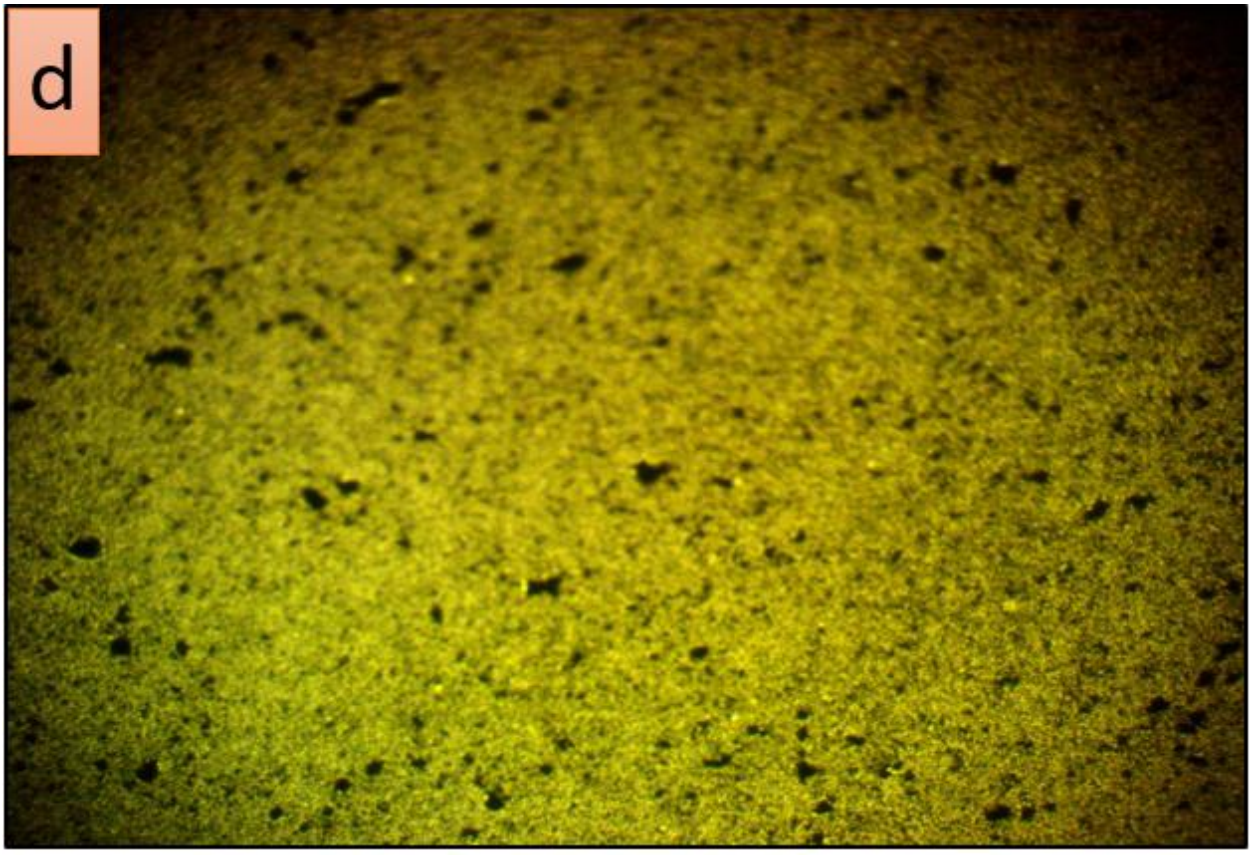
d

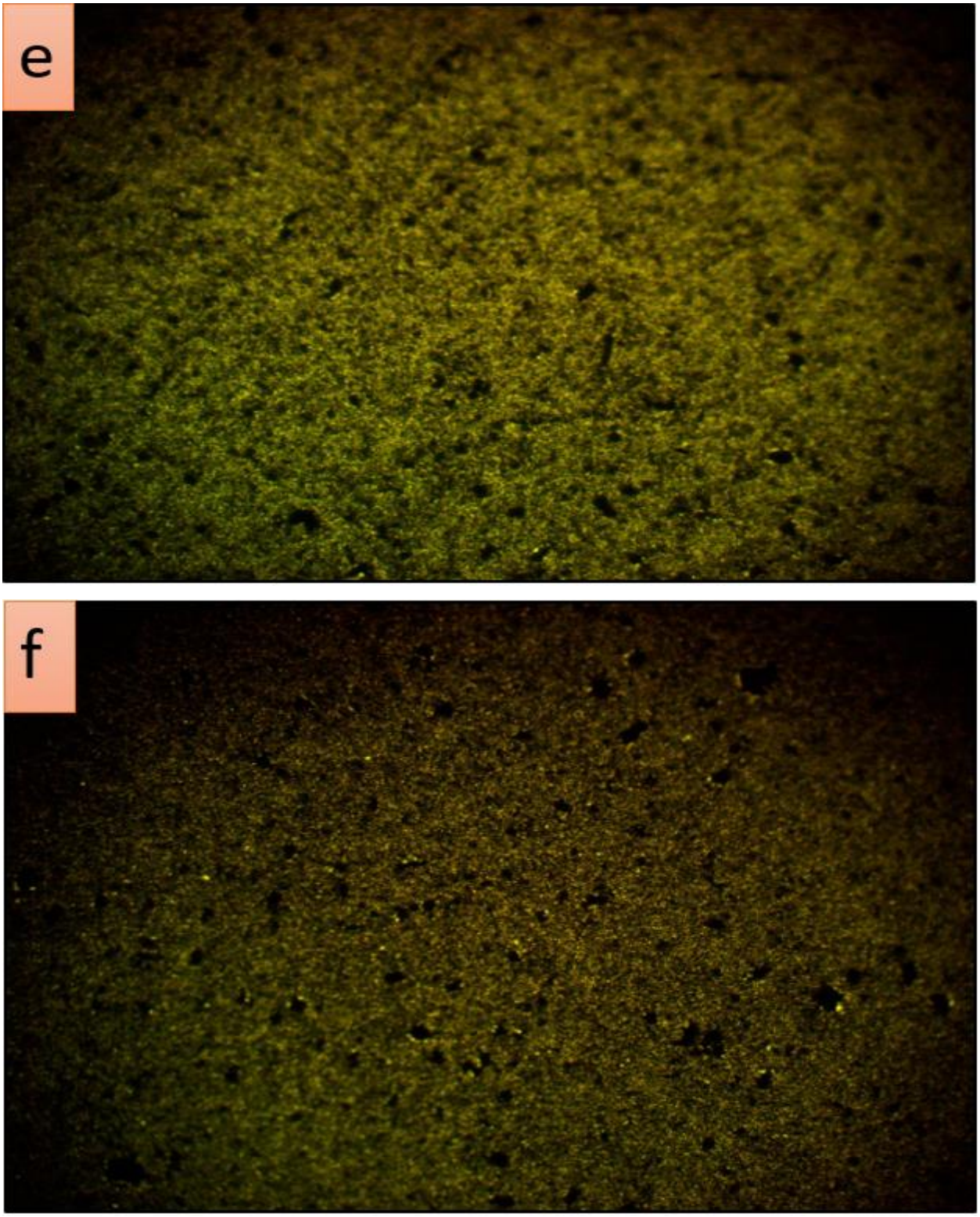

Fig (4.4): Photomicrographs (40x) for, a. (PVA-PVP) blend, b. (PVA-PVP/ 5wt.% ZnO), c. 1wt.% Ag, d. 2wt.% Ag, e. 3wt.% Ag and f. 4wt.% Ag NCs.

4.3 The Optical Properties

The main purpose of studying the optical properties is to identify the effect of adding 5wt.% ZnO and different (1, 2, 3 and 4) wt.% of Ag NPs on the optical properties of PVA-PVP polymer blend. The research covers the recording of the spectra of absorbance for the films at RT, knowledge the types of electronic transitions, calculating energy gaps, and optical constants.

4.3.1 Absorbance (A)

Figure (4.5) illustrate the UV-Vis-NIR absorption spectra of (PVA-PVP) blend and it's NCs with ZnO and different wt.% of Ag NP films carried out in the range of 190-1100 nm. The absorption edge for NC films was shifted toward higher wavelength side with adding ZnO and Ag NPs, causing a decrease in the energy gap. This may be attribute to the change in polymeric chain mobility during the blending process. Because of its large energy gap (3.37eV), the most noteworthy attribute of ZnO in the polymer is its effective UV absorption [94]. It can be seen that the absorption of NCs is much higher than that of blend. The higher absorption is attributed to the interfacial interaction between the NPs with the adjacent polar groups of blends, which were consistent with reported data [25].

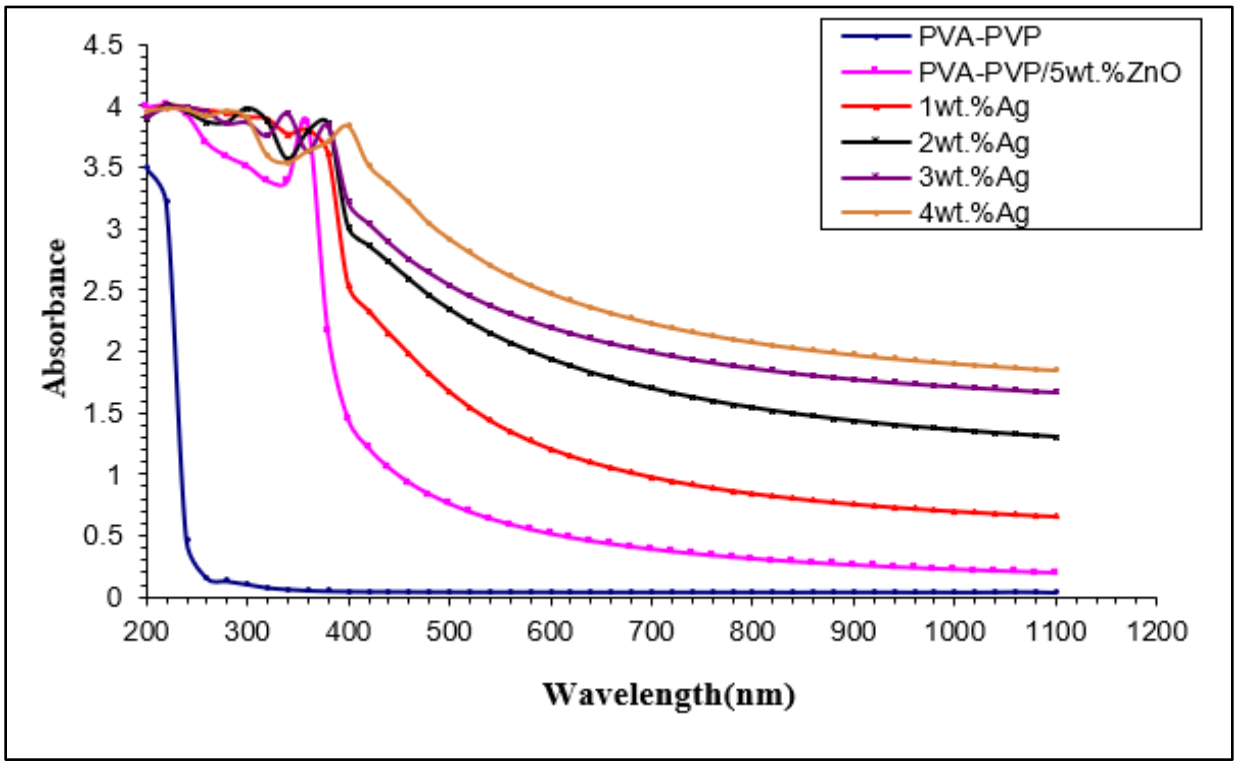

Fig. (4.5) : UV- Visible absorbance spectra (PVA-PVP) and it's NCs with ZnO and different wt. % of Ag NPs.

4.3.2 Transmittance (T)

Optical transmittance spectrum of (PVA-PVP) polymer blend and its NCs with 5wt.% ZnO and different wt.% of Ag films. Based on the results in figure (4.6), the optimal value of transmittance for pure polymer blend is about 98% in the regions Vis and NIR, but it decreases drastically with an increase in the wt.% Ag NPs. This property was due to the nature of the films surface and its absorption. Reduced the transmittance of the nanocomposite films towards ultraviolet rays qualifies it to use as a packaging for storage drugs regardless of cost.

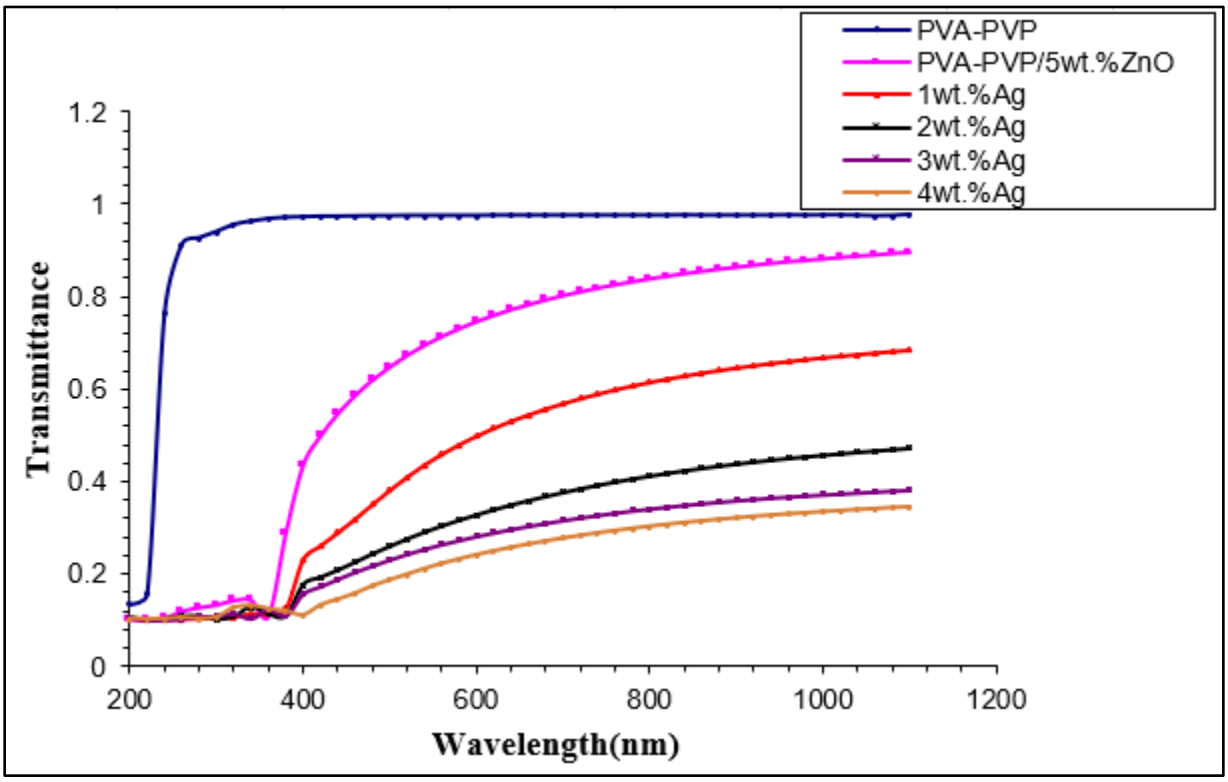

Fig. (4.6): UV-Visible transmittance spectra of (PVA-PVP) and NCs with 5wt.% ZnO and various weight % of Ag NPs.

4.3.3 Absorption coefficient (α)

The absorption coefficient (α) of the blended polymers and its NC films was calculated from eq. Lambert Beer's law (2.17), [63]:

Based on the absorption coefficient values of the prepared films ($\alpha < 10^4$ cm^{-1}) as in figure (4.7), indirect electronic transitions are extremely likely to occurs. α look smaller at high wavelength, that could relate to the little possibility of electron transition. The absorption of the electron is at high energies, which is agree with similar studies of Ag NPs [25].

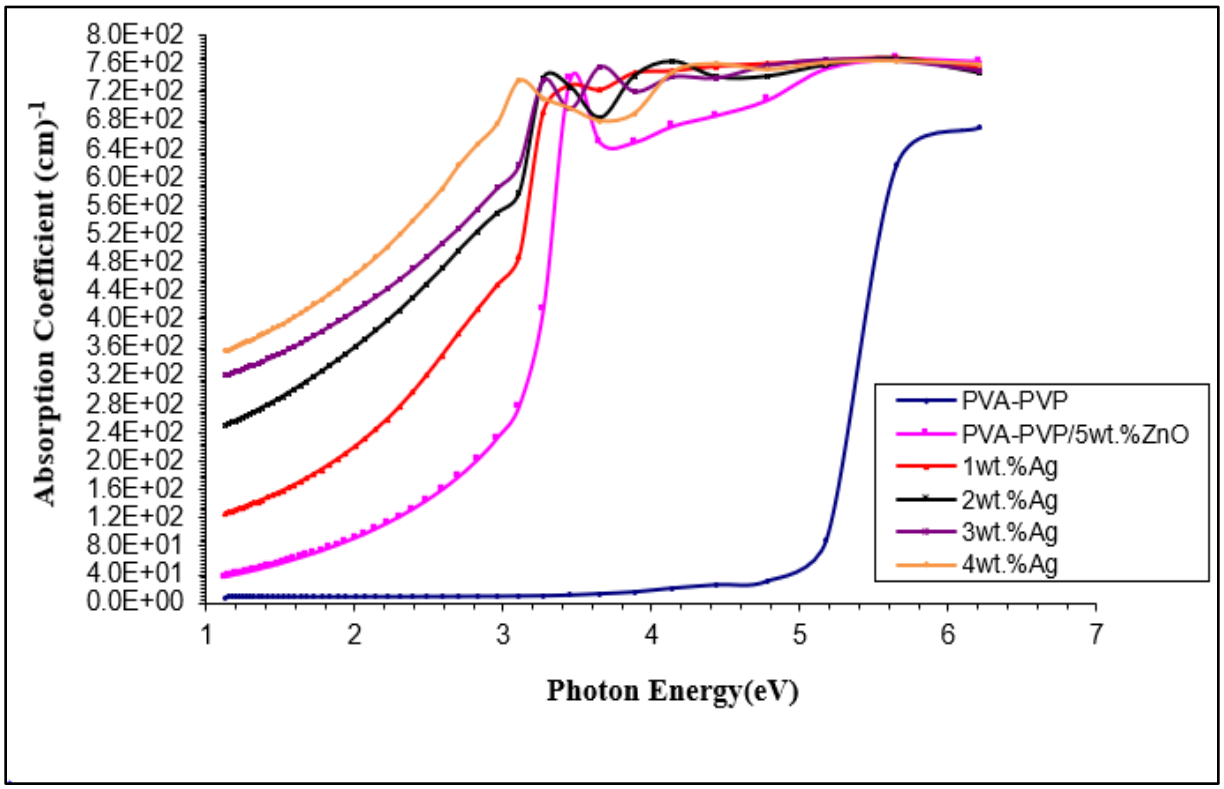

Fig. (4.7): Absorption coefficient of (PVA-PVP) blend and it's NCs with ZnO and different wt.% of Ag NPs.

4.3.4 Optical energy gaps of the allowed and forbidden indirect transition

Depending on the absorption coefficient the optical energy gap can be determined from the plot of $(\alpha h\nu)^{1/r}$ (where r = 2 for allowed and 3 for forbidden indirect transition) versus photon energy ($h\nu$) shown in the figures (4.8) and (4.9) using the Tauc relation (2.19), [66].

The both values allowed and forbidden indirect transitions are illustrated in Table (4.1). It is markedly that indirect E_g^{opt} reduce with additives of ZnO and Ag NPs. This reduce in E_g^{opt} is in good agreement with FT-IR studies and results reported on other polymeric materials [95]. The presence of silver and zinc ions in the as-prepared films increases the amount of ions available for charge transfer, and defects that lead to the irregular arrangement in the film may increase. Also, these

defects create energy states in the energy gap. Hence the increase in the deformation in the polymer matrix improves the conductivity.

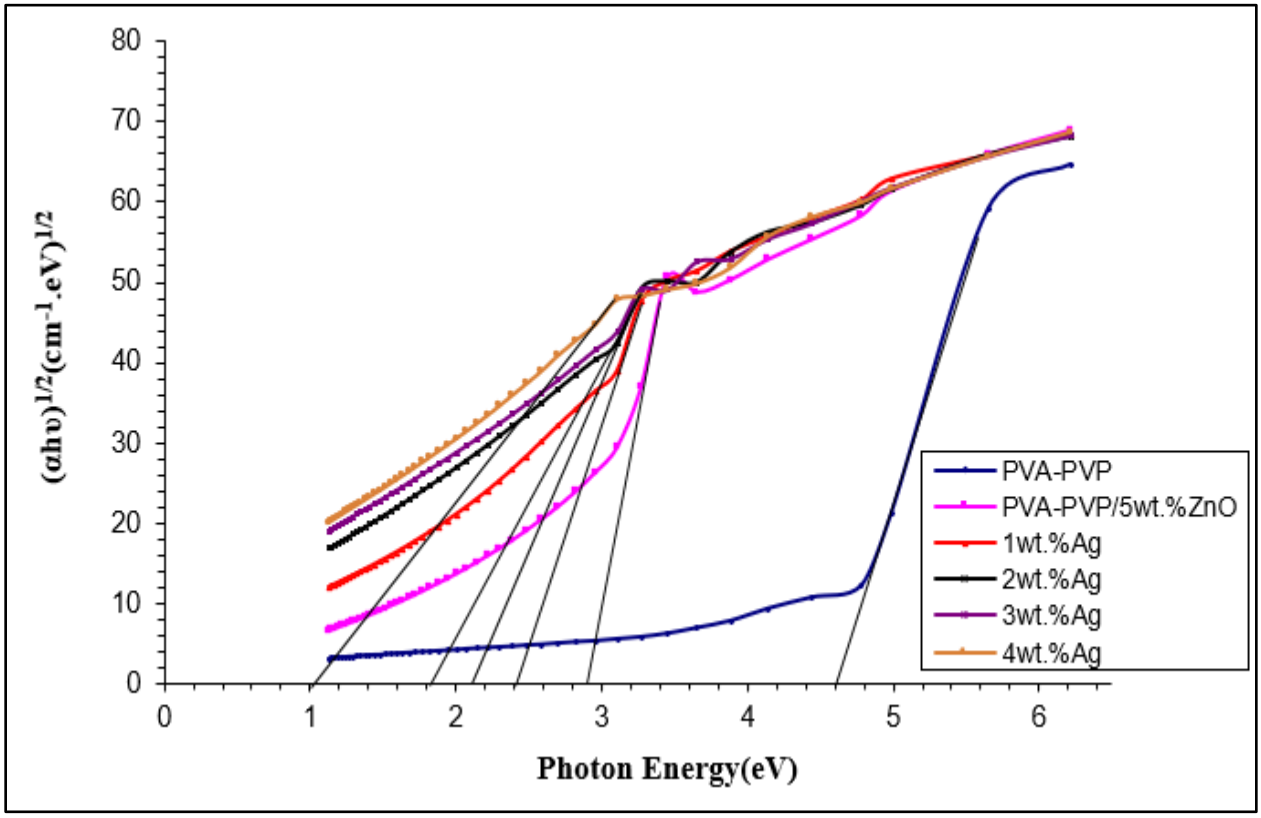

Fig. (4.8): Correlation between $(\alpha h\nu)^{1/2}$ vs. $(h\nu)$ for PVA-PVP blend and its NCs.

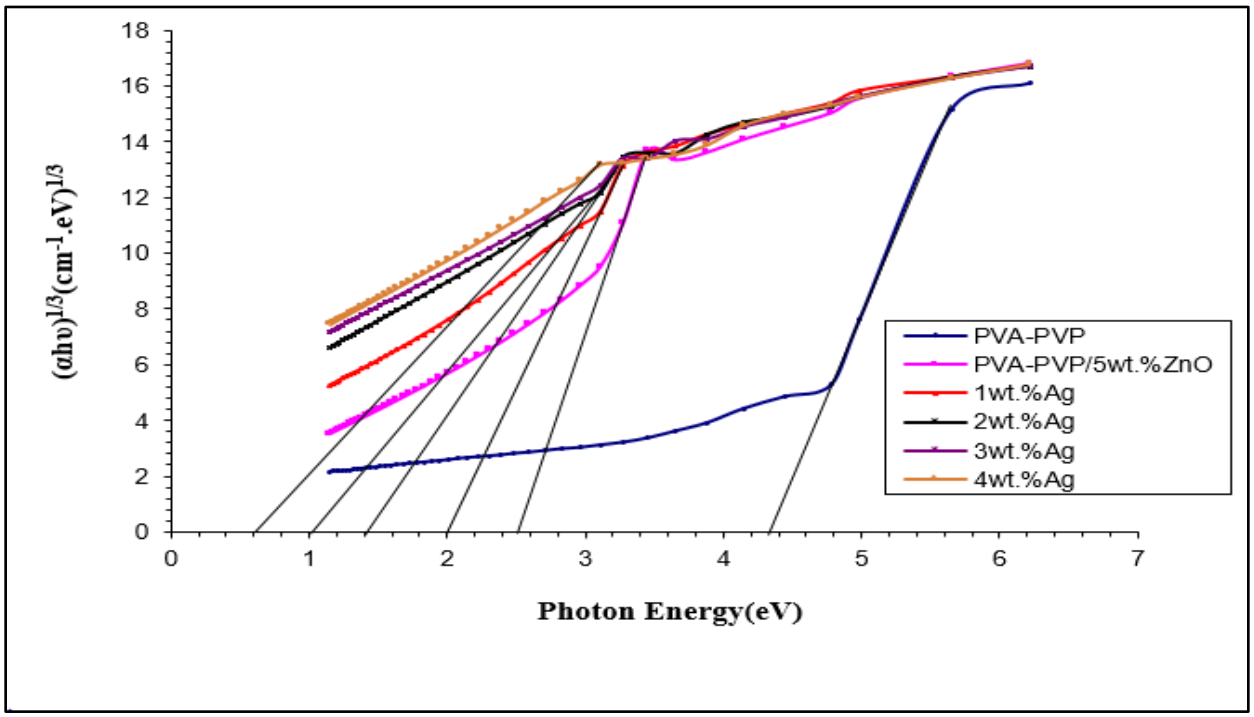

Fig. (4.9): Correlation between $(\alpha h\nu)^{1/3}$ vs. $(h\nu)$ for (PVA-PVP) blend and its NCs.

Table (4.1): E_g^{opt} values for indirect transition of (PVA-PVP) blend and its NCs.

Sample	Allowed (eV)	Forbidden (eV)
PVA-PVP	4.6	4.3
PVA-PVP/ ZnO	2.9	2.5
1wt.% Ag	2.4	2
2wt.% Ag	2.1	1.4
3wt.% Ag	1.8	1
4wt.% Ag	1	0.6

4.3.5 Refractive index(n), Polarizability(P), and extinction coefficient (K_o)

The Refractive Index (n), Polarizability (P) and Extinction Coefficient (K_o) of (PVA-PVP) polymer blend and its NCs with 5wt.% ZnO and different wt.% of

Ag films has been calculated from the eqs.(2.20), (2.22), and (2.24) respectively [96].

From the figure (4.10), it was found that the NC films is higher than that of pure blend in the Vis and NIR regions of the spectrum, due to the large index of Ag [97]. The decrease in refractive index values at UV region correlates with the behavior of the polarizability below.

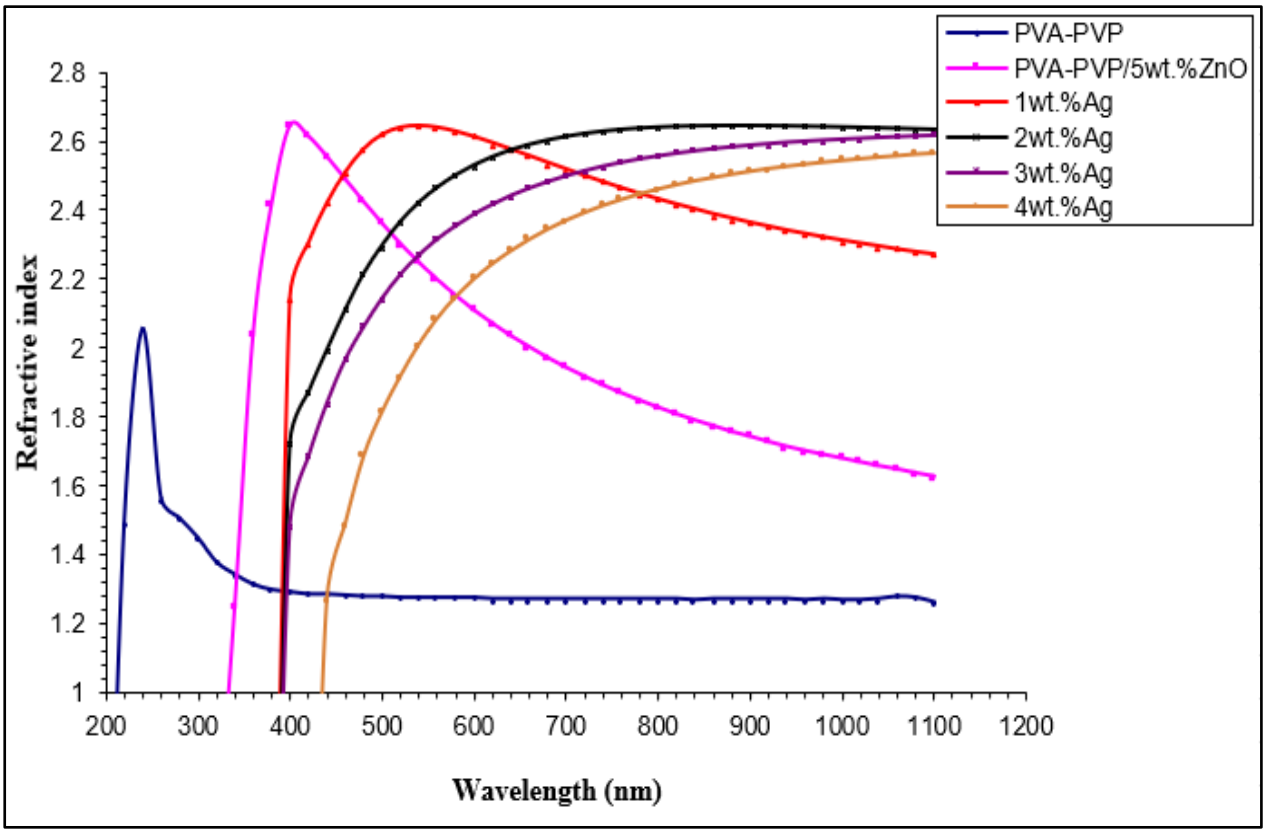

Fig. (4.10): Refractive index (n) of (PVA-PVP) blend and it's NCs with ZnO and different wt.% of Ag NPs.

From figure (4.11) it was found that P curves is identical to that of n, therefor the polarization follows the index of refractive. The refractive index is equal to 1 for materials that don't have any change in the speed of light. The polarizability increases with decreasing E_g^{opt} due to the transition of electrons to higher levels, therefore, the strength of its binding to the nucleus is small,

therefore P is greater. At UV region, a decrease in the polarization is due to the inability of the dipoles formed to keep up with the high frequency (low wavelength).

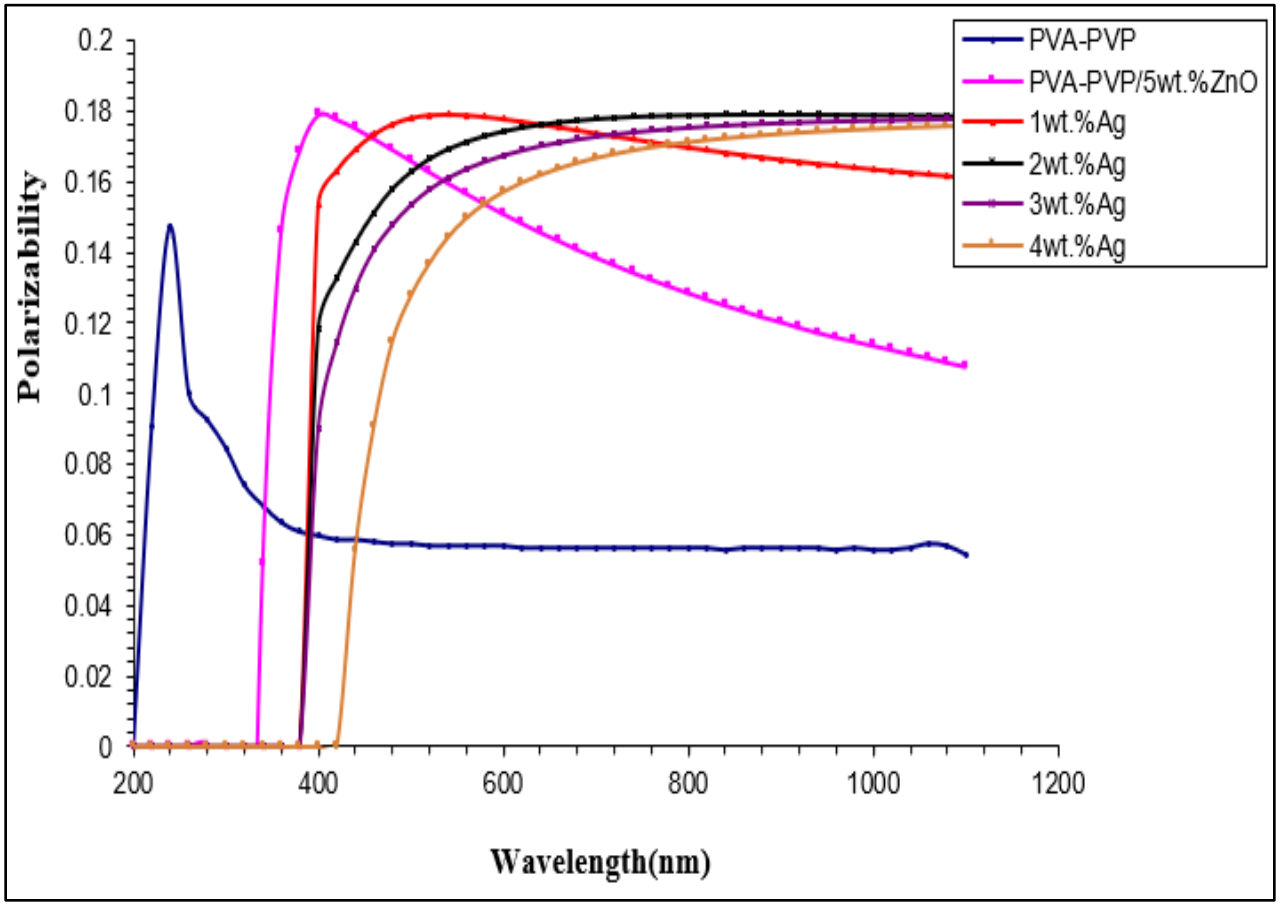

Fig. (4.11): Polarizability (P) of (PVA-PVP) blend and it's NCs with ZnO and different wt.% of Ag NPs.

From observation of the figure (4.12), it can be notice that the extinction coefficient results of the nanocomposites films are much larger than that of the pure polymer blend in all regions. This result was directly depended on the absorption of light.

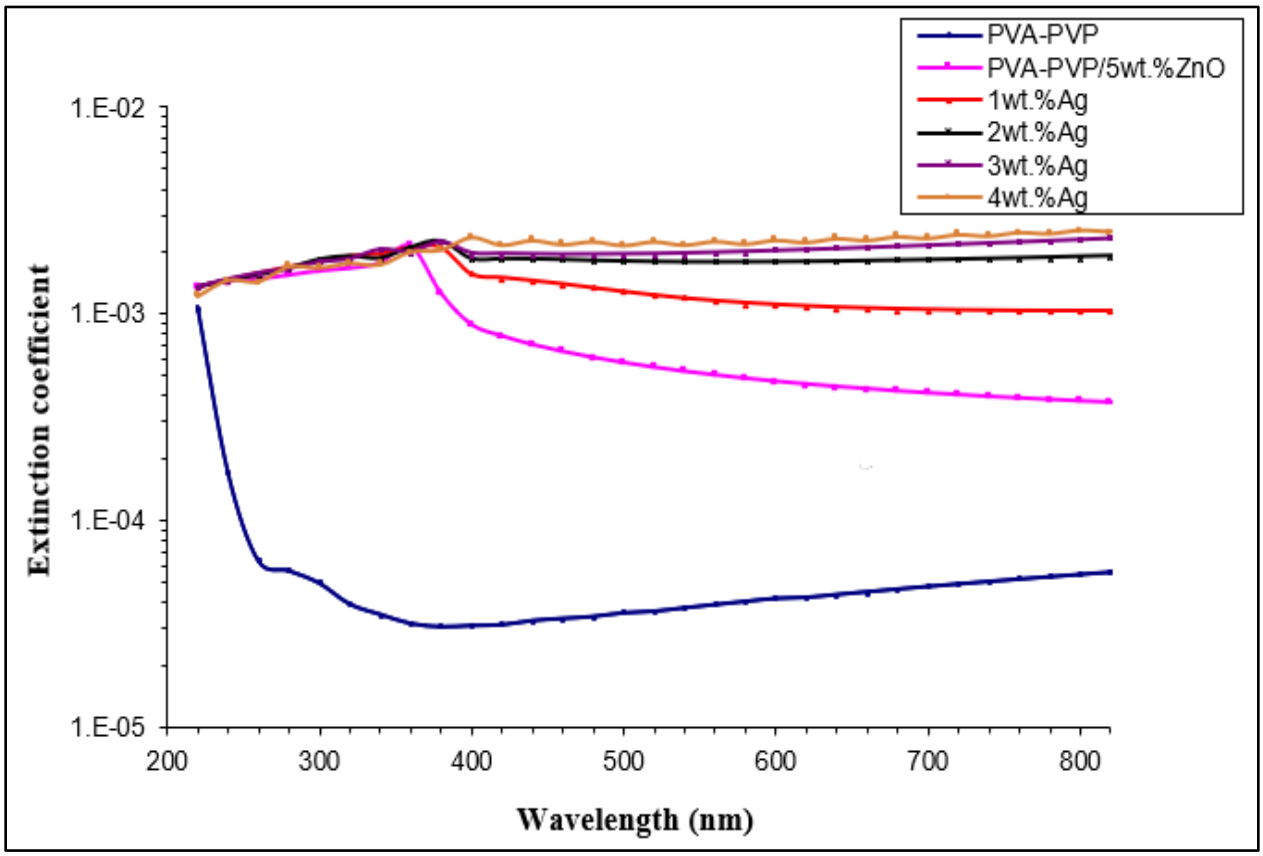

Fig. (4.12): Extinction coefficient of (PVA-PVP) blend and the NCs.

4.3.6 Real and imaginary parts of dielectric constant (ε_r, ε_i)

Figures (4.13) and (4.14) illustrated the variation of real ($\boldsymbol{\varepsilon_r}$) and imaginary ($\boldsymbol{\varepsilon_i}$) parts of the dielectric constant for pure polymer blend and its NC films with ZnO and different wt.% of Ag *NPs* as a function of wavelength. Equations (2.28) and (2.29) were used to obtain the real and imaginary dielectric constants. It can be seen from the figure that ($\boldsymbol{\varepsilon_r}$) considerably dependent on (n^2) due to the low value of (k^2). The real dielectric constant is increased with the increase of NPs [98]. ε_i is dependent on (k) values that are changing with the change of the absorption coefficient due to the relation between (α) and (k) [99].

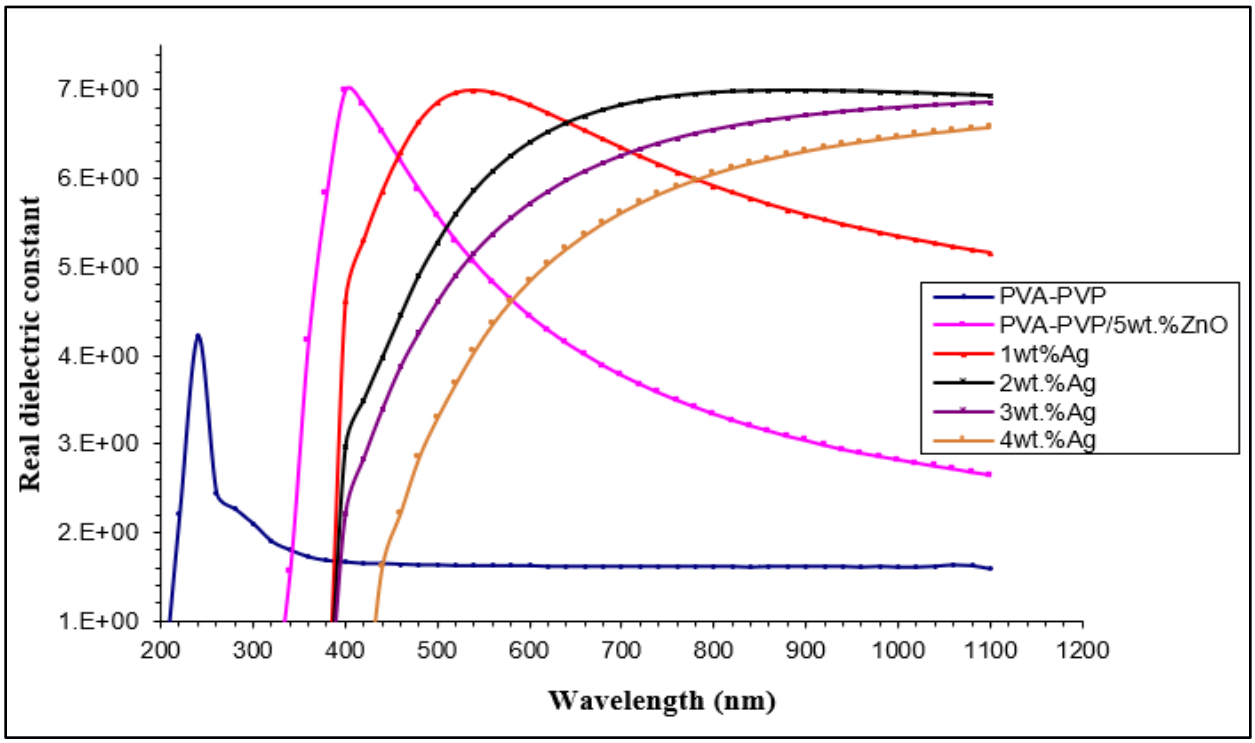

Fig. (4.13): ε_r of PVA-PVP and it's NCs with ZnO and various ratios of Ag NPs.

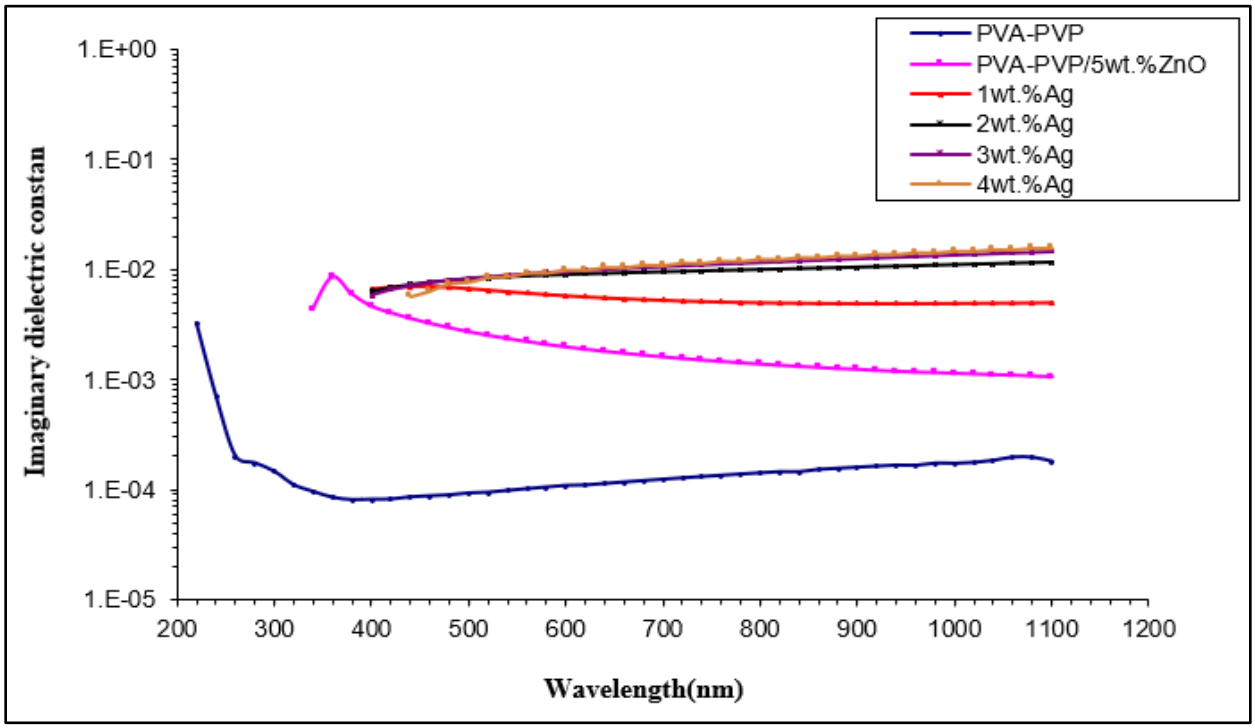

Fig. (4.14): ε_i of PVA- PVP and it's NCs with ZnO and various ratios of Ag NPs.

4.4 The A.C Electrical Properties

Dielectric constant, dielectric loss and A.C electrical conductivity for polymer blend and its NC films were studied in the RT over the frequency range 10^2 - 5×10^6 Hz. Figure (4.15) shows the dependence of dielectric constant on electric field frequency. Decreasing the dielectric constant with increasing frequency may be attributed to the tendencies of dipole in the samples for orienting themselves in the directions of the applied electrical fields and decreasing of space charge polarization. That means the space charge polarization becomes the more contributing type of polarization at low frequencies. The maximum dielectric constant, are (1.21, 1.24, 1.27, 1.29, 1.32 and 1.35) for polymer blend and its NCs with 5wt.% ZnO and different (1,2,3, and 4) wt.% of Ag NPs at 100Hz, respectively. The magnitude of dielectric constant indicates the ability of the material to store energy from the applied electric field. These are similar to the results of researcher [29].

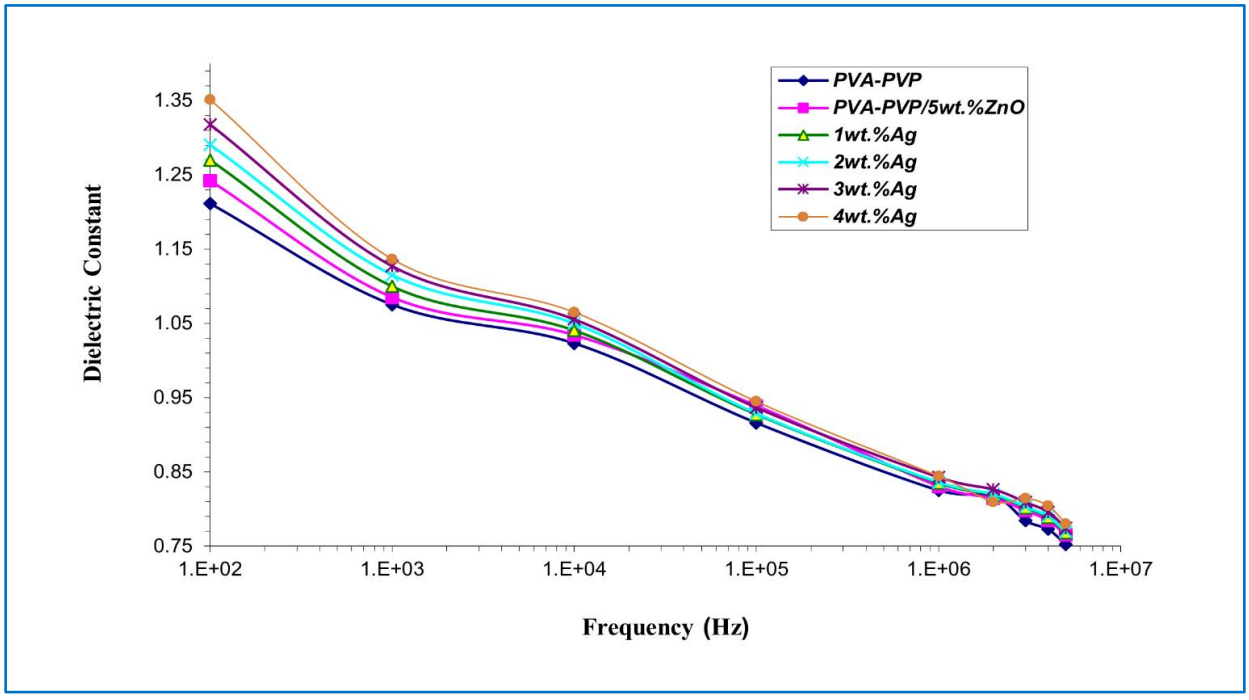

Fig. (4.15): Dependence dielectric constant from PVA-PVP on frequency and the additives NPs at RT.

The dielectric loss measures the lost electrical energy in the sample from the applied field which is transformed to thermal energy. The dependence of dielectric loss on electric field frequency range and the additives NPs (ZnO and Ag) for PVA-PVP blends at RT shown in figure (4.16). The maximum dielectric loss for pure polymer blend and its nanocomposites with 5wt.%ZnO and different (1, 2, 3, and 4) wt.% of Ag NPs at low frequency (100Hz), are (0.081, 0.090, 0.094, 0.099, 0.107 and 0.112) respectively, and decreases with increase the frequency of applied electric field. This behavior is attributed to a decrease of the space charge polarization contribution.

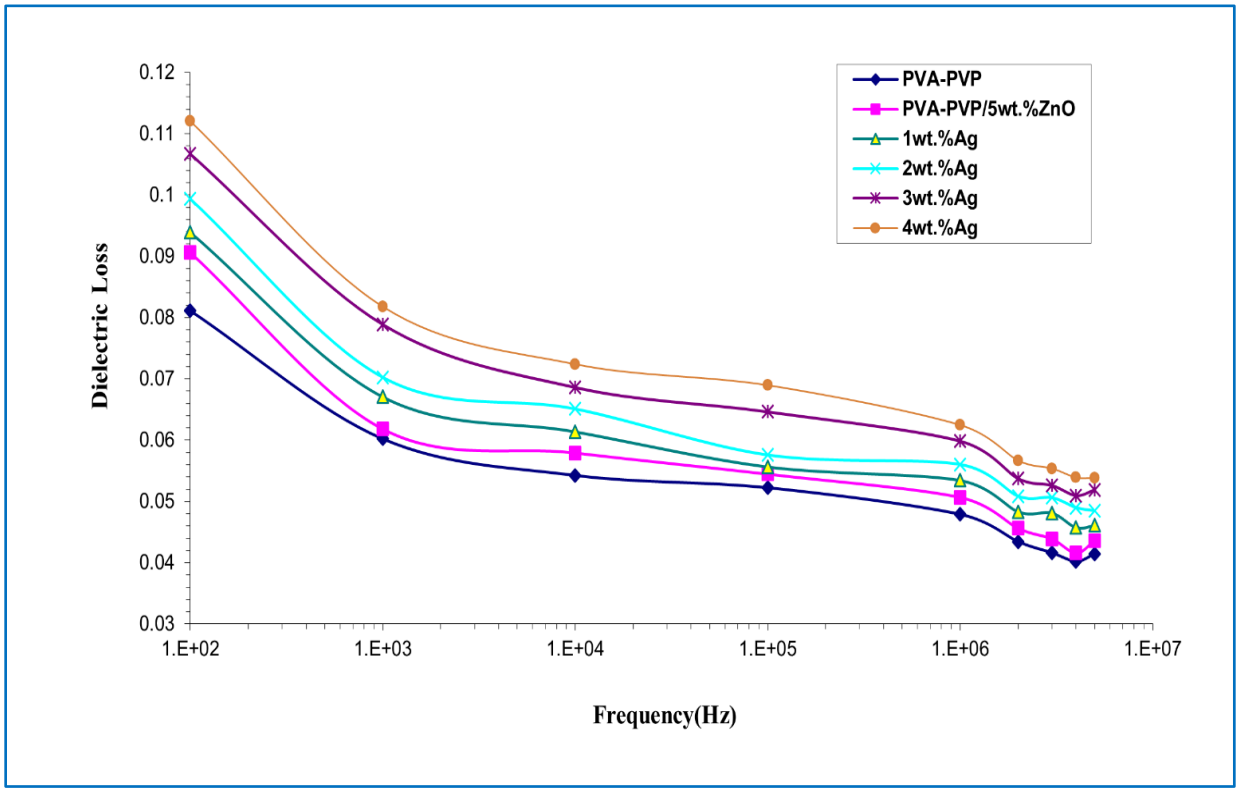

Fig. (4.16) dependence of dielectric loss of PVA-PVP blend on frequency and the additives NPs at RT.

The dependence of A.C electrical conductivity on electric field frequency range and the additives NPs (ZnO and Ag) for PVA-PVP blends at RT shown in figure (4.17). The A.C conductivity increases considerably with the increase of

electric field frequency for all samples. This is attributed to the space charge polarization at low frequencies, and to the motion of charge carriers by hopping process [100]. Also, the conductivity increases with the increasing of the wt.% of Ag NPs. This behavior is due to the effect of the space charge as a result of the increase the charge carriers, due to the regular distribution in the polymer matrix. This is in agreement with the results reached by the researcher [29].

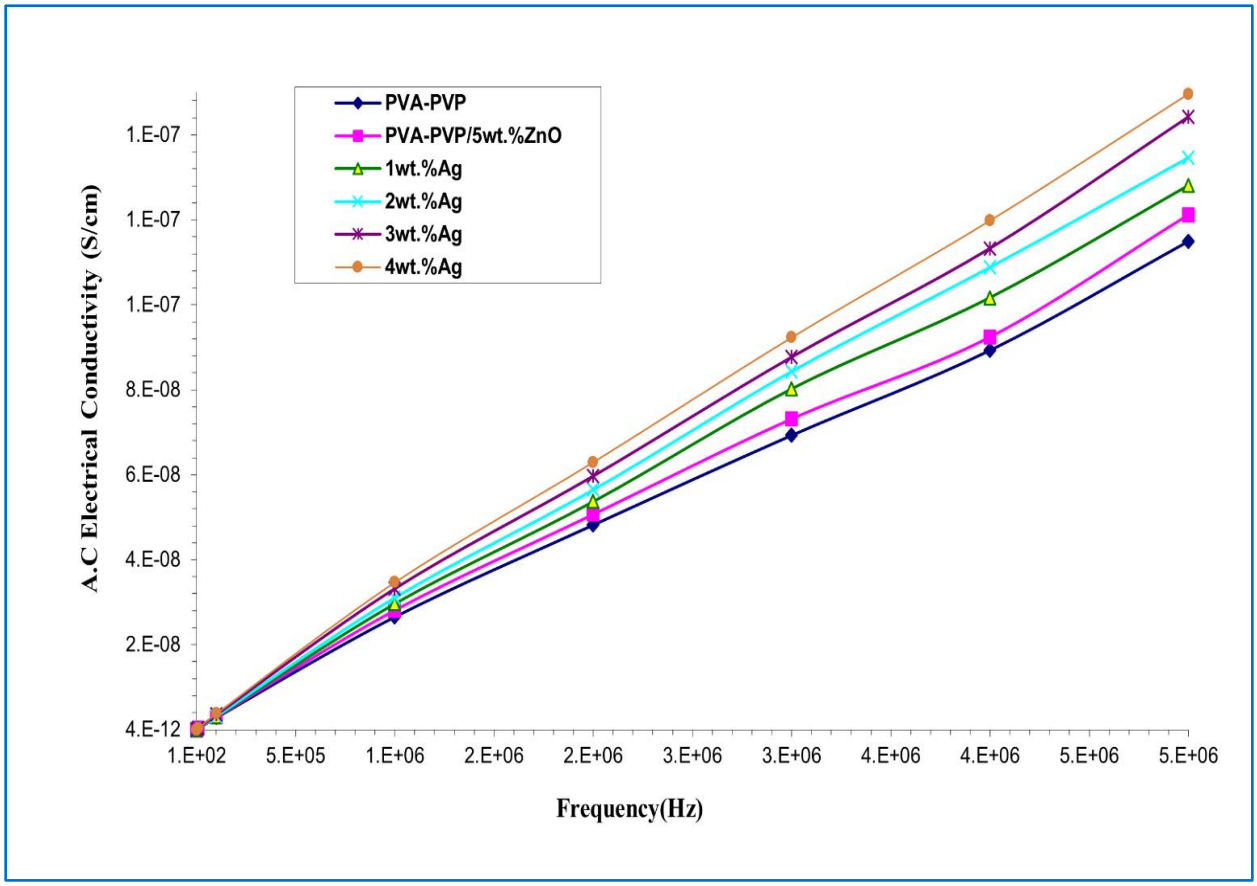

Fig. (4.17) The dependence of A.C electrical conductivity of (PVA-PVP) blend on frequency and additives NPs at RT.

4.5 Application of (PVA-PVP/ZnO and Ag) NCs for antibacterial activity

Nanoparticles are an attractive antibiotic choice because they have a broad spectrum antibacterial effect even at low concentrations [101]. PVA-PVP polymeric blend and its NCs with ZnO and different (1,2,3 and 4) wt.% of Ag NPs were used to study antibacterial activity towards two bacterial strains *Escherichia coli and Staphylococcus aureus* as showed in figure (4.18), were investigated by agar disk diffusion method and the antibacterial sensitivity was measured by determining the diameter of zones of inhibition in millimeter.

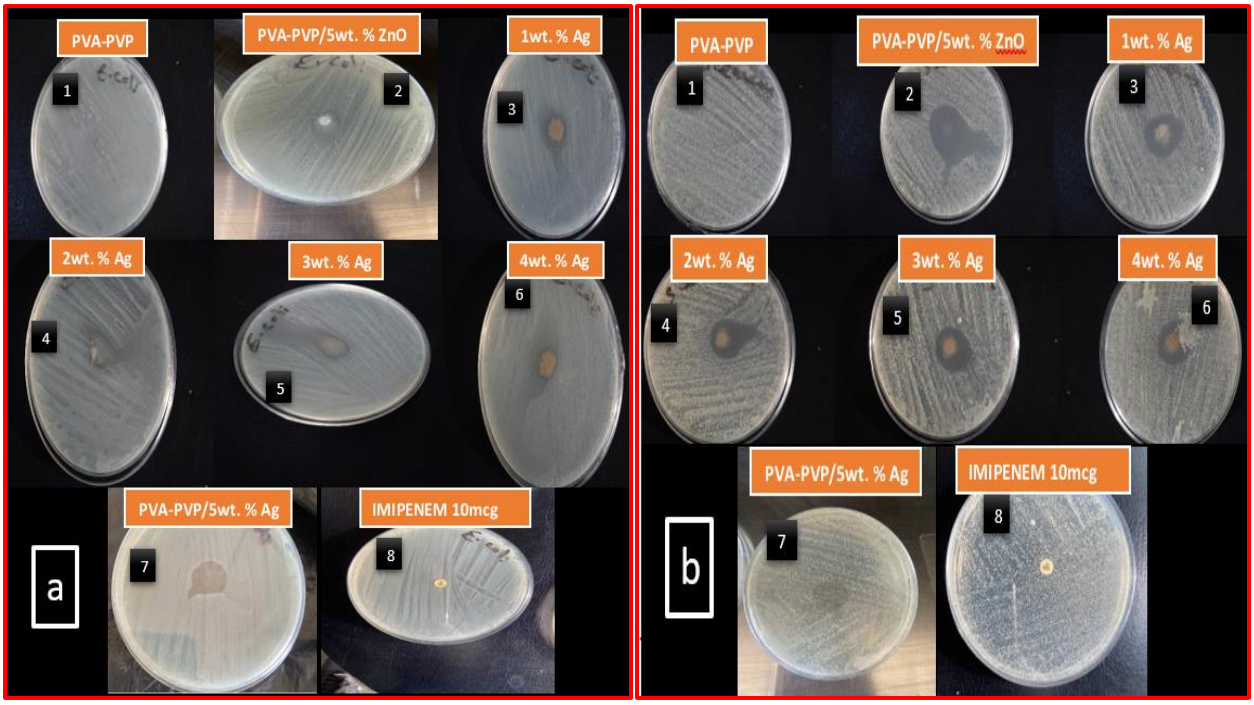

Fig. (4.18): Images for inhibition zones of PVA-PVP with ZnO and varied ratios of Ag nanocomposite films on (a) *E. coli* and (b) *S. aureus.*

The study showed that synthesized NC films have antibacterial effect against all tested bacteria, and at the same time the tested bacterial strains were not sensitive to the antibiotics (IMIPENEM 10mcg). Among the tested ratios of the synthesis pure PVA-PVP blend and its NCs with ZnO NPs and different wt.% of Ag NPs, best

growth inhibition was observed with ratio 4wt.% of Ag (34.567±3.066) against *E. coli* as tabulated in Table (4.3).

Furthermore it, the results showed that inhibition zone of *E. coli* bacteria increased by adding different ratios wt.% of Ag NPs, while the inhibition zone of *S. aureus* bacteria decreased with adding different ratios wt.% of Ag NPs. This result may be due to the difference of cell wall between gram-negative and gram-positive bacteria, so it is likely that the presence of Ag NPs with ZnO NPs on the polymer blend consisting of PVA-PVP reduces the inhibition activity of ZnO NPs for *S. aureus*, in contrast, their presence together increases the sensitivity of *E. coli* of NC films.

Table 4.2: Inhibition zones of NCs against different bacterial strains.

Zone of inhibition (diameter, mm)		
Bioactive agent	***E. Coli*** ***Mean±Sd***	***S. aureus*** ***Mean±Sd***
PVA-PVP	0.000±0.000 a	0.000±0.000 a
5wt.% ZnO	22.100±*2.762* b	31.600±8.062 e
5wt.% ZnO&1wt.% Ag	26.700±2.931 bcd	26.567±0.603 de
5wt.% ZnO&2wt.% Ag	30.500±2.451 cd	25.133±1.401 d
5wt.% ZnO&3wt.% Ag	33.633±4.123 cd	23.633±2.030 cd
5wt.% ZnO&4wt.% Ag	34.567±3.066 d	19.000±2.960 c
Anti IMIPENEM 10mcg	6.000±0.000 a	6.000±0.000 b
The similar letters of the vital coefficients indicate that there is no significant difference p>0.05		

The bacterial inhibition zone in *E. coli* colonies show's a significant difference between the pure polymer blend and its NCs also there are significant differences between ZnO at 5wt.% and the different ratios wt.% (2, 3, and 4) of Ag. While there are no significant differences among the other ratios.

The comparison between the pure polymer blend and its NCs for *S. aureus* showed significant differences ($p \leq 0.05$), also, there is a significant difference between ZnO at 5wt.% and the different ratios wt.% (2, 3, and 4) of Ag, significant differences was also found between 1wt.% of Ag and 4wt.% of Ag, finally there are significant differences between 2wt.% Ag and 4wt.% Ag. While there are no significant differences between the other materials ratios. It was also noted that there were significant differences between the antibiotic (IMIPENEM 10mcg) and the polymer with its NCs.

The ratios of silver NCs were correlated with the inhibition region in bacteria in a statistically significant manner as shown in figure (4.19 a and b), and it was found that the relationship was positively strong for *E. coli* bacteria, are illustrated in Table (4.3), this may be due to the synergistic effect, on the contrary, it was found that negative correlation between Ag ratios and the inhibition zone in bacteria *S. aureus* this may be due to the antagonistic effect, are illustrated in Table (4.4).

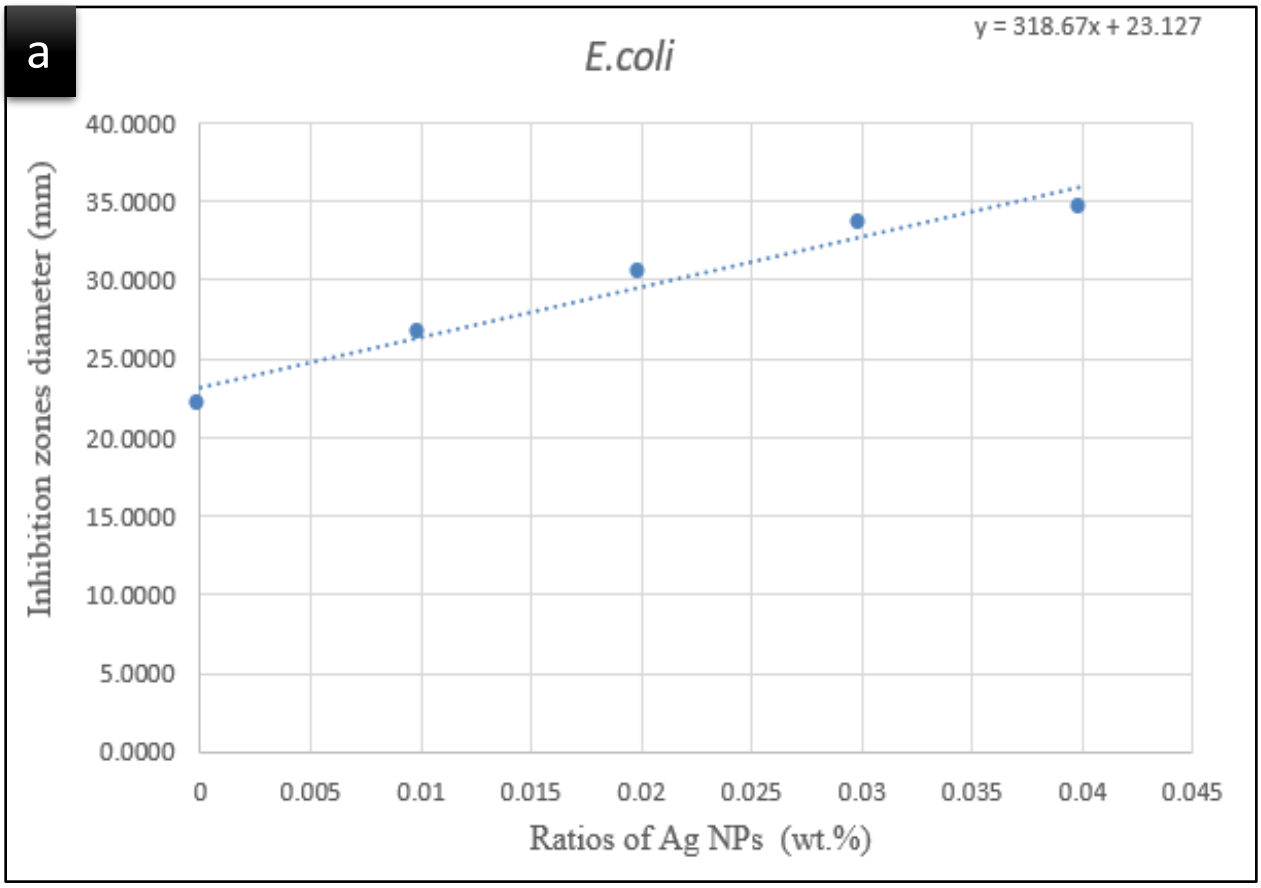
a
E.coli
y = 318.67x + 23.127
Inhibition zones diameter (mm)
40.0000
35.0000
30.0000
25.0000
20.0000
15.0000
10.0000
5.0000
0.0000
0
0.005
0.01
0.015
0.02
0.025
0.03
0.035
0.04
0.045
Ratios of Ag NPs (wt.%)

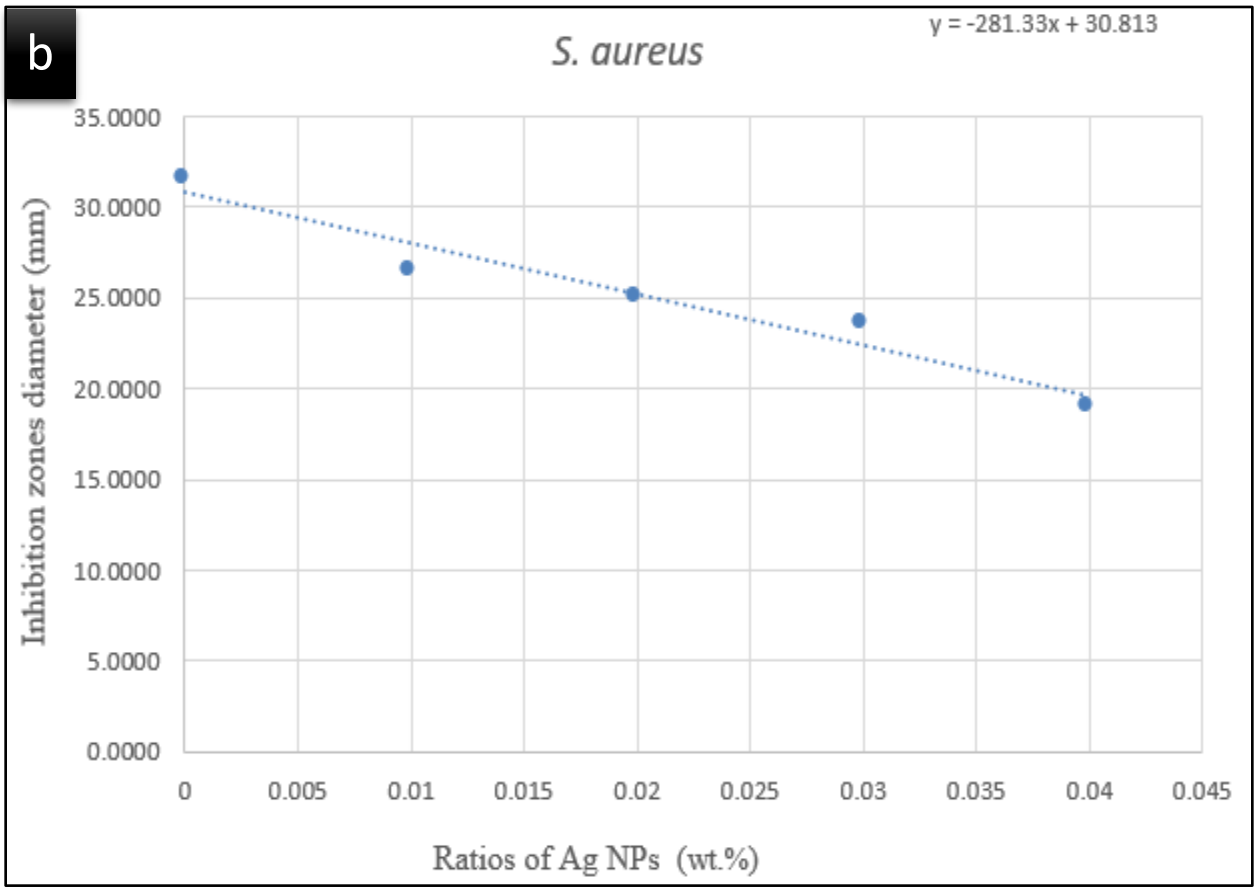

Fig. (4.19): correlation between Ag ratios and the inhibition zone in (a) *E. coli* and (b) *S. aureus.*

Table (4.3): Strong positive correlation in *E. coli* bacteria.

VAR00005	VAR00004	
.977**	1	Pearson Correlation VAR00004
.004		Sig. (2-tailed)
5	5	N
1	.977**	Pearson Correlation VAR00005
	.004	Sig. (2-tailed)
5	5	N

**. Correlation is significant at the 0.01 level (2-tailed).

Table (4.4): negative correlation between Ag ratios and the inhibition zone in bacteria *S. aureus.*

Correlations			
VAR00006	VAR00005		
-.972**	1	Pearson Correlation	VAR00005
.006		Sig. (2-tailed)	
5	5	N	
1	-.972**	Pearson Correlation	VAR00006
	.006	Sig. (2-tailed)	
5	5	N	

**. Correlation is significant at the 0.01 level (2-tailed).

4.6 Conclusions

At the end of the current study and based upon the experiment conducted and the results reach at, the following conclusions are put forward:

1. The FT-IR spectra indicates the presence of functional groups in polymer nanocomposite systems, and no obvious shifting is seen as a result of the addition of ZnO and different Ag ratios.
2. XRD measurements indicates the production of more crystalline nanocomposite films from the polymeric matrix.
3. FE-SEM images showed agglomeration of small and close packed group of elliptical particles in surface morphology as a result of adding different amount of nanoparticles.
4. The optical microscope images denote high homogeneity and fine distribution of ZnO, Ag NPs.
5. The optimal value of transmittance for polymer blend film is about 98% in the regions Vis and NIR, reduced the transmittance of the nanocomposite films towards ultraviolet rays qualifies it to be used as a packaging for storage drugs. The indirect allowed and forbidden transition energy gaps values decrease with increasing the Ag NPs content. All other parameters under search are also affected by the level of additives.
6. The dielectric constant and dielectric loss for all various weight percents of Ag particles decreases as the electric field frequency increases, according to the AC electrical characteristics.
7. The nanocomposite films have antibacterial activity for *S. aureus* and *E. coli*.

8. The work combines medical physics and nano technology, perform probable it can contribute significantly to the elimination of bacteria that are infectious and toxic to humans.

4.7 Future Works

Below are some ideas for future work to be conducted:

1. Study the mechanical properties (PVA-PVP/ ZnO and Ag) nanocomposites.

2. Study the thermal properties of (PVA-PVP/ ZnO and Ag) nanocomposites for energy storage and other thermal applications.

3. A study of the pressure sensors application of the (PVA-PVP/ZnO and Ag) nanocomposites.

References

[1] M. S. Jalil, “Physical Properties, Antibacterial and Antibiofilm Activities of PVA Polymer with Safranin Dye and Biosurfactant.” Ph. D Thesis, College of Science, Al-Mustansiriyah University, 2015.

[2] D. R. Paul and L. M. Robeson, “Polymer nanotechnology: nanocomposites,” *Polymer (Guildf).*, vol. 49, no. 15, pp. 3187–3204, 2008.

[3] J. E. Mark, *Physical properties of polymers handbook*, vol. 1076. Springer, 2007.

[4] A. P. Mouritz and A. G. Gibson, *Fire properties of polymer composite materials*, vol. 143. Springer Science & Business Media, 2007.

[5] S. Kubo and J. F. Kadla, “The formation of strong intermolecular interactions in immiscible blends of poly (vinyl alcohol)(PVA) and lignin,” *Biomacromolecules*, vol. 4, no. 3, pp. 561–567, 2003.

[6] B. Ben Doudou, A. Vivet, J. Chen, A. Laachachi, T. Falher, and C. Poilâne, “Hybrid carbon nanotube—silica/polyvinyl alcohol nanocomposites films: preparation and characterisation,” *J. Polym. Res.*, vol. 21, no. 4, pp. 1–9, 2014.

[7] B. M. Baraker and B. Lobo, “Experimental study of PVA-PVP blend films doped with cadmium chloride monohydrate,” 2016.

[8] E. M. Abdelrazek, I. S. Elashmawi, A. El-Khodary, and A. Yassin, “Structural, optical, thermal and electrical studies on PVA/PVP blends filled with lithium bromide,” *Curr. Appl. Phys.*, vol. 10, no. 2, pp. 607–613, 2010.

[9] A. H. O. Al-khayatt and M. D. Jaafer, “Annealing effect on the structural and optical properties of CuS thin film prepared by Chemical Bath Deposition (CBD),” *J. Kufa–Physics*, vol. 5, no. 1, pp. 79–90, 2013.

[10] K. K. Sadasivuni, D. Ponnamma, H.-U. Ko, H. C. Kim, L. Zhai, and J. Kim, “Flexible NO_2 sensors from renewable cellulose nanocrystals/iron oxide composites,” *Sensors Actuators B Chem.*, vol. 233, pp. 633–638, 2016.

[11] K. M. Reddy, K. Feris, J. Bell, D. G. Wingett, C. Hanley, and A. Punnoose, “Selective toxicity of zinc oxide nanoparticles to prokaryotic and eukaryotic systems,” *Appl. Phys. Lett.*, vol. 90, no. 21, p. 213902, 2007.

[12] D. S. Blanc, P. H. Carrara, G. Zanetti, and P. Francioli, “Water disinfection with ozone, copper and silver ions, and temperature increase to control Legionella: seven years of experience in a university teaching hospital,” *J. Hosp. Infect.*, vol. 60, no. 1, pp. 69–72, 2005.

[13] C. Zeitlin, S. B. Guetersloh, L. H. Heilbronn, and J. Miller, “Measurements of materials shielding properties with 1 GeV/nuc 56Fe,” *Nucl. Instruments Methods Phys. Res. Sect. B Beam Interact. with Mater. Atoms*, vol. 252, no. 2, pp. 308–318, 2006.

[14] A. K. Bajpai, S. K. Shukla, S. Bhanu, and S. Kankane, “Responsive polymers in controlled drug delivery,” *Prog. Polym. Sci.*, vol. 33, no. 11, pp. 1088–1118, 2008.

[15] A. Khan, “CdS nanoparticles with a thermoresponsive polymer: synthesis and properties,” *J. Nanomater.*, vol. 2012, 2012.

[16] D. Kim, S. Jeong, and J. Moon, “Synthesis of silver nanoparticles using the polyol process and the influence of precursor injection,” *Nanotechnology*, vol. 17, no. 16, p. 4019, 2006.

[17] A. A. ElBellihi, W. A. Bayoumy, E. M. Masoud, and M. A. Mousa, “Preparation, characterizations and conductivity of composite polymer electrolytes based on PEO-LiClO 4 and Nano ZnO filler,” *Bull. Korean Chem. Soc.*, vol. 33, no. 9, pp. 2949–2954, 2012.

[18] E. M. Masoud, “Montmorillonite incorporated polymethylmethacrylate matrix containing lithium trifluoromethanesulphonate (LTF) salt: thermally stable polymer nanocomposite electrolyte for lithium-ion batteries application,” *Ionics (Kiel).*, vol. 25, no. 6, pp. 2645–2656, 2019.

[19] R. K. Goyal, *Nanomaterials and nanocomposites: synthesis, properties, characterization techniques, and applications*. CRC Press, 2017.

[20] T. A. Söderberg, B. Sunzel, S. Holm, T. Elmros, G. Hallmans, and S. Sjöberg, “Antibacterial effect of zinc oxide in vitro,” *Scand. J. Plast. Reconstr. Surg. hand Surg.*, vol. 24, no. 3, pp. 193–197, 1990.

[21] Q. L. Feng T. N. Kimb, J. Wua, E. S. Parkb, J. Ock Kimb, D. Y. Limb, F. Z. Cuia, “Antibacterial effects of Ag-HAp thin films on alumina substrates,” *Thin Solid Films*, vol. 335, no. 1–2, pp. 214–219, 1998.

[22] Q. Feng, Z. Dang, N. Li, and X. Cao, "Preparation and dielectric property of Ag–PVA nano-composite," *Mater. Sci. Eng. B*, vol. 99, no. 1–3, pp. 325–328, 2003.

[23] Y. H. Kim, D. K. Lee, H. G. Cha, C. W. Kim, and Y. S. Kang, "Synthesis and characterization of antibacterial Ag− SiO_2 nanocomposite," *J. Phys. Chem. C*, vol. 111, no. 9, pp. 3629–3635, 2007.

[24] Z. A. Al-Ramadhan, J. A. Salman, and H. A. K. Hmud, "Optical and morphological properties of (PVA-PVP-Ag) Nanocomposites," *Int. J. Sci. Res.*, vol. 5, pp. 1828–1836, 2016.

[25] M. T. Ramesan, M. Varghese, and P. Periyat, "Silver-doped zinc oxide as a nanofiller for development of poly (vinyl alcohol)/poly (vinyl pyrrolidone) blend nanocomposites," *Adv. Polym. Technol.*, vol. 37, no. 1, pp. 137–143, 2018.

[26] M. Teodorescu, M. Bercea, and S. Morariu, "Biomaterials of PVA and PVP in medical and pharmaceutical applications: Perspectives and challenges," *Biotechnol. Adv.*, vol. 37, no. 1, pp. 109–131, 2019.

[27] A. M. Ismail, M. I. Mohammed, and E. G. El-Metwally, "Influence of Gamma irradiation on the structural and optical characteristics of Li ion-doped PVA/PVP solid polymer electrolytes," *Indian J. Phys.*, vol. 93, no. 2, pp. 175–183, 2019.

[28] P. Panchal, D. R. Paul, A. Sharma, P. Choudhary, P. Meena, and S. P. Nehra, "Biogenic mediated Ag/ZnO nanocomposites for photocatalytic and antibacterial activities towards disinfection of water," *J. Colloid Interface Sci.*, vol. 563, pp. 370–380, 2020.

[29] H. H. Jassim and F. S. Hashim, "Synthesis of (PVA/PEG: ZnO and Co_3O_4) Nanocomposites: Characterization and Gamma Ray Studies," *NeuroQuantology*, vol. 19, no. 4, p. 47, 2021.

[30] A. Muheisin, "Study of electrical conductivity for amorphous and semi crystalline polymers filled with Lithium Fluoride Additive," M. Sc. Thesis, University of Mustansiriah, College of Science, 2009.

[31] G.Akovali, *Hand Book of Composites Fabrication*. Ankara,Turkea, 2001.

[32] F. Haaf, A. Sanner, and F. Straub, "Polymers of N-vinylpyrrolidone: synthesis, characterization and uses," *Polym. J.*, vol. 17, no. 1, pp. 143–152, 1985.

[33] F. Hussain, M. Hojjati, M. Okamoto, and R. E. Gorga, "Polymer-matrix nanocomposites, processing, manufacturing, and application: an overview," *J. Compos. Mater.*, vol. 40, no. 17, pp. 1511–1575, 2006.

[34] G. A. Mansoori and T. A. F. Soelaiman, *Nanotechnology An introduction for the standards community*. ASTM International, 2005.

[35] R. Oslanec, A. C. Costa, R. J. Composto, and P. Vlcek, "Effect of block copolymer adsorption on thin film dewetting kinetics," *Macromolecules*, vol. 33, no. 15, pp. 5505–5512, 2000.

[36] A. Gautam and S. Ram, "Preparation and thermomechanical properties of Ag-PVA nanocomposite films," *Mater. Chem. Phys.*, vol. 119, no. 1–2, pp. 266–271, 2010.

[37] J. E. Mark, *Polymer data handbook*. New York : Oxford University Press, 1999.

[38] J. Tao, "Effects of Molecular weight and Solution Concentration on Electrospinning of PVA," *Worcester Polytech. Institute, USA*, 2003.

[39] K. H. H. Al-Attiyah, A. Hashim, and S. F. Obaid, "Fabrication of novel (carboxy methyl cellulose–polyvinylpyrrolidone–polyvinyl alcohol)/lead oxide nanoparticles: structural and optical properties for gamma rays shielding applications," *Int. J. Plast. Technol.*, vol. 23, no. 1, pp. 39–45, 2019.

[40] H.-D. Wu, I.-D. Wu, and F.-C. Chang, "The interaction behavior of polymer electrolytes composed of poly (vinyl pyrrolidone) and lithium perchlorate ($LiClO_4$)," *Polymer (Guildf).*, vol. 42, no. 2, pp. 555–562, 2001.

[41] M. T. Razzak, S. P. Dewi, H. Lely, and E. Taty, "The characterization of dressing component materials and radiation formation of PVA–PVP hydrogel," *Radiat. Phys. Chem.*, vol. 55, no. 2, pp. 153–165, 1999.

[42] R. M. Tilaki and S. M. Mahdavi, "Stability, size and optical properties of silver nanoparticles prepared by laser ablation in different carrier media," *Appl. Phys. A*, vol. 84, no. 1, pp. 215–219, 2006.

[43] T. Klaus-Joerger, R. Joerger, E. Olsson, and C.-G. Granqvist, "Bacteria as workers in the living factory: metal-accumulating bacteria and their potential for materials science," *TRENDS Biotechnol.*, vol. 19, no. 1, pp. 15–20, 2001.

[44] L. H. K. S. Chandravathanam, V. Chidambaram, M. Helen, S. P.Indra Neel , C.M. Janet , P. S. Kishore, G. Mahesh, T. Maiy-alagan, and and B. V. Navaladian , J. Rajeswari , M.Sankaran, M. Sathiesh, Ch.Venkateswara Rao, *Nanomaterials - A Sojourn*. National Centre for Catalysis Research Department of chemistry, 2006.

[45] Ü. Özgür Ya. I. Alivov, C. Liu, A. Teke, M. A. Reshchikov, S. Doğan, V. Avrutin, S.-J. Cho, and H. Morkoç, "A comprehensive review of ZnO materials and devices," *J. Appl. Phys.*, vol. 98, no. 4, p. 11, 2005.

[46] A. Hezam, K. Namratha, Q. A. Drmosh,b Deepalekshmi Ponnamma, Adel Morshed Nagi Saeed, V. Ganesh, B. Neppolian and K. Byrappa, "Direct Z-scheme Cs_2 O–Bi_2O_3–ZnO heterostructures for photocatalytic overall water splitting," *J. Mater. Chem. A*, vol. 6, no. 43, pp. 21379–21388, 2018.

[47] J. Y. W. and R. P. H. C. H. Cao, Y.G. Zhao, H.C.Ong, S.T.Ho, J.Y.Dai, "Applied Physics Letters," 25, 1998.

[48] R. Ghosh, S. Fujihara, and D. Basak, "Studies of the optoelectronic properties of ZnO thin films," *J. Electron. Mater.*, vol. 35, no. 9, pp. 1728–1733, 2006.

[49] A. Bakin, A. El-Shaer, A. C. Mofor, M. Al-Suleiman, E. Schlenker, and A. Waag, "ZnMgO-ZnO quantum wells embedded in ZnO nanopillars: Towards realisation of nano-LEDs," *Phys. status solidi c*, vol. 4, no. 1, pp. 158–161, 2007.

[50] D. B. Murphy, *Fundamentals of light microscopy and electronic imaging*. John Wiley & Sons, 2002.

[51] S.-N. Wang, F.-D. Zhang, A.-M. Huang, and Q. Zhou, "Distinction of four Dalbergia species by FTIR, 2nd derivative IR, and 2D-IR spectroscopy of their ethanol-benzene extractives," *Holzforschung*, vol. 70, no. 6, pp. 503–510, 2016.

[52] W. S. Lau, *Infrared characterization for microelectronics*. World scientific, 1999.

[53] A. A. Bunaciu, E. G. UdriŞTioiu, and H. Y. Aboul-Enein, "X-ray diffraction: instrumentation and applications," *Crit. Rev. Anal. Chem.*, vol. 45, no. 4, pp. 289–299, 2015.

[54] L. Reimer, *Transmission electron microscopy: physics of image formation and microanalysis*, vol. 36. Springer, 2013.

[55] C. J. Brinker and G. Cao, "Annual Review of Nano Research," 2006.

[56] Y. I. Sirotin and M. P. Shaskolskaya, "Fundamentals of Crystal Physics, Mir Publ." Moscow, 1982.

[57] C. Kittle, *Introduction to Solid State Physics*. John Wiley and Sons Inc., 2005.

[58] S. L. Erlandsen, C. Frethem, and Y. Chen, "Field emission scanning electron microscopy (FESEM) entering the 21st century: nanometer resolution and molecular topography of cell structure," *J. Histotechnol.*, vol. 23, no. 3, pp. 249–259, 2000.

[59] O. Stenzel, *The physics of thin film optical spectra*. Springer, 2015.

[60] M. A. Omar, *Elementary solid state physics*. Addison-Wesley Pub. Co., 1975.

[61] T. K. Hamad, "Refractive index dispersion and analysis of the optical parameters of (PMMA/PVA) Thin film," *Al-Nahrain J. Sci.*, vol. 16, no. 3, pp. 164–170, 2013.

[62] D. A. Neamen, *Semiconductor physics and devices*. Mexico: Irwin, 1992.

[63] J. I. Pankove, *Optical processes in semiconductors*. New York, 1971.

[64] A. M. I. F.H. Abdi El-kidder, N.A. Hakeem, I.S Ela Shumway, "Structural, Optical and Thermal Characterization of ZnO Nanoparticles Doped in PEO/PVA Blend Films," *Aust. J. Basic Appl. Sci.*, vol. 7, no. 10, pp. 608–619, 2013.

[65] G. B. S. man C.M Wolfe, N. Hoouyak, *Physical Properties of Semiconductors*. Harlow, United Kingdom: Pearson Education Limited, 1989.

[66] J. Tauc, A. Menth, and D. L. Wood, "Optical and magnetic investigations of the localized states in semiconducting glasses," *Phys. Rev. Lett.*, vol. 25, no. 11, p. 749, 1970.

[67] K. L. Chopra, P. D. Paulson, and V. Dutta, "Thin-film solar cells: an overview," *Prog. Photovoltaics Res. Appl.*, vol. 12, no. 2-3, pp. 69–92, 2004.

[68] H. A. Macleod, *Thin Film Optical Filter*. New York, 2001.

[69] A. Loopy, *Microwaves in organic synthesis*. Germany, 2006.

[70] N. A. Azahari, N. Othman, and H. Ismail, "Biodegradation studies of polyvinyl alcohol/corn starch blend films in solid and solution media," *J. Phys. Sci.*, vol. 22, no. 2, pp. 15–31, 2011.

[71] M. Y. Nadeem and W. Ahmed, "Optical properties of ZnS thin films," *Turkish J. Phys.*, vol. 24, no. 5, pp. 651–659, 2000.

[72] M. Ghanipour and D. Dorranian, "Effect of Ag-nanoparticles doped in polyvinyl alcohol on the structural and optical properties of PVA films," *J. Nanomater.*, vol. 2013, 2013.

[73] M. Davies, N. Hill, W. E. Vaughan, and A. H. Price, "Dielectric properties and molecular behaviour," *Hill,.., Vaughan, WE, Price, AH, Davies, M., Eds*, 1969.

[74] K. Obeid, "Preparation and Study Some of Electrical and Thermal Properties of a Nematic Liquid Crystal Material Prepared from Schiff Bases and Some its Complexes." M. Sc. Thesis, Babylon University, College of Science, 2010.

[75] H. Fröhlich, *Theory of dielectrics: dielectric constant and dielectric loss*, vol. 190. Oxford University Press, USA, 1958.

[76] L.L.Hench and and J. K. West, *Principles of Electronic Ceramics*. New York, United States: John Wiley and Sons Ltd, 1990.

[77] R. C. Dorf, *The Electrical Engineering Hand Book*. New Jersey, USA: CRC Press LLC, 2000.

[78] R. S. Al-Khafaji, "Study the Effect of Iraqi Bentonite Clay addition on the Properties of Porcelain Body Prepared from Local Clays," PhD. Thesis, College of Education/Ibn Al-Haithem, University of Baghdad,Iraq, 2009.

[79] A. R. Blythe, T. Blythe, and D. Bloor, *Electrical properties of polymers*. Cambridge university press, 2005.

[80] H. Li, Q. Chen, J. Zhao, and K. Urmila, "Enhancing the antimicrobial activity of natural extraction using the synthetic ultrasmall metal nanoparticles," *Sci. Rep.*, vol. 5, no. 1, pp. 1–13, 2015.

[81] I. Armentano, C. R. Arciola, E. Fortunati, D. Ferrari, S. Mattioli, C. F. Amoroso, J. Rizzo, Jose M. Kenny, M. Imbriani, and L. Visai, "The interaction of bacteria with engineered nanostructured polymeric materials: a review," *Sci. World J.*, vol. 2014, 2014.

[82] W. Gao, S. Thamphiwatana, P. Angsantikul, and L. Zhang, "Nanoparticle approaches against bacterial infections," *Wiley Interdiscip. Rev. nanomedicine nanobiotechnology*, vol. 6, no. 6, pp. 532–547, 2014.

[83] B. Luan, T. Huynh, and R. Zhou, "Complete wetting of graphene by biological lipids," *Nanoscale*, vol. 8, no. 10, pp. 5750–5754, 2016.

[84] A. Raghunath and E. Perumal, "Metal oxide nanoparticles as antimicrobial agents: a promise for the future," *Int. J. Antimicrob. Agents*, vol. 49, no. 2, pp. 137–152, 2017.

[85] W. Levinson and E. Jawetz, *Medical microbiology & immunology: examination & board review*, 7th edition. New York: McGraw-Hill, 2002.

[86] A. Y. Itah and J. P. Essien, "Growth profile and hydrocarbonoclastic potential of microorganisms isolated from tarballs in the Bight of Bonny, Nigeria," *World J. Microbiol. Biotechnol.*, vol. 21, no. 6, pp. 1317–1322, 2005.

[87] Z. L. Wang, "Zinc oxide nanostructures: growth, properties and applications," *J. Phys. Condens. matter*, vol. 16, no. 25, p. R829, 2004.

[88] A. M. Cole, S. TAHK, A. OREN, D. YOSHIOKA, Y. KIM, A. PARK, and T. GANZ, "Determinants of Staphylococcus aureus nasal carriage," *Clin. Diagnostic Lab. Immunol.*, vol. 8, no. 6, pp. 1064–1069, 2001.

[89] O. P. Sah, "Prescribing and sensitivity patterns of antimicrobials in uncomplicated urinary tract infections in females," *J. Drug Deliv. Ther.*, vol. 4, no. 2, pp. 1–8, 2014.

[90] P. R. Murray, E. J. Baron, J. H. Jorgensen, M. L. Landry, and M. A. Pfaller, *Manual of clinical microbiology*, 9th ed. Washington, D.C. : ASM Press, 2007.

[91] A. L. Cogen, V. Nizet, and R. L. Gallo, "Skin microbiota: a source of disease or defence?," *Br. J. Dermatol.*, vol. 158, no. 3, pp. 442–455, 2008.

[92] K. R. Park and Y. C. Nho, "Preparation and characterization by radiation of hydrogels of PVA and PVP containing Aloe vera," *J. Appl. Polym. Sci.*, vol. 91, no. 3, pp. 1612–1618, 2004.

[93] F. Khan, S.-H. Baek, and J. H. Kim, "Enhanced charge transport properties of Ag and Al co-doped ZnO nanostructures via solution process," *J. Alloys Compd.*, vol. 682, pp. 232–237, 2016.

[94] H. Miyazaki, Y. Teranishi, and T. Ota, "Fabrication of uv-opaque and visible-transparent composite film," *Sol. energy Mater. Sol. cells*, vol. 90, no. 16, pp. 2640–2646, 2006.

[95] M. M. Abutalib and A. Rajeh, "Influence of ZnO/Ag nanoparticles doping on the structural, thermal, optical and electrical properties of PAM/PEO composite," *Phys. B Condens. Matter*, vol. 578, p. 411796, 2020.

[96] K. M. E. Miedzinska, B. R. Hollebone, and J. G. Cook, "An assigment of the optical absorption spectrum of mixed valence Co_3O_4 spinel films," *J. Phys. Chem. Solids*, vol. 48, no. 7, pp. 649–656, 1987.

[97] B. Coşkun, "Investigation of dielectric properties of Ag-doped ZnO thin films," *J. Mol. Struct.*, vol. 1209, p. 127970, 2020.

[98] S.-W. Zhao, C.-R. Guo, Y.-Z. Hu, Y.-R. Guo, and Q.-J. Pan, "The preparation and antibacterial activity of cellulose/ZnO composite: A review," *Open Chem.*, vol. 16, no. 1, pp. 9–20, 2018.

[99] T. S. Bachari, "Electric properties of Polyvinyl Acetate (PVA)-Polyol and prepared Sulfonated Phenol formaldehyde Resin (SPF) bulk samples composite," *Asian J. Appl. Sci. Eng.*, vol. 3, no. 2, pp. 33–44, 2014.

[100] B. Abd-Alkareem, "Effect of Nano-Copper Oxide on the Electrical and Optical Properties of (PMMA) Polymer." College of Education for Pure Sciences, University of Babylon, 2016.

[101] A. Herman and A. P. Herman, "Nanoparticles as antimicrobial agents: their toxicity and mechanisms of action," *J. Nanosci. Nanotechnol.*, vol. 14, no. 1, pp. 946–957, 2014.

Appendix (A)

The original images of the pure blend (PVA-PVP) from the FT-IR device.

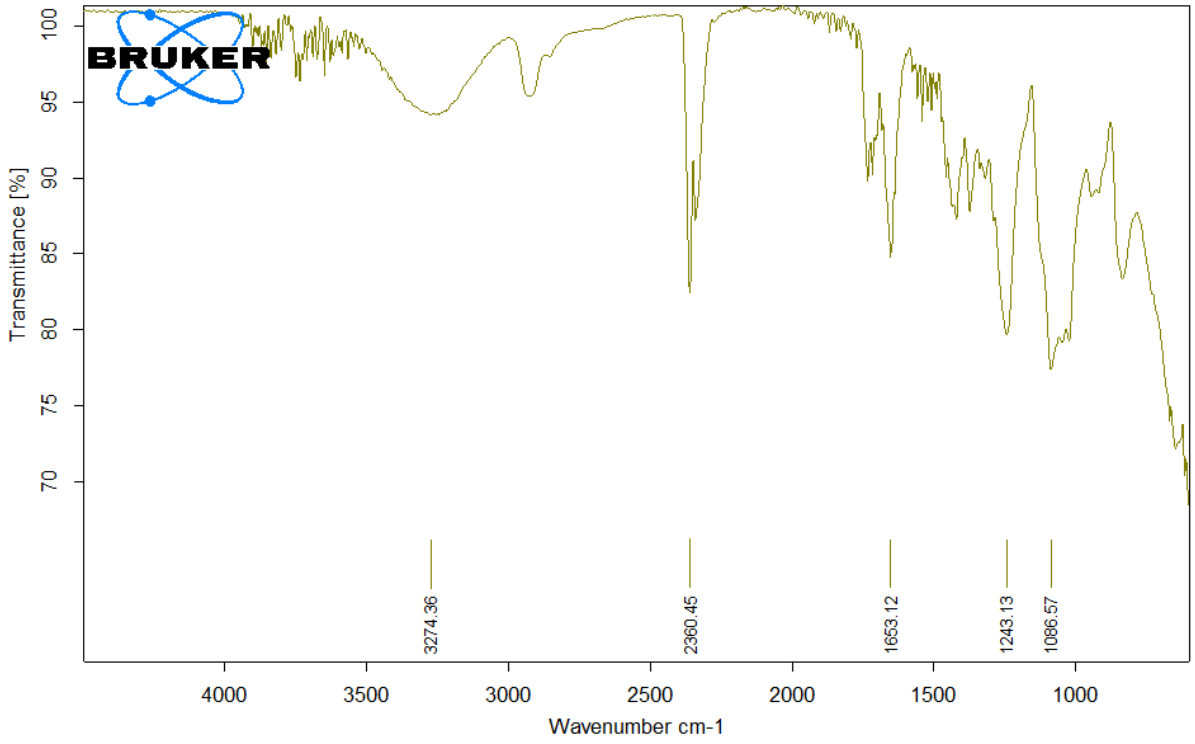

C:\OPUS_7.2.139.1294\MEAS\Sample description.1527	Sample description	Instrument type and / or accessory	14/12/2021

Page 1/1

Appendix (A)

The original image of the (PVA-PVP) blend with 5wt.% ZnO NCs film, from the FT-IR device.

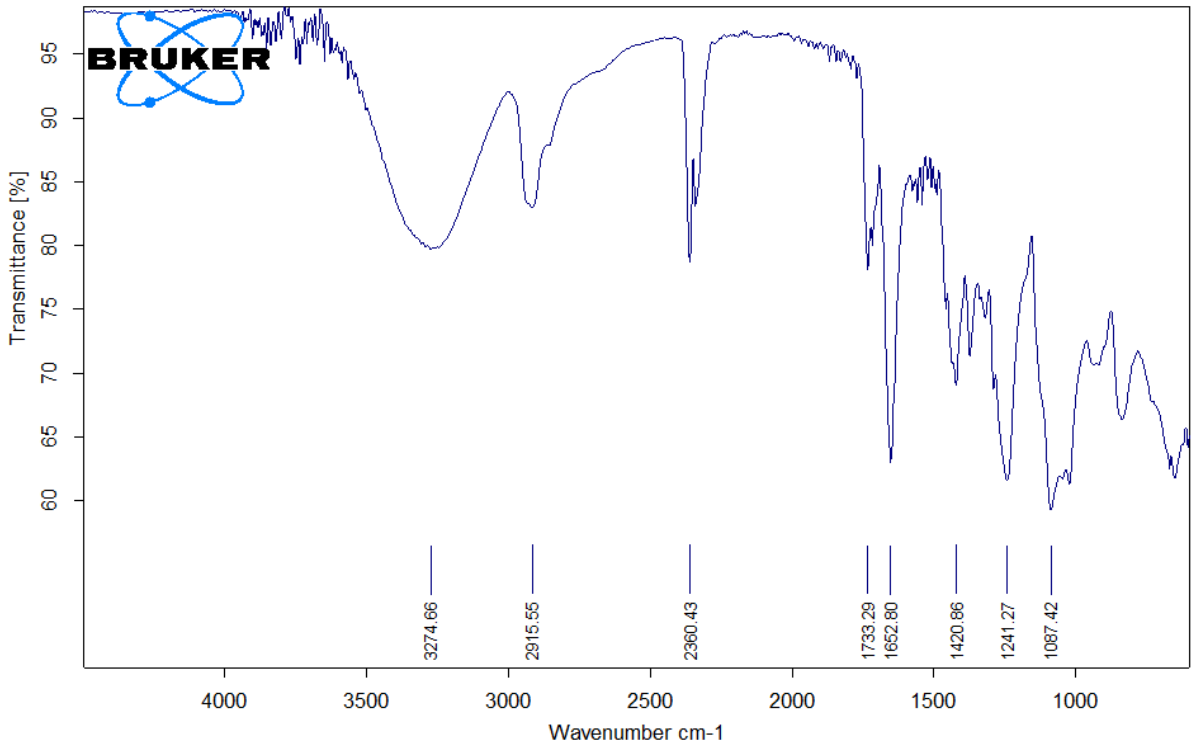

C:\OPUS_7.2.139.1294\MEAS\Sample description.1528	Sample description	Instrument type and / or accessory	14/12/2021

Page 1/1

Appendix (A)

The original image of the (PVA-PVP) blend with 5wt.% ZnO and 1wt.% of Ag nanocomposite film, from the FT-IR device.

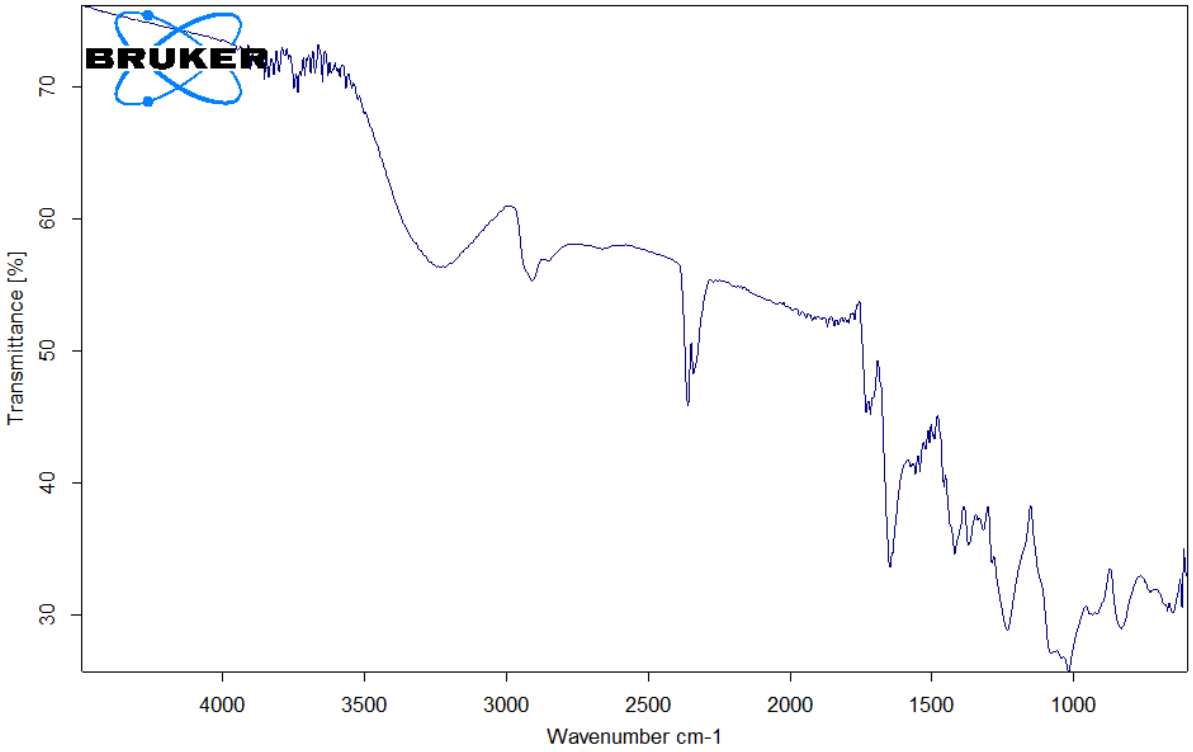

C:\OPUS_7.2.139.1294\MEAS\Sample description.1529	Sample description	Instrument type and / or accessory	14/12/2021

Page 1/1

Appendix (A)

The original image of the (PVA-PVP) blend with 5wt.% ZnO and 2wt.% of Ag nanocomposite film, from the FT-IR device

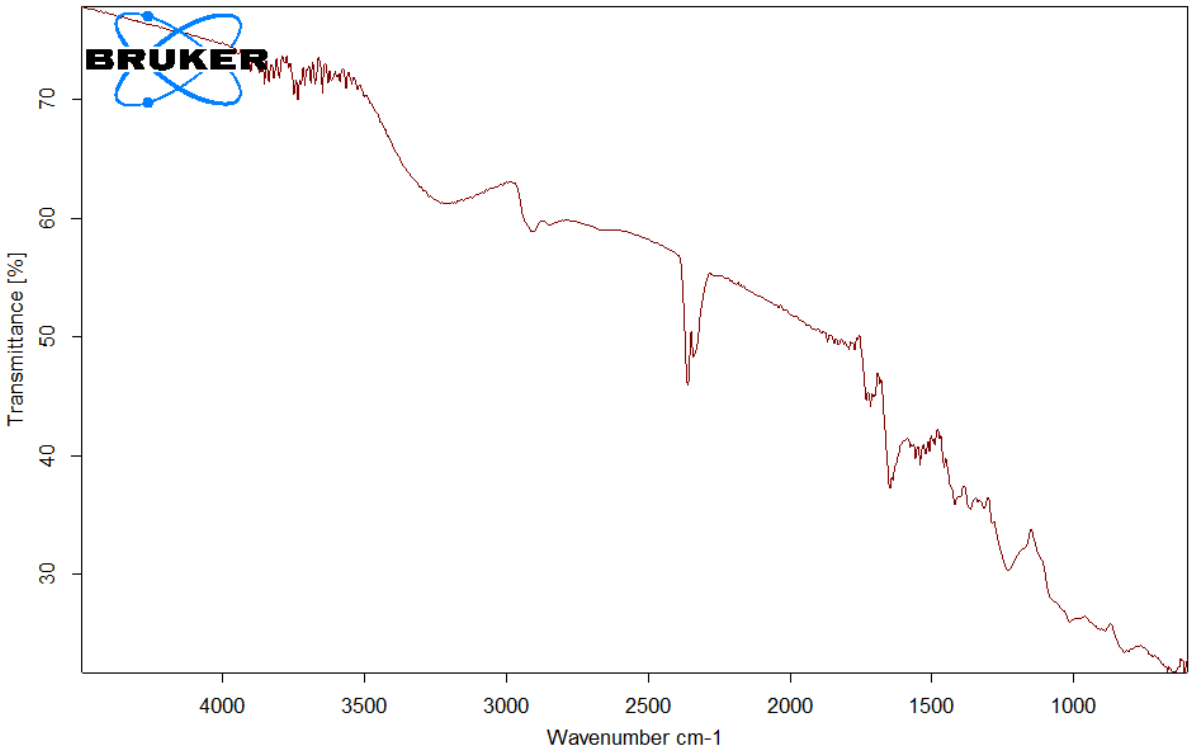

C:\OPUS_7.2.139.1294\MEAS\Sample description.1530	Sample description	Instrument type and / or accessory	14/12/2021

Page 1/1

Appendix (A)

The original image of the (PVA-PVP) blend with 5wt.% ZnO and 3wt.% of Ag nanocomposite film, from the FT-IR device

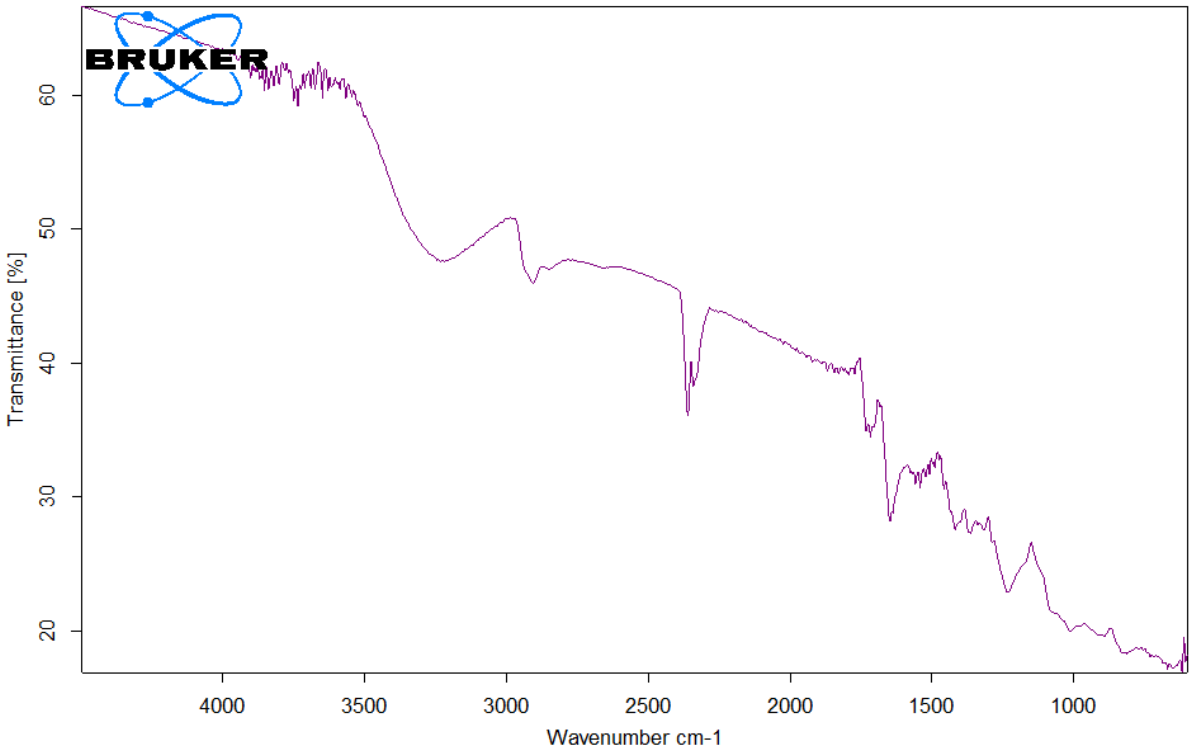

C:\OPUS_7.2.139.1294\MEAS\Sample description.1531	Sample description	Instrument type and / or accessory	14/12/2021

Page 1/1

Appendix (A)

The original image of the (PVA-PVP) blend with 5wt.% ZnO and 4wt.% of Ag nanocomposite film, from the FT-IR device

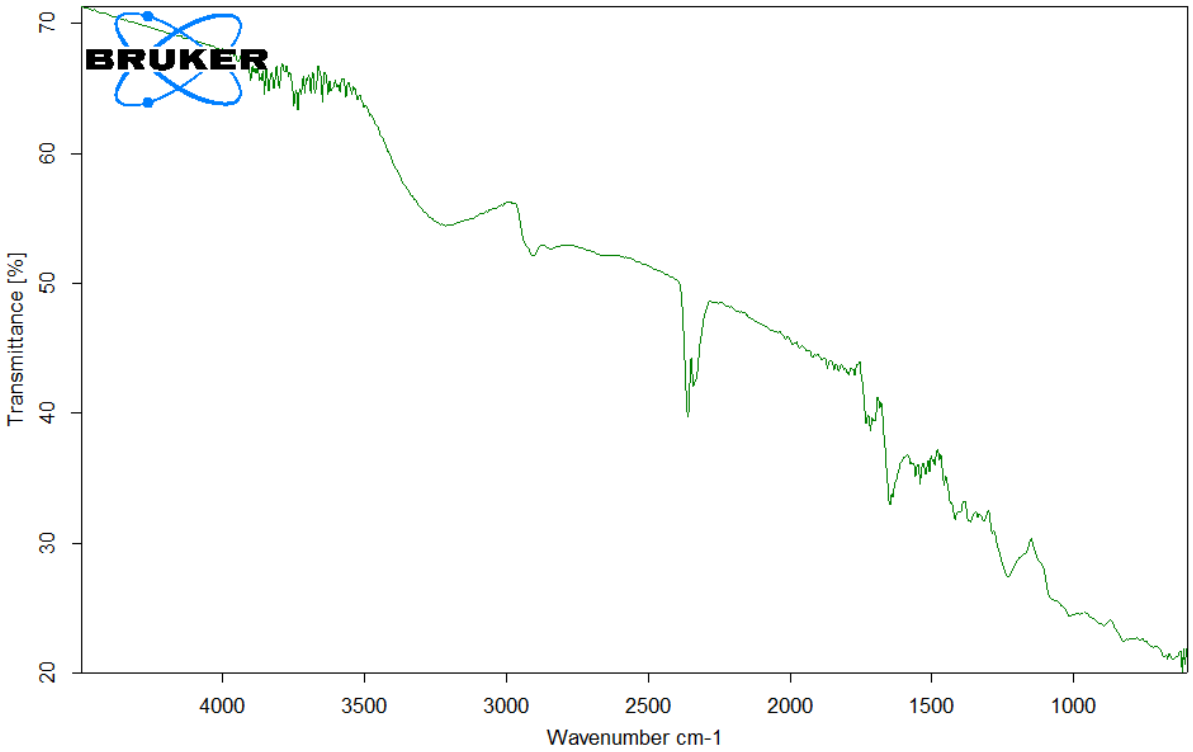

Appendix (B)

XRD Pattern of Polymer blend (PVA-PVP)

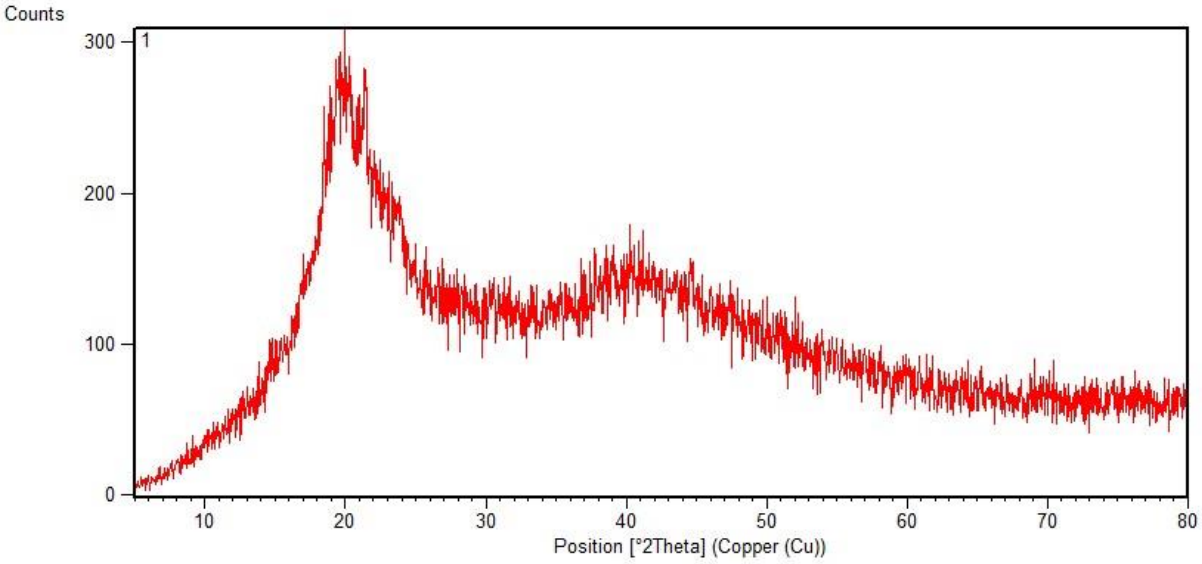

XRD Pattern of PVA-PVP/ZnO

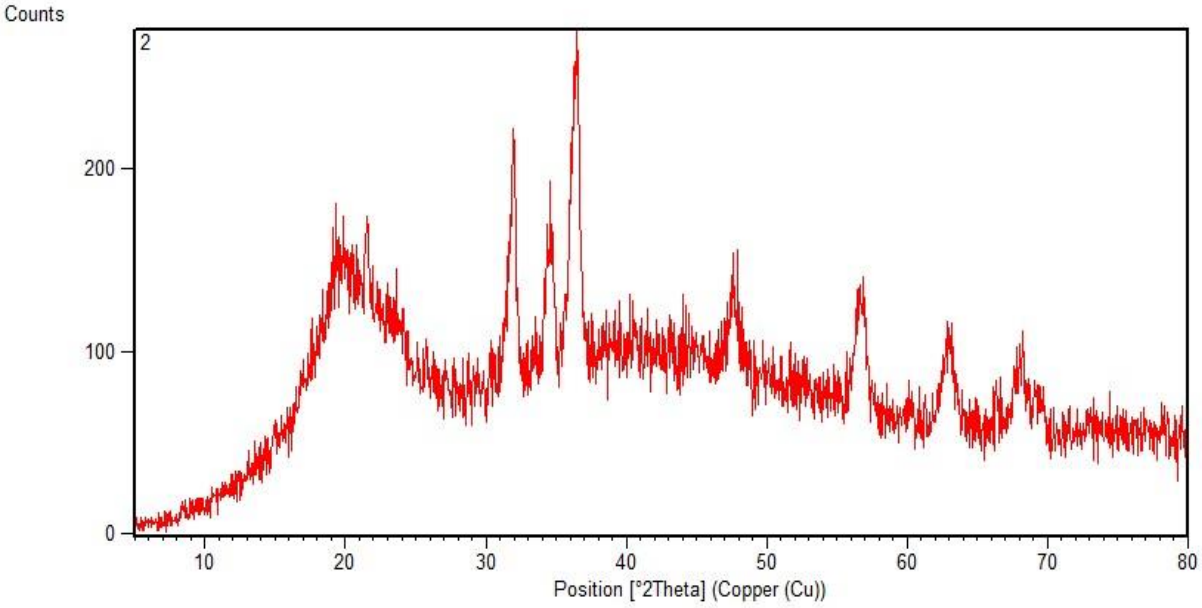

Appendix (B)

XRD Pattern of PVA-PVP/ ZnO and 1wt.% of Ag

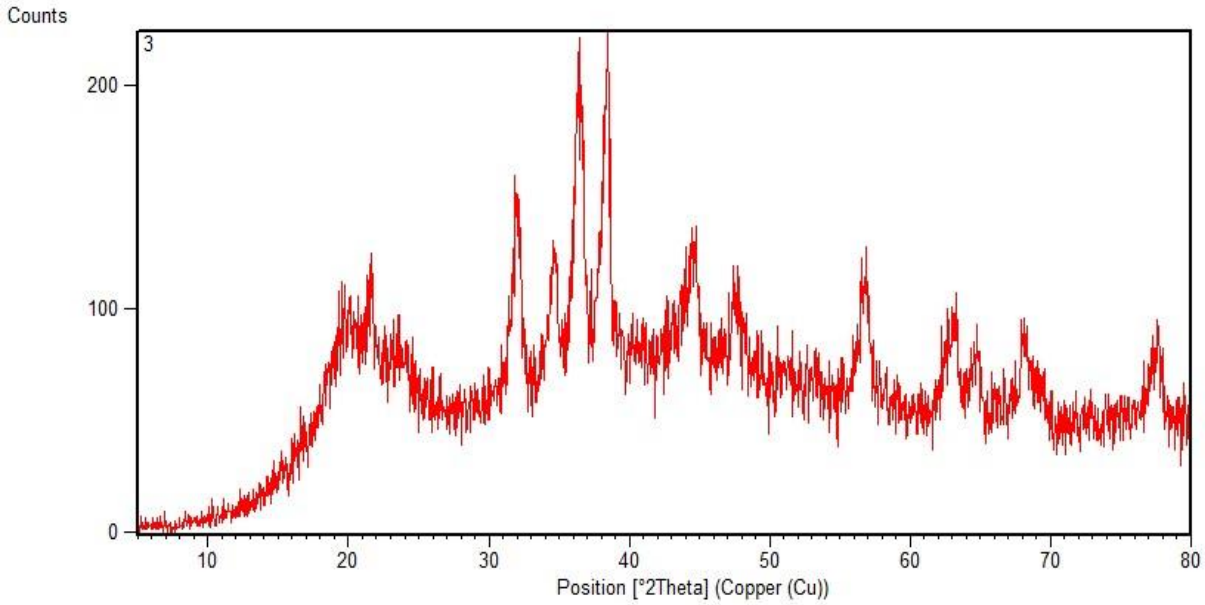

XRD Pattern of PVA-PVP/ ZnO and 2wt.% of Ag

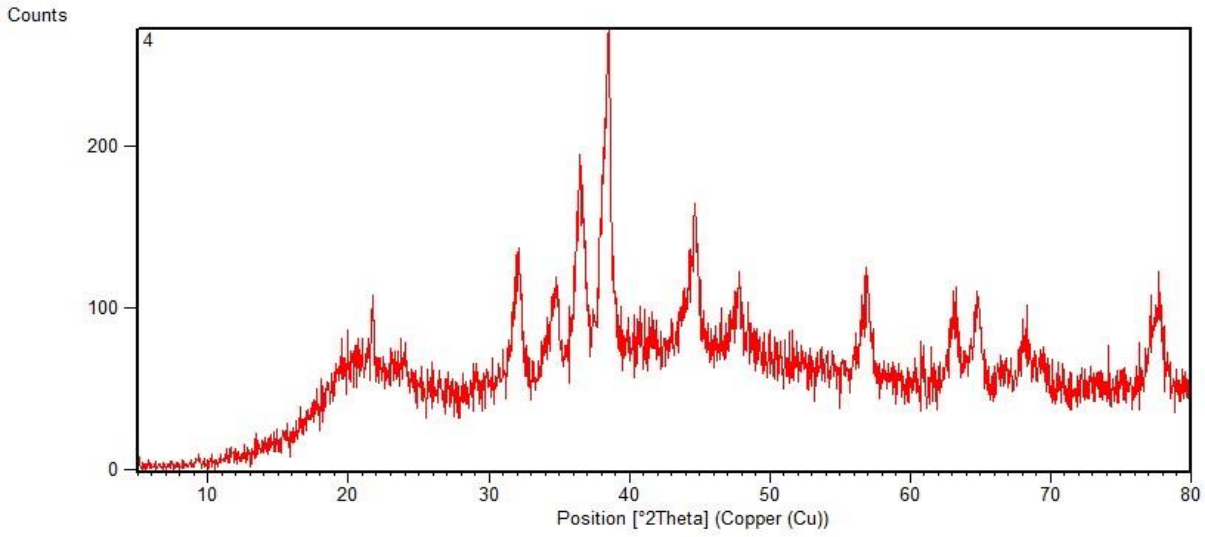

Appendix (B)

XRD Pattern of PVA-PVP/ ZnO and 3wt.% of Ag

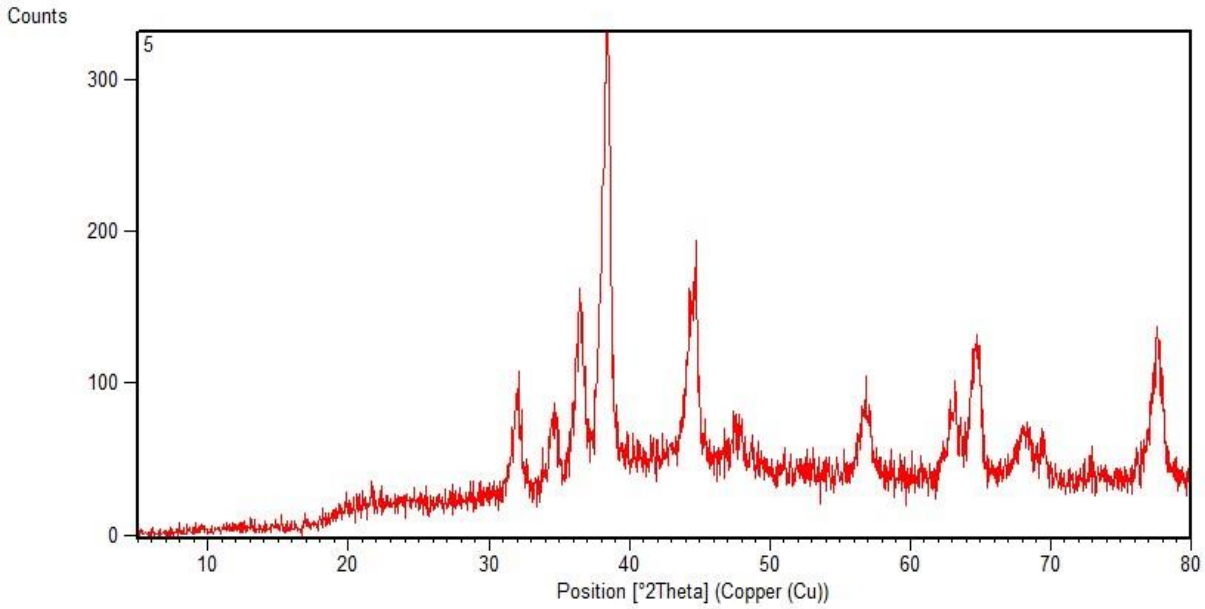

XRD Pattern of PVA-PVP/ ZnO and 4wt.% of Ag

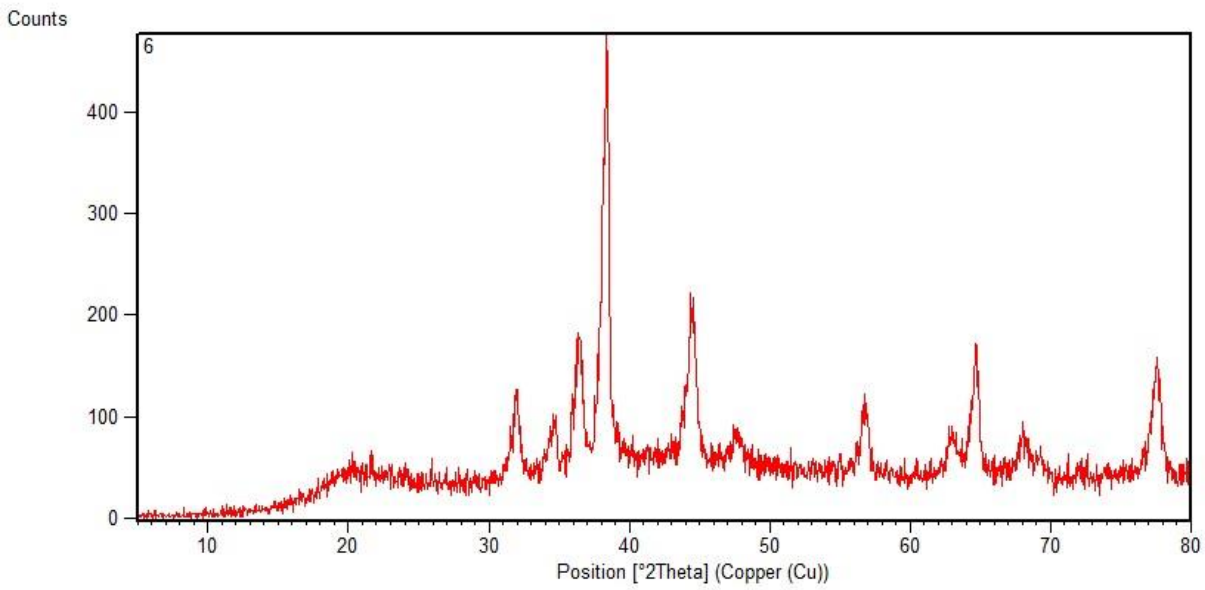

الخلاصة

تم تحضير مزيج بوليمر PVA-PVP ومركباته النانوية بنسبة وزنية 5% من ZnO ونسب مختلفة بالوزن (4,3,2,1) % من جسيمات الفضة النانوية باستخدام طريقة صب المحلول. تم تحديد النتائج عن طريق التحليل الطيفي للأشعة تحت الحمراء لتحويل فورييه (FT-IR)، حيود الاشعة السينية (XRD)، المجهر الالكتروني لمسح انبعاث المجال (FE-SEM)، المجهر البصري (OM) التحليل الطيفي للأشعة فوق البنفسجية المرئية، الخواص الكهربائية (AC) وتطبيقه كنشاط مضاد للجراثيم.

اكدت أطياف FT-IR على انتاج المجموعات الوظيفية الموجودة في أنظمة البوليمر النانوية. أكد تحليل XRD ان اغشية التكوين النانوية أكثر بلورية من مزيج البوليمر. أظهرت صور FE-SEM تكتلا لمجموعة صغيرة ومغلقة من الجسيمات الاهليجية على سطح خليط البوليمر نتيجة لإضافة كمية مختلفة من NPs . تشير الصور المجهرية الضوئية الى تجانس جيد وتوزيع جيد للجسيمات النانوية ZnO وAg، بالإضافة الى نقل الشحنة والتكوين المعقد داخل أغشية البوليمر الممزوجة.

اظهر التحليل الطيفي للأشعة فوق البنفسجية المرئية ان القيمة المثلى للنفاذية لفلم مزيج البوليمر تبلغ حوالي 98% في منطقتي Vis و NIR. يؤهل انخفاض نفاذية أفلام NC تجاه الاشعة فوق البنفسجية لاستخدامها كغلاف لتخزين الادوية بغض النظر عن التكلفة. تم تحديد فجوات الطاقة الانتقالية غير المباشرة المسموح بها والممنوعة من طيف الامتصاص، والتي انخفضت قيمها مع زيادة محتوى جسيمات الفضة النانوية. أظهرت الخواص الكهربائية AC ان ثابت العزل وفقد العزل الكهربائي لجميع الاغشية يتناقص مع زيادة تردد المجال الكهربائي، وان قيمه تزداد مع زيادة الوزن % من جسيمات الفضة النانوية.

تم اجراء اختبار الحساسية لمضادات الجراثيم للـ NCs المصنع بطريقة انتشار قرص الاجار ضد عزلتين من البكتيريا سالبة الجرام (*Escherichia coli*) والبكتيريا إيجابية الجرام (*Staphylococcus aureus*). أظهرت النتائج ان اغشية NC ذات نشاط مضاد للجراثيم مرتفع مقارنة بالمضاد الحيوي IMIPENEM 10mcg ولوحظت أفضل منطقة لتثبيط النمو البكتيري بنسبة 4% بالوزن من الفضة (34.567±3.066) ضد الاشريكية القولونية.

جمهورية العراق
وزارة التعليم العالي والبحث العلمي
جامعة بابل - كلية التربية للعلوم الصرفة
قسم الفيزياء

تحضير وتوصيف أغشية متراكبات نانوية كأنموذج للتطبيقات المضادة للبكتريا

رسالة مقدمة إلى

مجلس كلية التربية للعلوم الصرفة / جامعة بابل وهي جزء من متطلبات

نيل درجة الماجستير في التربية / فيزياء

من قبل

سرمد منذر عبد الكاظم حسين

بكالوريوس تربية فيزياء 2013 م

جامعة بابل

بإشراف

أ.د. فؤاد شاكر هاشم **أ.د. بهاء حسين صالح**

1444 هـ 2022 م